

A computational study of metastable states of CO²⁺

Felicja Mrugała^{a)}

Institute of Physics, Nicolaus Copernicus University, Grudziadzka 5, PL 87-100 Toruń, Poland

(Received 7 January 2008; accepted 28 May 2008; published online 13 August 2008)

Extensive calculations of energies and lifetimes of vibronic and rovibronic states of the CO²⁺ dication are performed using the electronic energy potentials and spin-orbit couplings published recently by Šedivcová *et al.* [J. Chem. Phys. **124**, 214303 (2006)] and by Eland *et al.* [J. Phys. B **37**, 3197 (2004)]. Siegert quantization, bound-continuum configuration mixing, two-potential, and semiclassical methods are exploited in the calculations. Lifetimes for predissociation and tunneling, varying over a wide range, are determined, demonstrating a very good agreement between results yielded by the different methods. Dependence of the calculated predissociation characteristics (level widths and shifts) on the individual potentials and couplings is analyzed. The potentials of Šedivcová *et al.*, especially the repulsive potential of the ³Σ⁻ state, are found insufficiently accurate in the medium range of the internuclear distance to be useful in simulations of the decay of the lowest vibronic states of the ion, X ³Π(*v*=0,1) and a ¹Σ⁺(*v*=0,1). Combining the potentials of Eland *et al.* with the SO couplings of Šedivcová *et al.* is demonstrated to provide the best description of metastability of the ion so far. Purely vibronic models constructed in this way give lifetimes in a reasonable agreement with all existing experimental values and estimates. The largest deviations, $\tau^{\text{expt}}/\tau^{\text{calc}} \approx 20$, occur in the X ³Π(*v*=1,2) cases. Strong evidence is provided that accounting for rotational motion of nuclei, spin-uncoupling perturbations, and diagonal spin-orbit couplings can reduce these deviations substantially, approximately ten times. The predissociation lifetimes of the rovibronic states A ³Σ_{0,1}⁺(*Jv*) are predicted to be, with no exception, more than 100 times shorter than radiative lifetimes of these states. © 2008 American Institute of Physics. [DOI: 10.1063/1.2948389]

I. INTRODUCTION

Investigations of multiply charged molecules have a long history and constitute an important branch of contemporary molecular sciences. Several review articles on different aspects of these investigations have been published; the most recent ones are Refs. 1–3. Of basic interest are diatomic dications, most of which can exist only in metastable states, at energies above charged-separated dissociation limits. Determining the energies and lifetimes of the metastable states, providing information on their quantum identity, and explaining mechanisms of their decay belong to the main objectives of experimental^{4–16,20,22} and theoretical^{6,7,9,14,17–25} studies in the field.

CO²⁺ has played a special role in the studies of stability of multiply charged molecules. It was the first molecular dication observed, in 1932, to live at least 1 μs (Ref. 4) before unimolecular fragmentation into atomic cations C⁺ and O⁺. It was used in the work⁹ reported in 1993 to provide “the first experimental evidence that a doubly charged molecule can be stable on a time scale of seconds.” More recently, the CO²⁺ ion served as the first test case of new experimental techniques which have been developed^{11,13,14} to allow measurements of lifetimes with vibrational level resolution.

The theoretical studies on metastability of the CO²⁺ ion have become possible with the publishing, in 1961, of the

first work¹⁷ on electronic energy potentials for doubly positive diatomic ions. Semiempirical potentials of the ground electronic state of CO²⁺ constructed according to the procedure proposed in that work were used in the early calculations^{6,18} which attempted to explain the observed^{5,6} stability of the ion on the microsecond time scale in terms of tunneling predissociation. Though these attempts seemed successful, the first *ab initio* computations of the potentials¹⁹ of several electronic states of CO²⁺ have given rise to a supposition that electronic predissociation might be a more important mechanism. The subsequent refined calculations of the potentials^{7,20,21} and the first evaluations of the electronic predissociation rates²¹ have fully confirmed this supposition.

Tunneling through the sizable barrier that occurred in the accurate potential of the ground state, X ³Π, and through even larger barriers in the potentials of the states that converge to the first excited dissociation limit, a ¹Σ⁺, b ¹Π, and A ³Σ⁺, have been found insignificant as decay routes of the vibrational levels of the ion which could be accessed in the experiments. Spin-orbit (SO) predissociation by purely repulsive state ³Σ⁻, having a common dissociation limit with the ground state, was found²¹ to proceed in some cases with rates which were close to the observed range of 10⁴–10⁸ s⁻¹. However, contrary to what had been expected before^{19,20} on the basis of general intensity considerations of spin-changing and spin-conserving transitions, those long-lived states were actually the *v*=0 and *v*=1 levels of the X ³Π state and not levels of the b ¹Π state. The *v*=1 level of

^{a)}Electronic mail: felicja@fizyka.umk.pl.

the lowest singlet state $a^1\Sigma^+$ was indicated as the only other candidate likely to live for microseconds and the lowest vibrational level of this state was predicted to be practically stable.

Predissociation lifetimes of levels in some excited electronic states, $A^3\Sigma^+$ and $d^1\Sigma^+$, were considered with reference to the question about the possibilities to observe photon emission in CO^{2+} . The estimate provided for the lifetime of $v=0$ level of the state $A^3\Sigma^+$ and the suggested stability of some spin components of this state have given rise to the later search^{8,16,22} for the emission due to the $A^3\Sigma^+ \rightarrow X^3\Pi$ transition.

The approach taken in Ref. 21 to evaluate the predissociation rates was the simplest implementation of the bound-continuum configuration mixing (CM) theory,^{26–29} accounting for interaction of a discrete level in single potential (of the $X^3\Pi$, $b^1\Pi$, or $A^3\Sigma^+$ state) with single continuum (of the $^3\Sigma^-$ state). Semiempirical estimates of SO couplings³⁰ were inserted for the bound-continuum interactions.

The theoretical description of the CO^{2+} ion has been advanced significantly in result of calculations performed in Ref. 9. Together with further improved potential curves for the four lowest electronic states, $X^3\Pi$, $^3\Sigma^-$, $A^1\Sigma^+$, and $b^1\Pi$, the SO couplings between the $X^3\Pi-^3\Sigma^-$, $a^1\Sigma^+-^3\Sigma^-$, and $a^1\Sigma^+-X^3\Pi$ states have been determined as functions of the internuclear distance. The predissociation rates of vibrational levels of the $a^1\Sigma^+$ and $X^3\Pi$ states have been generated from these potentials and couplings in a nonperturbative manner, using the complex rotated finite element method.³¹ Due to accounting for indirect $a^1\Sigma^+ \rightarrow X^3\Pi \rightarrow ^3\Sigma^-$ decay route, the levels $a^1\Sigma^+(v=0,1)$ have been found to live much shorter than the corresponding levels of the ground state. $X^3\Pi(v=0)$ has been established as the longest-lived vibrational level of the ion. However, the lifetime of 20 ms calculated for this level was definitely too small to match the experimental finding reported in the same paper, of a level living longer than 3.8 s. Similarly, the second largest lifetime calculated for the $a^1\Sigma^+(v=0)$ level was by far too small to serve identifying precursor states of two lifetimes which were observed in the millisecond range (0.8 and 6 ms). It was therefore hypothesized that the higher excited state $d^1\Sigma^+$, strictly tunneling from its double-well potential, might be responsible for these observations. An additional argument in favor of the hypothesis was the small detected fractional population of levels giving rise to the millisecond lifetimes, which would presumably be unattainable if the levels belonged to any of the states $X^3\Pi$, $a^1\Sigma^+$, or $b^1\Pi$.

The experimental studies on stability of individual vibronic states of the CO^{2+} ion carried out in later years^{11,13,14} have provided information which enabled a partial verification of the theory developed up to 1993. Namely, lifetimes of three states of the $^{12}\text{C}^{16}\text{O}^{2+}$ ion, $a^1\Sigma^+(v=1)$, $X^3\Pi(v=2)$, and $b^1\Pi(v=0)$, have been measured and found to be 0.7, 0.2, and 0.026 μs , respectively, and the two lower states $X^3\Pi(v=0,1)$ and $a^1\Sigma^+(v=0)$ have been found to live longer than 10 μs . Lifetimes of above 20 higher vibronic states, including $d^1\Sigma^+(v=0,1)$, have been estimated¹¹ to be in the interval of 1×10^{-14} – 5×10^{-8} s. In four important cases at least, $X^3\Pi(v=1,2)$ and $a^1\Sigma^+(v=0,1)$, these data

could not be reproduced theoretically¹⁴ using the potentials and couplings of Ref. 9. The calculated lifetimes of the states $X^3\Pi(v=2)$ and $a^1\Sigma^+(v=1)$ were nearly three orders of magnitude too small. This striking discrepancy between calculations and measurements together with the finding of low stability of the state $d^1\Sigma^+$ cast some doubts on the original explanation of the slow decay observed in the experiment of Ref. 9. It has been therefore proposed¹³ that the 0.8 and 6 ms lifetimes be ascribed just to states $X^3\Pi(v=1)$ and $a^1\Sigma^+(v=0)$, respectively. Obviously, a need has emerged for still higher accuracy calculations of the electronic structure of the CO^{2+} ion.

Two such calculations have been reported recently.^{23,24} The calculations of Ref. 23 have provided potentials of seven lowest states, $X^3\Pi$, $^3\Sigma^-$, $a^1\Sigma^+$, $b^1\Pi$, $A^3\Sigma^+$, $c^1\Delta$, and $d^1\Sigma^+$. The potentials have been tested in a simulation of double photoionization spectrum of CO. Very good consistency has been achieved with the vibrationally resolved spectra recorded in the experiments of Refs. 10, 12, and 15. Even larger set of potentials (for nine states) and all SO coupling curves between the lowest six states have been generated in Ref. 24. Using these data, calculations of predissociation lifetimes of several lowest vibronic states of the $^{12}\text{C}^{16}\text{O}^{2+}$ ion have been performed in the same work, demonstrating the desired tendency of the results; they are substantially larger than the lifetimes calculated previously. The lifetime calculations of Ref. 24 had evidently a very preliminary character. The two standard methods employed, the stabilization³² and the complex-scaling³³ methods, gave numbers differing by hundreds of percent in most (eight of ten) cases presented. No number could be provided for lifetimes of the three lowest vibronic states. The interesting confrontation with the experimental data in the millisecond range could not thus be made. Summarizing, the new electronic structure data for CO^{2+} are very promising. Taking fuller advantages of them to improve the existing theoretical description of dissociation dynamics of the ion is desirable. This is the general goal of the present study. The particular questions investigated are listed at the beginning of Sec. IV, after the presentation of the assumed model Hamiltonians (Sec. II) and the chosen methods for resonance calculations (Sec. III).

II. MODELS

The models of dynamics of the CO^{2+} ion which are tried in the present study involve maximally five lowest electronic states, $X^3\Pi$, $^3\Sigma^-$, $a^1\Sigma^+$, and $b^1\Pi$, and $A^3\Sigma^+$, and account for SO interactions between these states. The respective electronic energy potentials, taken from Refs. 24 and 23, are presented in Fig. 1(a), and the SO coupling curves from Ref. 24 are shown in Fig. 2. Of this electronic structure input, four models are formed to study the vibrational motion of the ion; they are called hereafter the JCP06 original, the JCP06, the JP04 model, and the JP04A model, respectively.

The term “JCP06 original” signifies the four-state model (without the state $A^3\Sigma^+$) which was constructed in Ref. 24 by a global analytical fitting to the *ab initio* generated points of the potentials and couplings. However, using the formulas and parameters provided in the supplementary material to

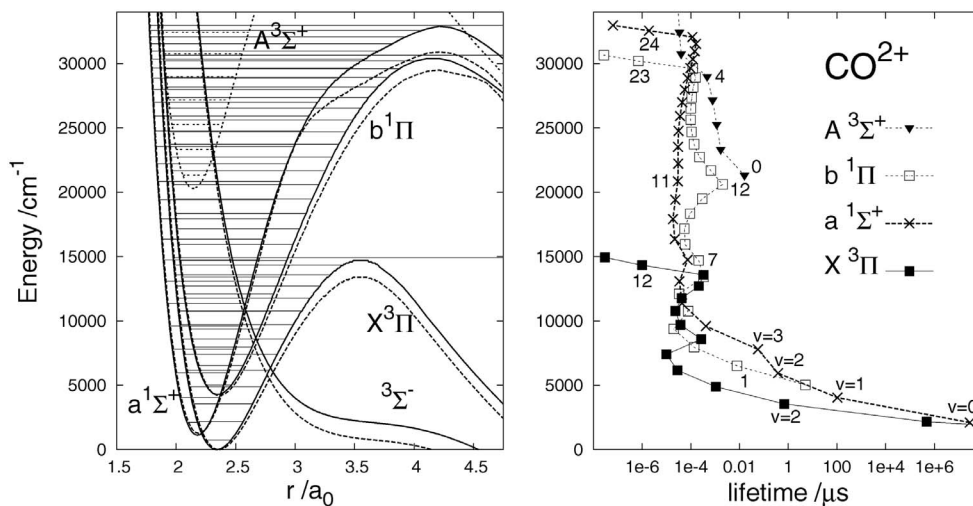


FIG. 1. (a) Left panel: Electronic energy potentials of four lowest states of CO²⁺. Solid line curves are from the analytical model of Ref. 24 (the JCP06 model). Dashed curves represent the *ab initio* results of Ref. 23 (the JP04 model). In each model, $E=0$ is set at the minimum of the well of the $X^3\Pi$ state potential. The separations of the well minima $V_a^{\min} - V_X^{\min}$ and $V_b^{\min} - V_X^{\min}$ are 0.005 110 and 0.019 488 E_H in the JCP06 model and 0.005 744 and 0.019 129 E_H in the JP04 model. The barrier heights $V_s^{\max} - V_s^{\min}$ of the JCP06 potentials, 0.067 086, 0.144 68, and 0.119 169 E_H for $s=X, a, b$, exceed their JP04 counterparts by 0.005 937, 0.009 734, and 0.003 940 E_H , respectively. [Adapted from T. Šedivcová, P. R. Zdánská, V. Špirko, and J. Fišer, J. Chem. Phys. **124**, 214303 (2006), ©2006 AIP, by permission of American Institute of Physics, and from J. H. D. Eland, M. Hochlaf, G. C. King, P. S. Kreynin, R. J. Le Roy, I. R. McNab, and J. M. Robbe, J. Phys. B **37**, 3197 (2004), ©2004 IOP Publishing Ltd., by permission of IOP Publishing Ltd.] (b) Right panel: Lifetimes of metastable vibronic states formed within the potential wells—results of the present four-coupled channel calculations. The lifetimes of the $A^3\Sigma^+(v)$ levels are from the JP04A model (see text). The other lifetimes are from the JCP06 model.

that paper, one obtains coupling curves which in two cases differ significantly from the curves shown in the main text. In particular, the largest coupling determined in the *ab initio* calculations of that work, $^1\Sigma^+ - ^3\Sigma^-$, is totally suppressed in the model. Moreover, the formulas are evidently not designed to account for the asymptotic behavior of the potentials (for example, the potential of the ground state starts to grow at C–O distances around $13a_0$). Unfortunately, no *ab initio* data are disclosed in Ref. 24 which would help to eliminate these deficiencies. Thus, the $a^1\Sigma^+ - ^3\Sigma^-$ and $a^1\Sigma^+ - X^3\Pi$ curves are modified here to make them look as the ones shown in Fig. 2 of Ref. 24. The JCP06 original model with the two couplings corrected, as demonstrated in Fig. 2 by the dashed lines, gives the JCP06 model. The model is assumed to match reasonably well the *ab initio* data in the range of C–O distance extending up to $9.9 a_0$. Beyond this range, the potentials are extrapolated with the function $1/r + V^{\text{th}}$. (Atomic units are used throughout the text). In the case of the $^3\Sigma^-$ state, the function $1/r + c/r^4 + V^{\text{th}}$ is used for the extrapolation. The threshold position V^{th} is deduced in this case from the numbers provided in Ref. 24 for the kinetic energy release in the predissociation of $X^3\Pi(v=2)$, $a^1\Sigma^+(v=1)$, and $b^3\Pi(v=0)$ states.

Replacing the potentials of the JCP06 model with the ones determined in Ref. 23 and retaining the SO couplings give what is called the JP04 model. “JP04A” labels a version of the JP04 model designated solely to study the decay of the vibrational states formed in the potential of the fifth excited electronic state $A^3\Sigma^+$. The role of state $a^1\Sigma^+$ in this decay is assumed to be negligible. The states included are $X^3\Pi$, $^3\Sigma^-$, $b^1\Pi$, and $A^3\Sigma^+$. Since Ref. 23 provides the potentials in numerical form, cubic spline interpolation is performed to generate smooth curves in the ranges covered by the data. Extrapolation of each curve to large r -values is made with

one-parameter function $1/r + V^{\text{th}}$. Some details on the potentials used in the present study are listed in the caption of Fig. 1.

Thus, 4×4 matrix Hamiltonian emerges from each of the four models for the investigation of vibrational motion of the CO²⁺ ion,

$$\mathbf{H}(r) = -\frac{1}{2\mu} \mathbf{I} \frac{d^2}{dr^2} + \mathbf{V}(r). \quad (1)$$

Obviously, the diagonal part of \mathbf{V} is built of the potentials of the electronic states considered, the off-diagonal part con-

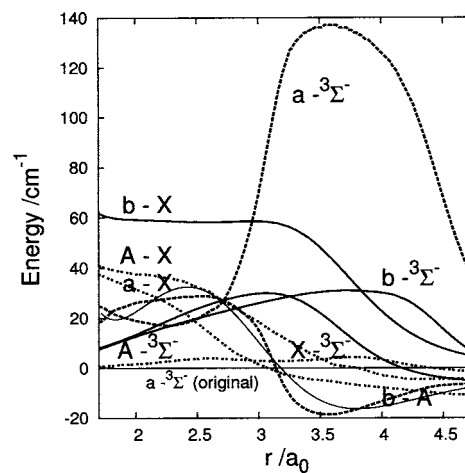


FIG. 2. SO couplings between the five lowest electronic states of CO²⁺. Full line curves are from the analytical model of Ref. 24. Dashed curves represent couplings corrected here to match the ones calculated *ab initio* and shown in Fig. 2 of Ref. 24. Dotted lines represent couplings included into the JP04A model; they are also reproduced from Fig. 2 of Ref. 24. [Adapted with permission from T. Šedivcová, P. R. Zdánská, V. Špirko, and J. Fišer, J. Chem. Phys. **124**, 214303 (2006), ©2006 American Institute of Physics.]

tains the SO couplings, \mathbf{I} denotes the unit matrix, and μ is the reduced mass. The $^{12}\text{C}^{16}\text{O}^{2+}$ isotopomer is mostly considered in this work for which the value $\mu=12\,497.592\,m_e$ is adopted. Some calculations are also done for $^{13}\text{C}^{16}\text{O}^{2+}$ with $\mu=13\,072.140\,m_e$.

Metastable vibronic states of the CO^{2+} ion are the focus of the present study. However, a substantial part of the work is devoted also to estimating how much the lifetimes of these states can be influenced by rotation of the nuclear framework. In this part, the following matrix Hamiltonians are exploited:

$$\mathbf{H}^{Jp}(r) = -\frac{1}{2\mu}\mathbf{I}\frac{d^2}{dr^2} + \mathbf{V}^{Jp}(r) \quad \text{for } p=e,f, \quad (2)$$

with

$$\mathbf{V}^{Jp} = \mathbf{V}_{\text{EL}}^{Jp} + \mathbf{V}_{\text{SO}}^{Jp} + \mathbf{V}_{\text{ROT}}^{Jp}, \quad (3)$$

where J is the quantum number associated with the total angular momentum operator $\mathbf{J}=\mathbf{L}+\mathbf{S}+\mathbf{R}$ with \mathbf{L} , \mathbf{S} , and \mathbf{R} representing the total electronic orbital angular momentum, the total electronic spin, and the nuclear rotation operators, respectively, and p is the parity label. Elements of the matrices \mathbf{H}^{Jp} are enumerated by a composite index s_Ω with $s \equiv 2S+1\Lambda$ labeling the electronic state (spin multiplet) and Ω identifying the multiplet component. S , Λ , and Ω are the quantum numbers associated with \mathbf{S}^2 and with the projections on the internuclear axis of \mathbf{L} and \mathbf{J} , respectively. (Here, symbols Λ and Ω are used for unsigned values of the projections, i.e., $\Lambda=|\Lambda|$ and $\Omega=|\Omega|$.) The matrices $\mathbf{V}_{\text{EL}}^{Jp}$ are diagonal in both s and Ω indices,

$$[\mathbf{V}_{\text{EL}}^{Jp}(r)]_{s_\Omega, \tilde{s}_\Omega'} = \delta_{s,s'}\delta_{\Omega,\Omega'}V_{s,s}(r), \quad (4)$$

and include the electronic energy potentials $V_{s,s}(r)$ of the five states of CO^{2+} listed at the beginning of this section. Obviously, the fact that there are only definite parity $\Omega=0$ components of odd-multiplicity Σ states³⁰ is accounted for. The potentials of Ref. 23 (i.e., those used in the JP04 and JP04A models) are used for this vibrational study.

The matrices $\mathbf{V}_{\text{SO}}^{Jp}$ are built of the SO coupling functions $V_{s,s}(r)$ plotted in Fig. 2, respecting the $\Delta\Omega=0$ selection rule

$$[\mathbf{V}_{\text{SO}}^{Jp}(r)]_{s_\Omega, \tilde{s}_\Omega'} = \delta_{\Omega,\Omega'}[(1-\delta_{s,s'})V_{s,s}(r)\alpha + \delta_{s,s'}A_\Lambda(r)\Lambda(\Omega-\Lambda)]. \quad (5)$$

The factor $\alpha=\sqrt{2}$ is inserted when s_Ω or \tilde{s}_Ω' is a $2S+1\Sigma_0$ state; otherwise $\alpha=1$. An important new ingredient as compared to the vibronic (nonrotating molecule) JP04 and JCP06 models is the SO ‘‘constant’’ $A_\Lambda(r)$. This function for the $X^3\Pi$ state is taken from Ref. 22.

The matrices $\mathbf{V}_{\text{ROT}}^{Jp}$ include the following parts of the matrix elements of the operator $(1/2\mu r^2)\mathbf{R}^2$ in Hund's case (a) angular momentum basis set³⁰

$$[\mathbf{V}_{\text{ROT}}^{Jp}(r)]_{s_\Omega, \tilde{s}_\Omega'} = \delta_{s,s'}[\delta_{\Omega,\Omega'}E^J(s_\Omega; r) + \delta_{\Omega',\Omega\pm 1}C_{\Omega,\Omega\pm 1}^{Jp}(s; r)], \quad (6)$$

where the diagonal part is the rotational energy,

$$E^J(2S+1\Lambda_\Omega; r) = \frac{1}{2\mu r^2}[J(J+1) + S(S+1) - \Omega^2 - \Sigma^2], \quad (7)$$

with $\Sigma=\Omega-\Lambda$, and the second part is the S-uncoupling perturbation,³⁰

$$C_{\Omega,\Omega\pm 1}^{Jp}(2S+1\Lambda; r) = -\frac{1}{2\mu r^2}[J(J+1) - \Omega(\Omega\pm 1)]^{1/2} \times [S(S+1) - (\Sigma\pm 1)\Sigma]^{1/2} \times N^p(2S+1\Lambda_\Omega)N^p(2S+1\Lambda_{\Omega\pm 1}), \quad (8)$$

where $N^p=1$ except for $N^p(2S+1\Sigma_0) = \frac{1\pm(-1)^{-S+\epsilon}}{\sqrt{2}}$ with $\pm \Leftrightarrow p=e$ and $\epsilon=0 \Leftrightarrow \Sigma^\pm$.

The matrix Hamiltonians $\mathbf{H}_{8\times 8}^{Je}$ and $\mathbf{H}_{7\times 7}^{Jf}$ for vibration-rotation motion defined by Eqs. (2) and (4)–(6) and (8) together with the used electronic structure input constitute what is called here the JP04r-v model. In some tests the model is supplemented with terms which are intended to simulate L-uncoupling perturbations³⁰ in the system

$$[\mathbf{V}_{\text{ROT}}^{Jp}(r)]_{s_\Omega, \tilde{s}_\Omega'} = -\frac{1}{2\mu r^2}\delta_{s,s'}\delta_{\Lambda,\Lambda\pm 1}\delta_{\tilde{\Omega},\Omega\pm 1}\delta_{\tilde{\Sigma},\Sigma}G^{Jp}(s_\Omega, \tilde{s}_\Omega'; r). \quad (9)$$

The terms are given proper J -dependent factors but their electronic factors $\langle \Lambda|L^+|\Lambda-1\rangle$ are all set arbitrarily to $\sqrt{2}$.³⁴

The used formulas are $G^{Jf} = \mp [2J(J+1)]^{1/2}$ and $[2J(J+1) - 4]^{1/2}$ for $(s_\Omega, \tilde{s}_\Omega') = ({}^3\Pi_0, {}^3\Sigma_1)$ and $({}^3\Pi_2, {}^3\Sigma_1)$, respectively, and $G^J(\Pi_1, \Sigma_0) = 2[J(J+1)]^{1/2}$.

Obviously, within the models presented here it is possible to account for two mechanisms of decay of the (ro)vibrational states of the CO^{2+} ion, the SO predissociation, and the tunneling. It can be deduced from the lifetime calculations of Ref. 23 that tunneling is unimportant in the decay of most of the vibrational levels drawn in Fig. 1(a), in particular, of those investigated experimentally. Thus, for the purpose of confronting the models with experiment, one could concentrate on the SO predissociation mechanism only. It should be noted, however, that tunneling widths, even the unrealistically small ones, can be of theoretical interest as sensitive indicators of the size of the potential barriers. Besides, there are interesting methodological aspects associated with accurate determination of these widths. For these reasons, the tunneling widths are also given some consideration here.

III. METHODS

Well-known methods of three distinct categories were exploited in the calculations on the metastable states of the CO^{2+} ion. The methods are described shortly in the following subsections. Emphasis is put on the most important features of their present implementation.

A. An exact quantum-mechanical method

The Siebert-quantization (SQ) method^{35–38} consists in solving the following eigenvalue problem:

$$[\mathcal{E}\mathbf{I} - \mathbf{H}(r)]\Psi(r; \mathcal{E}) = 0, \quad (10)$$

$$\Psi(0; \mathcal{E}) = 0, \quad (11)$$

$$\left[\mathbf{I} \frac{d}{dr} - \mathbf{L}_{O^+}(r_\infty; \mathcal{E}) \right] \Psi(r; \mathcal{E})|_{r=r_\infty} = 0, \quad (12)$$

with the characteristic asymptotic boundary condition requiring that there be only outgoing-wave components in the eigenfunctions. The condition is imposed at a distance r_∞ which is large enough to allow for the approximation

$$V_{s,s'}(r) \approx \delta_{s,s'} \left(\frac{1}{r} + V_s^{\text{th}} \right) \quad \text{for } s, s' = 1, \dots, 4 \quad (13)$$

at $r \geq r_\infty$. Thus, the log-derivative matrix of the outgoing waves at the r_∞ -boundary,

$$[\mathbf{L}_{O^+}(r_\infty; \mathcal{E})]_{s,s'} = \delta_{s,s'} \frac{d}{dr} \ln O_s^+(r; \mathcal{E})|_{r=r_\infty} \quad (14)$$

for $s = 1, \dots, 4$, should be built of Coulomb functions, i.e.,

$$O_s^+(r; \mathcal{E}) = \frac{C}{\sqrt{k_s}} [G_{L=0}(\rho_s; \eta_s) + iF_{L=0}(\rho_s; \eta_s)], \quad (15)$$

where

$$k_s = \sqrt{2\mu(\mathcal{E} - V_s^{\text{th}})}, \quad \rho_s = k_s r, \quad \eta_s = \frac{\mu}{k_s},$$

$F_L(\rho; \eta)$ and $G_L(\rho; \eta)$ denote the regular and irregular Coulomb functions³⁹ normalized to unit Wronskian, $(d/d\rho)F_L G_L - (d/d\rho)G_L F_L = 1$. From among possible eigenvalues \mathcal{E} (an infinite set of complex numbers, see, e.g., Ref. 40, are references therein) only the ones which correspond to resonances are of interest here. A complex eigenvalue \mathcal{E} describes a resonance of energy E_{res} and width Γ ,

$$\mathcal{E} = E_{\text{res}} - i \frac{\Gamma}{2} = \frac{1}{2\mu} k_s^2 + V_s^{\text{th}}, \quad (16)$$

if $\text{Im } k_s < 0$ and $-\text{Im } k_s \ll \text{Re } k_s$ when $E_{\text{res}} > V_s^{\text{th}}$ and $\text{Im } k_s \gg -\text{Re } k_s > 0$ when $E_{\text{res}} < V_s^{\text{th}}$. The eigenvalue should be stable against an increase of the distance r_∞ .

In the procedure adopted here, the resonance eigenvalues are determined as roots of the equation³⁷

$$\det[\mathbf{L}(r_m; \mathcal{E}) - \bar{\mathbf{L}}(r_m; \mathcal{E})] = 0, \quad (17)$$

where $\mathbf{L}(r; \mathcal{E})$ and $\bar{\mathbf{L}}(r; \mathcal{E})$ denote the log-derivative matrices of solutions of Eq. (10), which at any \mathcal{E} satisfy only one boundary condition, Eqs. (11) and (12), respectively. The values of \mathbf{L} and $\bar{\mathbf{L}}$ at $r = r_m$, where $0 < r_m < r_\infty$, are obtained by integrating the Riccati equation,

$$\frac{d}{dr} \mathbf{L} + \mathbf{L}^2 + \mathbf{W} = 0 \quad \text{with} \quad \mathbf{W}(r; \mathcal{E}) \equiv 2\mu[\mathcal{E}\mathbf{I} - \mathbf{V}(r)], \quad (18)$$

in the intervals $[0, r_m]$ and $[r_\infty, r_m]$, respectively,

$$[\mathbf{L}(0; \mathcal{E})]^{-1} = 0, \quad (19)$$

$$\bar{\mathbf{L}}(r_\infty; \mathcal{E}) = \mathbf{L}_{O^+}(r_\infty; \mathcal{E}). \quad (20)$$

The integration is done with the help of the log-derivative method.^{41,42} Some caution is required in choosing an appropriate form of the asymptotic boundary condition (Eq. (20)) especially when the value r_∞ cannot be enlarged freely for some reason.

For the planned discussion of the accuracy of models and methods, it is desirable to have a set of reference results for the predissociating states generated from each of the considered models which are free of any impact of the uncertain, extrapolated parts of the potentials. Hence, a need arises to achieve a reasonable stability of the resonance eigenvalues at relatively small distances r_∞ , possibly not larger than $9 - 9.5a_0$. Several ways of evaluations of the matrices $\mathbf{L}_{O^+}(r_\infty; \mathcal{E})$ can be tried.³⁸ Tests described in the supplementary material⁴³ (Table AI) reveal that it is most suitable to resort to the WKB form of \mathbf{L}_{O^+} ,

$$\mathbf{L}_{O^+}^{\text{WKB}}(r_\infty; \mathcal{E}) = i\mathbf{k}_\infty(r, \mathcal{E}) - \frac{1}{2} \frac{d}{dr} \ln \mathbf{k}_\infty(r, \mathcal{E})|_{r=r_\infty}, \quad (21)$$

with

$$\mathbf{k}_\infty(r, \mathcal{E}) \equiv \sqrt{\mathbf{W}_\infty(r; \mathcal{E})} \quad \text{and} \quad \mathbf{W}_\infty(r; \mathcal{E}) \equiv \mathbf{k}^2(\mathcal{E}) - \frac{2\mu}{r} \mathbf{I}, \quad (22)$$

and to account for small differences that exist between the values of the potentials and their asymptotic counterparts at the boundary r_∞ by means of the following simple modification of the local wavenumbers:

$$\mathbf{k}_\infty(r, \mathcal{E}) \rightarrow \mathbf{k}(r, \mathcal{E}) \equiv \sqrt{\text{diag } \mathbf{W}(r; \mathcal{E})}. \quad (23)$$

The branch of the square root function is chosen to assure that $\text{Im } k_s(r_\infty, \mathcal{E})$ be negative (positive) when $r_\infty > r_s^{\text{tm}}$ ($r_\infty < r_s^{\text{tm}}$), where r_s^{tm} are the turning points $\text{Re}[\mathbf{W}_\infty(r_s^{\text{tm}}; \mathcal{E})]_{s,s} = 0$, for $s = 1, \dots, 4$. Obviously, no similar restrictions on r_∞ can be imposed when determining the eigenvalues which describe tunneling resonances (the use of the extrapolated parts of the potentials is unavoidable in these cases). Exact values of \mathbf{L}_{O^+} can thus be inserted into the asymptotic boundary condition (see Table AII in Ref. 43).

The nonlinear equation [Eq. (17)] is solved with the help of the procedure NEWT of Ref. 44. Typically large (even huge) disproportion between the real and imaginary parts of the roots (E_{res} and Γ) is an unfavorable circumstance for the procedure to work as a globally convergent one. Therefore a sufficiently good initial guess for the root sought is needed. Actually, having a good guess is much more essential for the resonance energy than for the width. Very good estimates of resonance positions deeply inside the potential wells are obtainable easily by solving a real-energy eigenvalue problem for Hamiltonian (1) with the boundary conditions $\Psi(0; E) = 0$ and $\Psi(\bar{r}; E) = 0$ and with the outer boundary \bar{r} placed close to the potential barrier maximum.

B. Perturbative quantum-mechanical methods

The standard resonance theories—the **bound-continuum configuration-mixing (CM) approach** to pre-

dissociation and ionization^{26–29} and the Feshbach⁴⁵ operator-partitioning theory—can obviously be applied to the problem of SO predissociation in CO²⁺. Thus, devising an efficient scheme which would exploit the smallness of the SO couplings is mostly a matter of adopting an appropriate partitioning of the configuration space available to the system at energies in the vicinity of predissociating levels into subspaces of bound and continuum configurations, called traditionally^{45,46} the Q and the P subspace, respectively. A well-chosen Q subspace should support reasonable zero-order approximations to the predissociating states.

At each energy in the range of interest here, $V_X^{\min} \leq E \leq V_X^{\min} + 30\,000 \text{ cm}^{-1}$ [cf. Fig. 1(a)], there are four open scattering channels allowed by Hamiltonian (1). Consequently, there are four outgoing scattering states,

$$[\mathbf{E}\mathbf{I} - \mathbf{H}(r)]\Psi^{(+)}_s(r; E) = 0 \quad \text{for } s = 1, \dots, 4, \quad (24)$$

which take asymptotically the form

$$[\Psi^{(+)}_s(r; E)]_{s'} \xrightarrow{r \rightarrow \infty} \delta_{s',s} O_s^{+*}(r; E) - O_{s'}^+(r; E) S_{s',s}(E) \quad (25)$$

for $s' = 1, \dots, 4$, with the Coulomb functions O_s^+ as defined in Eq. (15); the factor $C = \sqrt{\mu/2\pi}$ is inserted to assure the energy normalization of the states: $\langle \Psi^{(+)}_s(E) | \Psi^{(+)}_{\bar{s}}(\bar{E}) \rangle = \delta_{s,\bar{s}} \delta(E - \bar{E})$. Obviously, not all the open scattering channels are practically available for the decay of the vibrational states which are formed behind the barriers of the potentials included in \mathbf{H} . Because of the size of the barriers, the asymptotic regions of the potentials V_a and V_b are almost completely inaccessible for the decay of nearly all the states. Similarly, the X state continuum can be treated as a closed channel when describing the predissociation in the energy range well below the barrier top of V_X . Thus, in most cases of interest it is evident to which subspace, P or Q , each of the four-channel Hamiltonians $\mathbf{H}_{s,s}$ should be assigned. Moreover, the channels in the Q subspace can be made strictly closed by means of the following modification:

$$V_s(r) \rightarrow U_s(r) \equiv \begin{cases} V_s(r) & \text{for } r \leq R_s \\ V_s(R_s) \equiv V_s^m & \text{for } r > R_s \end{cases} \quad \text{and } s \in Q, \quad (26)$$

where R_s denotes the position of the barrier top of s -state potential. Summarizing, the partitioning $P+Q = \{^3\Sigma^-\} + \{X, a, b\}$ is adopted in the treatment of the vibronic states $X^3\Pi(v=0-12)$, $a^1\Sigma^+(v=0-6)$, and $b^1\Pi(v=0-6)$. For the treatment of $a^1\Sigma^+(v)$ and $b^1\Pi(v)$ states having energies above $V_X(R_X)$, the X -channel is shifted to the P subspace. Since there is no a - b coupling, one-channel subspaces $Q_1 = \{a\}$ and $Q_1 = \{b\}$, respectively, are used. Further simplification is made by neglecting the $X-^3\Sigma^-$ coupling in the P subspace.

Different choices of P and Q subspaces are obviously required for adequate perturbative treatment of states $A^3\Sigma^+(v)$ within the JP04A model. For $v \leq 4$ states, the partitioning $Q+P = \{A, b\} + \{^3\Sigma^-, X\}$ is appropriate. For higher

states, the b -channel becomes open and should be placed in the P subspace. Again, all couplings within the P subspace are neglected.

Having fixed an appropriate partitioned counterpart of Eq. (24),

$$\begin{pmatrix} \mathbf{E}\mathbf{I}_P - \mathbf{H}_{PP} & -\mathbf{H}_{PQ} \\ -\mathbf{H}_{QP} & \mathbf{E}\mathbf{I}_Q - \tilde{\mathbf{H}}_{QQ} \end{pmatrix} \begin{pmatrix} \Psi_P^{(+)} \\ \Psi_Q^{(+)} \end{pmatrix} = 0 \quad (27)$$

for $s = 1, \dots, N_P$, where N_P denotes the dimension of the P subspace and tilde indicates the block of \mathbf{H} affected by the modification (26), one derives the respective effective Hamiltonian in the Q subspace,^{45,46}

$$\mathcal{H}_Q(E) = \tilde{\mathbf{H}}_{QQ} + \mathbf{H}_{QP} \lim_{\varepsilon \rightarrow 0^+} [(E + i\varepsilon)\mathbf{I}_P - \mathbf{H}_{PP}]^{-1} \mathbf{H}_{PQ}, \quad (28)$$

from which the information on energies and widths of the predissociating states can be extracted. Generally, a search for poles of $\mathcal{G}_Q(\mathcal{E}) \equiv [\mathcal{E}\mathbf{I}_Q - \mathcal{H}_Q(\mathcal{E})]^{-1}$ in the lower half of complex energy plane is needed.⁴⁷ The smallness of the \mathbf{H}_{QP} couplings permits exploitation of the simplest, Golden rule, version of the search procedure. It consists in (i) determining bound state energies and functions of $\tilde{\mathbf{H}}_{QQ}$,

$$[E_i^{(0)}\mathbf{I}_Q - \tilde{\mathbf{H}}_{QQ}]\Phi_i = 0, \quad (29)$$

and (ii) evaluating the matrix elements $\langle \Phi_i | \mathcal{H}_Q(E) | \Phi_i \rangle \equiv \mathbf{H}_{i,i}^{\text{eff}}(E)$, which give

$$E_i \approx \text{Re } \mathbf{H}_{i,i}^{\text{eff}}(E_i^{(0)}) = E_i^{(0)} + E_i^{\text{shf}} \quad (30)$$

and

$$\Gamma_i \approx -2 \text{Im } \mathbf{H}_{i,i}^{\text{eff}}(E_i^{(0)}).$$

Step (ii) of the procedure is actually based on the additional assumption that the resonances are isolated. The majority of vibronic levels of CO²⁺ resulting from both the JCP06 and the JP04 model are indeed well separated from each other. A few coincidences are, however, seen in Fig. 1(a) and a case of even stronger near-degeneracy occurs in the JP04 model. To these cases, slightly extended version of the search procedure was applied (see Table AV in Ref. 43).

The two-potential (TP) approach of Gurvitz⁴⁸ is exploited in the part of perturbative one-channel calculations whose aim is a quantitative description of the small tunneling through the barriers of the potentials V_s for $s = X, a, b$. Following this approach, the respective Hamiltonian $\mathbf{H}_{s,s}(r)$, denoted here by $H = K + V$, is split into zero-order part and a perturbation, $H = H^{(0)} + W$, by choosing $W = V - U \equiv \tilde{W} - V^m$ with U and V^m defined in Eq. (26). Thus, $W(r) = 0$ for $r \leq R$ and $\tilde{W}(r)$ is identical with the full potential $V(r)$ on the outer side of its barrier ($r \geq R$). If $E_v^{(0)}$ is a discrete eigenvalue of $H^{(0)}$ and Φ_v is the corresponding eigenfunction, then the energy shift $E_v - E_v^{(0)} = E_v^{\text{shf}}$ to a nearby metastable state of H and the width of the state are obtained from the following formula:

$$\Gamma_v^{\text{shf}} - i\frac{1}{2}\Gamma_v \approx \langle \Phi_v | W \Phi_v \rangle + \langle \Phi_v | W G_W^{(+)}(E_v^{(0)}) W \Phi_v \rangle, \quad (31)$$

where $G_W^{(+)}(E) \equiv [E + i0^+ - K - \tilde{W}]^{-1}$. The adequacy of this formula relies on the smallness of overlapping in the outer region between the function $\Phi_v(r)$ and functions representing continuum states of $K + \tilde{W}$ at energies near $E_v^{(0)}$, especially when $E_v^{(0)} \ll V^m$.

In the numerical implementation of both the CM and TP approaches, use is made of the generalized log-derivative method for the evaluation of second-order transition amplitudes⁴⁹ (see Ref. 50 for previous applications of the method).

C. Semiclassical methods

Whereas the above quantum-mechanical methods are chosen for their expected ability to give accurate results for all the metastable states of the CO²⁺ ion within the considered models, use of semiclassical (SC) methods is made to assist discussion of the results. Strictly, the well-known analytical expressions of the SC theory of predissociation by curve crossing,⁵¹ for widths and shifts⁵² of energy levels in a well of potential V_1 due to weak coupling V_{12} with a repulsive potential V_2 , are applied here to seven pairs of crossing potentials: $V_s - V_{3\Sigma^-}$ for $s = X, a, b, A$, $V_A - V_X$, $V_a - V_X$, and $V_A - V_b$. The two latter crossings are describable by these expressions when the barriers in the potentials V_X and V_b can be neglected, i.e., in cases of the states $a^1\Sigma^+v \geq 7$ and $A^1\Sigma^+v \geq 5$, respectively. Generally, the expressions involve a number of phase integrals with the wavenumber functions $k_i(r, E) = [(2\mu/\hbar^2)(E - V_i(r))]^{1/2}$ for $i = 1, 2$ over intervals which are determined by the classical turning points r_1 and $r_2 (> r_1)$ in the potential V_1 , the turning point r_3 in the potential V_2 , $k_2(r_3, E) = 0$, and the crossing point r_c , $V_1(r_c) = V_2(r_c)$. For concreteness in the discussion, the essential factors of the expression for the width should be listed here,

$$\Gamma_v = \hbar T_v^{-1} P_v^{\text{LZ}} P_v \equiv \Gamma_v^0 P_v. \quad (32)$$

These are (i) the vibrational period $T_v = 2\hbar(d/dE)\alpha|_{E=E_v^{\text{BS}}}$ being related to the phase integral $\alpha(E) = \int_{r_1}^{r_2} k_1(r, E) dr$ at energy satisfying the Bohr–Sommerfeld quantization condition, $\alpha(E_v^{\text{BS}}) = \pi(v + \frac{1}{2})$, (ii) the Landau–Zener curve-crossing transition parameter $P_v^{\text{LZ}} = 2\pi V_{12}^2(r_c) \hbar u_v(r_c) \Delta F(r_c)$ with $u_v(r_c) = \frac{\hbar}{\mu} |k_i(r_c, E_v^{\text{BS}})|$ and $\Delta F = \frac{d}{dr} V_1 - \frac{d}{dr} V_2$, and (iii) the factor $P_v = P[\xi(E_v^{\text{BS}})]$ involving the Airy function, $P(\xi) = 4\pi\sqrt{|\xi|} Ai^2(-\xi)$. The quantity ξ is negative at energies below $V_i(r_c)$, where it is defined as $\xi(E) = -[\frac{3}{2}\Delta\phi(E)]^{2/3}$ with $\Delta\phi(E) = \int_{r_2}^{r_c} |k_1(r, E)| dr + \int_{r_c}^{r_3} |k_2(r, E)| dr$ if $r_2 < r_c < r_3$ (the outer crossing).

The formulas of the SC theory of shape resonances^{53,54} are also exploited in the present study. The primary goal is to provide a reference for an assessment of usefulness of the TP approach.

IV. RESULTS AND DISCUSSION

Results of calculations performed in this work are presented in Figs. 1(b) and 3–8 and in Tables I–VIII of this

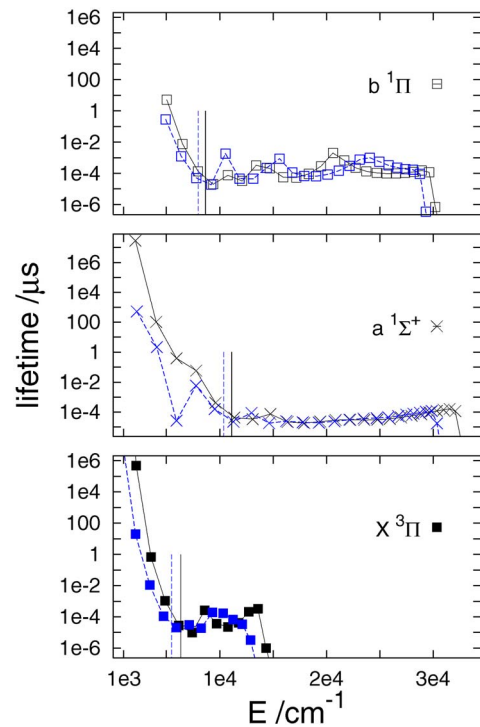


FIG. 3. (Color online) Comparison of energies and lifetimes of vibronic states of CO²⁺ from the JCP06 and JP04 models (blue dashed lines). The vertical lines mark energies at crossings of the JCP06 and JP04 potentials of the $3\Sigma^-$ state. The lowest vibrational level shown in the bottom panel is $v = 1$. The peak of the dashed curve in the middle panel is a manifestation of accidental degeneracy between the $a^1\Sigma^+(v=2)$ and $X^3\Pi(v=4)$ states in the JP04 model (see Table AV in Ref. 43).

paper and in Figs. A2–A10 and Tables AIII–AXIII of the supplementary material.⁴³ This material permits a discussion of the following subjects:

- (1) overall picture of metastable vibronic states of the CO²⁺ ion emerging from the (purely vibronic) model of dynamics in which the vibrational motion of the nuclei is governed by four (of five) lowest electronic energy potentials coupled by (off-diagonal) SO interactions,
- (2) sensitivity of lifetimes of the states to features (accuracy) of the electronic structure input to the model,
- (3) comparison of the best available potentials and couplings^{9,23,24} with respect to their ability to reproduce the existing experimental data^{9,11–14} for lifetimes of vibronic states of the ¹³C¹⁶O²⁺ and ¹²C¹⁶O²⁺ ions,
- (4) impact of rotational motion of nuclei on lifetimes of the ion, and
- (5) efficient determination in quantum-mechanical calculations of long and ultra-long lifetimes.

A. Vibronic states

1. Qualitative description

As shown in Fig. 1(b), there are 12+24+23 vibrational states of the CO²⁺ ion bound by the $X^3\Pi$, $a^1\Sigma^+$, and $b^1\Pi$ potentials, respectively, which are characterized by lifetimes longer than 1 ps. The corresponding JP04 potentials give one state less of the same property (12+23+23). The potential

TABLE I. Energies and widths (all in cm^{-1}) of $X^3\Pi(v)$ states of CO^{2+} from the JCP06 model. Comparison of four-channel SQ results with results obtained within the perturbative CM approach. Entries in lower lines concern $^{13}\text{C}^{16}\text{O}^{2+}$.

v	E^a	Γ	$E^{\text{shf } b}$	$\delta E^{\text{shf } c}$	$\delta\Gamma^d$
0	732.20 ^e	1.48(-24)	-0.022	0.0	-0.9
	716.0	3.23(-25)			
1	2 168.28	1.10(-11)	-0.033	0.0	-1.0
	2 123.5	2.54(-12)			
2	3 548.53	7.70(-6)	-0.046	0.0	-0.2
3	4 883.30	4.97(-3)	-0.082	0.0	-0.1
4	6 167.37	1.88(-1)	-0.168	0.0	-0.0
5	7 399.92	5.43(-1)	0.061	0.0	0.0
6	8 578.88	2.00(-2)	0.012	-0.1	0.0
7	9 702.94	1.43(-1)	0.125	-0.0	-0.1
8	10 769.09	2.33(-1)	0.052	0.5	0.0
9	11 774.63	1.29(-1)	0.004	-1.1	0.0
10	12 713.96	2.51(-2)	0.022	0.9	-0.0
11	13 577.11	1.61(-2)	f		
12	14 335.42	5.31	f		

^aZero of energy is at V_X^{min} .

^bEvaluated within the CM approach.

^cDefined as $[E^{\text{shf}}/(E-E^{(0)})-1]\times 100\%$, where $E^{(0)}$ denotes energy of related bound state in the Q subspace.

^dDefined as $[\Gamma^{\text{CM}}/\Gamma-1]\times 100\%$.

^eThe level lies (presumably) 41.229 eV above the energy of the $X^1\Sigma^+(v=0, J=0)$ state of CO. The value listed in Table I of Ref. 24 contains evidently a typographical error.

^fThe state decays by tunneling. Present choice of P and Q subspaces is inadequate. See Tables VIII and AXII-AXIII for results of a perturbative treatment of tunneling.

$A^3\Sigma^+$ has 16 vibrational states that live longer than 1 ps, five of which lie at energies below the top of the $b^1\Pi$ state potential barrier. The variation in energy of the lifetimes of vibrational levels of the $X^3\Pi(v)$, $a^1\Sigma^+(v)$, and $b^1\Pi(v)$ states exhibits features which are typical of the two decay mechanisms involved. The short lifetimes of the two levels closest to the barrier tops of the bounding potentials are certainly caused by the tunneling mechanism. The other parts of the curves drawn in the figure are determined by the SO couplings and the potential crossings, mostly by the outer (c^+

type⁵⁵) crossings with the repulsive $^3\Sigma^-$ potential. There are parts of rapid increase of lifetimes of levels which depart from the crossing points toward lower energies and characteristic oscillatory parts above these points. The smoother shape of the curve $a^1\Sigma^+$ (of its vertical fragment) testifies on involvement of another type of crossing, which is the one between the $a^1\Sigma^+$ and $X^3\Pi$ potentials (a c^i crossing⁵⁵). The feature of nonuniformness seen in the lower part of this curve, at $v=3$, should be attributed to the change of the pathway of transition to the repulsive state, from indirect (via the

TABLE II. Energies and widths (all in cm^{-1}) of $a^1\Sigma^+(v)$ and $b^1\Pi(v)$ states of CO^{2+} from the JCP06 model. Comparison of the SQ results with results obtained within the perturbative CM approach.

v	$a^1\Sigma^+$					$b^1\Pi$				
	E^a	Γ	$E^{\text{shf } b}$	$\delta E^{\text{shf } c}$	$\delta\Gamma^d$	E^a	Γ	$E^{\text{shf } b}$	$\delta E^{\text{shf } c}$	$\delta\Gamma^d$
0	2101.82	1.85(-13)	-0.008	0.0	-1.2	5030.78	1.04(-6)	-0.024	0.0	0.1
^c	2077.9	1.50(-13)				5014.1	7.27(-7)			
1	4044.63	5.06(-8)	-0.012	0.0	-0.0	6511.49	6.84(-4)	-0.037	0.0	0.1
2	5942.05	1.39(-5)	-0.015	0.0	-0.0	7959.13	3.92(-2)	-0.076	-0.0	-0.0
3	7796.46	9.40(-5)	-0.021	0.1	-0.1	9373.76	2.69(-1)	-0.051	-0.0	0.0
4	9606.04	1.28(-2)	-0.039	0.1	0.2	10755.37	6.99(-2)	0.076	-0.4	-0.0
5	11369.41	1.24(-1)	-0.056	0.1	-0.0	12103.61	1.63(-1)	0.005	-0.4	0.0
6	13084.68	1.58(-1)	0.050	-0.0	0.0	13418.66	1.62(-2)	0.002	-1.8	0.3
7	14749.49	7.22(-2)	0.046	0.3	2.6	14700.42	2.56(-2)	0.757	-0.1	-4.0
8	16362.12	2.44(-1)	0.129	-0.3	-0.1	15948.70	9.30(-2)	0.737	-0.1	-2.9
9	17919.75	2.91(-1)	0.090	-0.1	-0.2	17163.37	9.82(-2)	0.693	-0.0	-2.8
10	19419.74	2.32(-1)	0.064	0.1	0.0	18344.32	5.76(-2)	0.662	0.0	-2.7

^aZero of energy is at V_X^{min} .

^bEvaluated within the CM approach.

^cDefined as $[E^{\text{shf}}/(E-E^{(0)})-1]\times 100\%$, where $E^{(0)}$ denotes energy of related bound state in the Q subspace.

^dDefined as $[\Gamma^{\text{CM}}/\Gamma-1]\times 100\%$.

^eFor $^{13}\text{C}^{16}\text{O}^{2+}$.

TABLE III. Energies and widths (all in cm⁻¹) of lowest vibrational states of CO²⁺(A ³Σ⁺) from the JP04A model. The SQ results, E and Γ , are compared with results obtained within the perturbative CM approach. In the last two columns, the CM results are compared to SC results obtained as sums of contributions of two $A-\tilde{s}$ curve crossings with $\tilde{s}=X, {}^3\Sigma^-$ for $v=0-4$, and of the third crossing with $\tilde{s}=b$ for $v\geq 5$.

v	E^a	E^{shf}	$\delta E^{\text{shf } b}$	Γ	$\delta\Gamma^c$	$\Gamma_{v\rightarrow\tilde{s}}^{\text{CM}}/\Gamma^{\text{CM}}\times 100\%$			SC vs CM	
						$\tilde{s}={}^3\Sigma^-$	$\tilde{s}=X$	$\tilde{s}=b$	$\delta E^{\text{shf } d}$	$\delta\Gamma^d$
0	21 320.56	0.085	0.0	3.36(-4)	-0.7	46	54		-1.8	5.2 ^e
1	23 324.53	0.086	0.0	3.16(-3)	-1.5	71	29		-2.8	-4.1
2	25 275.56	0.090	0.0	4.59(-3)	-0.7	39	61		-3.5	4.1
3	27 169.47	0.091	-0.0	6.79(-3)	-0.1	7	93		-3.3	0.5
4	28 999.49	0.094	0.1	1.14(-2)	-0.9	4	96		-3.9	1.6
5	30 757.66	0.175	-0.4	1.34(-1)	-1.9	1	13	86	-1.4	0.4
6	32 438.58	0.166	-0.3	1.57(-1)	-1.8	0	16	84	-1.2	1.1

^aBecause of accuracy of the input potentials, the energies can be physically meaningful only up to ~ 0.1 cm⁻¹. The way of listing the numbers here is adjusted to the purpose of demonstrating the numerical consistency which is achieved in evaluation of the energy shifts with the SQ and CM methods.

^b $[E^{\text{shf}}/(E-E^{(0)})-1]\times 100\%$, where $E^{(0)}$ denotes energy of related bound state in the Q subspace.

^c $[\Gamma^{\text{CM}}/\Gamma-1]\times 100\%$.

^d $[X^{\text{SC}}/X^{\text{CM}}-1]\times 100\%$ for $X=E^{\text{shf}}, \Gamma$.

^eThere are some contributions to the widths $\Gamma_{v\leq 4}$, stemming from interference between the direct ($A\rightarrow{}^3\Sigma^-$ and $A\rightarrow X$) and indirect ($A\rightarrow b\rightarrow{}^3\Sigma^-$ and $A\rightarrow b\rightarrow X$) pathways of decay, which are not accounted for by the SC results (see Table AVII and Figs. A4 and A5 for a more detailed comparison of SC and CM results).

X state) to direct. In the variation in lifetimes of the seven lowest $A {}^3\Sigma^+(v)$ levels shown in the figure, two similar cases of sudden drop occur at energies just above the $A {}^3\Sigma^+-{}^3\Sigma^-$ potential crossing and above the $b {}^1\Pi$ potential barrier, respectively. The latter case signifies undoubtedly the opening of the b state as a channel of predissociation. The former stems from an interplay between predissociation to the ${}^3\Sigma^-$ and to the $X {}^3\Pi$ state. It will be demonstrated in Sec. IV C that lifetimes of the $A {}^3\Sigma^+(v\geq 2)$ states are determined by two c^- -type crossings: $A {}^3\Sigma^+-X {}^3\Pi$ and $A {}^3\Sigma^+-b {}^1\Pi$.

The lifetimes of states $X {}^3\Pi(v)$, $a {}^1\Sigma^+(v)$, and $b {}^1\Pi(v)$ that result from the JP04 model are shown separately in Fig. 3. Their energy variation is compared to the behavior of the respective lifetimes from the JCP06 model. The most striking difference exhibited is the much slower increase of the JP04 lifetimes when energy decreases below the crossing points with the repulsive potential. In cases of the two lowest energy levels shown, $a {}^1\Sigma^+(v=0)$ and $X {}^3\Pi(v=1)$, the discrepancies between the JCP06 (solid curves) and JP04 (dashed curves) lifetimes exceed four orders of magnitude. A

TABLE IV. Predissociation of vibrational states of CO²⁺(s) for $s=X {}^3\Pi$, $b {}^1\Pi$, and $a {}^1\Sigma^+$ in the two-crossing-curve description (s curve+ ${}^3\Sigma^-$). Comparison of SC results for level shifts and widths with results of two-channel SQ calculations (see Table AVI for a comparison of two- and four-channel SQ results). Comparison of different factors of SC expression for the width evaluated using the JCP06 and JP04 models.

v	JCP06						JP04				$x^{\text{JP04}}/x^{\text{JCP06}}$	
	$E^{\text{shf } a}$	$\delta E^{\text{shf } b}$	Γ^a	$\delta\Gamma^c$	Γ^0^d	ξ^e	$E^{\text{shf } a}$	$\delta E^{\text{shf } b}$	Γ^a	$\delta\Gamma^c$	$x=\Gamma^0(p^{\text{LZ}})$	$x=\xi$
$X {}^3\Pi$												
0	-2.32(-2)	-0.1	1.47(-24)	-3.6	7.63(-2)	-11.54	-2.64(-2)	-0.2	5.56(-14)	15.5 ^f	1.06(1.09)	0.66
1	-3.20(-2)	-0.3	1.24(-11)	10.6 ^f	8.55(-2)	-6.61	-3.77(-2)	-0.6	2.72(-7)	-3.5	1.08(1.11)	0.68
2	-4.70(-2)	-0.9	7.78(-6)	-2.0	1.01(-1)	-3.69	-5.91(-2)	-2.4	4.97(-4)	-1.5	1.13(1.17)	0.69
3	-8.00(-2)	-4.9	5.05(-3)	-1.1	1.34(-1)	-1.80	-1.24(-1)	-2.2	4.88(-2)	-1.0	1.33(1.39)	0.50
4	^g		1.92(-1)	-0.6	3.66(-1)	-0.21	-1.20(-1)	0.3	4.74(-1)	-0.2	0.60(0.62)	-2.54
5	6.20(-2)	-1.7	5.57(-1)	0.1	1.46(-1)	1.20	1.63(-1)	0.2	1.79(-1)	0.9	0.76(0.80)	1.56
$b {}^1\Pi$												
0	-2.28(-2)	-0.7	9.07(-7)	-7.1	4.62(-2)	-4.04	-2.60(-2)	-1.1	1.67(-5)	-6.7	1.07(1.09)	0.82
1	-3.51(-2)	-3.1	6.42(-4)	-2.6	5.87(-2)	-2.24	-4.35(-2)	-5.4	4.08(-3)	-2.4	1.14(1.17)	0.72
2	-7.64(-2)	4.1	3.76(-2)	-1.2	1.00(-1)	-0.70	^g		1.03(-1)	-1.0	2.12(2.17)	0.21
3	-4.98(-2)	1.1	2.61(-1)	-0.1	9.77(-2)	0.68	2.53(-2)	-2.6	2.74(-1)	0.3	0.74(0.75)	1.74

^aGiven in cm⁻¹.

^b $\delta E^{\text{shf}}=[E^{\text{shf}}/(E(2)-E^{(0)})-1]\times 100\%$, where $E(2)$ denotes the result of two-channel SQ calculations and $E^{(0)}$ is the energy of the related bound state in the potential U_s [cf. Eq. (26)].

^c $\delta\Gamma=[\Gamma/\Gamma(2)-1]\times 100\%$.

^dThe factor of Γ defined in Eq. (32), $\Gamma^0=\hbar/T\times p^{\text{LZ}}$.

^eThe argument of the factor $P(\xi)=\Gamma/\Gamma^0$ defined in Eq. (32). For $\xi\ll -1$, $P(\xi)\approx \exp(-\frac{4}{3}|\xi|^{3/2})$.

^fThis relatively large deviation may be connected with the fact that the classical turning point r_3 [cf. Eq. (32)], occurs in a very flat part of the curve $V_{3\Sigma^-}(r)$ [see Fig. 1(a)].

^gThe level lies too close to the crossing point (see Fig. 4). The SC formula for E^{shf} becomes inadequate (see Fig. A5 for an exposition of this problem in the case of the inner crossing $A-X$).

TABLE V. Lifetimes τ (in μs) of lowest vibronic states of CO^{2+} calculated from the JCP06, JP04, and JP04A models. Comparison with experimental data and with result calculated from potentials and couplings of Ref. 9 (denoted here as PRL93). Data in lines marked with an asterisk concern $^{13}\text{C}^{16}\text{O}^{2+}$.

Electronic state	v	Expt.	Calc.	JCP06		JP04	$\log_{10} \tau^{\text{calc}} / \tau^{\text{expt}}$		
				Ref. 24	This work	This work	PRL93	JCP06	JP04
$X^3\Pi$	0	$>10^a$	$7.2 \times 10^3^b$	>10	3.6×10^{18}	1.1×10^8			
	*	$>3.8 \times 10^6^c$	$2 \times 10^4^c$		1.6×10^{19}	3.0×10^8	[-2] ^d	[12]	[2]
	1	$>10^a$	0.17^b	>10	4.8×10^5	2.0×10^1			
	*	$800 \pm 200^{c,e}$	0.3^c		2.1×10^6	3.7×10^1	-3.4	3.4	-1.3
	2	0.2 ± 0.1^a 0.32 ± 0.22^b	$2.9 \times 10^{-4}^b$	0.61	6.9×10^{-1}	1.1×10^{-2}	-2.8	0.5	-1.3
$a^1\Sigma^+$	3-10	$<0.05^f$		$\leq 1.2 \times 10^{-3}$	$\leq 1.1 \times 10^{-3}$	$\leq 2.0 \times 10^{-4}$			
	0	$>10^a$	0.78^b	>10	2.9×10^7	5.1×10^2			
	*	$6000 \pm 2000^{c,e}$	2.0^c		3.5×10^7	1.1×10^3	-3.5	3.8	-0.7
	1	$0.67 \pm 0.05^{b,g}$ $0.7^{+0.2}_{-0.1}^a$ $0.6 \pm 0.1^{f,g}$	$8.8 \times 10^{-4}^b$	0.67^h	1.0×10^2	2.1	-2.9	2.2	0.5
	2	$<0.05^f$		0.028^h	3.8×10^{-1}	$2.6 \times 10^{-5}^i$		{+1} ^d	{-3}
$b^1\Pi$	0	0.026 ± 0.005^b $0.2^{+0.15}_{-0.2}^a$	$3 \times 10^{-3}^j$	8.3	5.1	2.8×10^{-1}		2.3	1.0
	1-10	$<0.05^f$		$\leq 2.2 \times 10^{-4}$	$\leq 7.8 \times 10^{-3}$	$\leq 1.8 \times 10^{-3}$		{-1}	{-1}
$A^3\Sigma^+$	0-2	$<0.05^f$	$<2.8 \times 10^{-1}^j$	$\leq 7.1 \times 10^{-2}^k$		$\leq 1.6 \times 10^{-2}$		{+0}	{-0}

^aReference 13.^bReference 14.^cReference 9.^dThe numbers in brackets (braces) show differences in orders of magnitude between the calculated values and the experimental lower (upper) bounds.^eAs assigned in Ref. 13.^fReference 11.^gAs assigned in Ref. 12.^hThe meaning of this number is uncertain; it seems to pertain to a significantly altered model, undocumented in Ref. 24 (see Table AVIII in the subsidiary material for a comparison of all results calculated in Ref. 24 with the present results from the JCP06 model, also from the "original JCP06" version).ⁱExceptionally small since affected by accidental degeneracy with the $X(v=4)$ state (see Fig. 3).^jDetermined in Ref. 21 from potentials generated in that work using the semiempirical value of 59 cm^{-1} for the SO coupling and the value of 1 cm^{-1} for the coupling.^kObtained in Ref. 25 with the complex-scaling method (see Table AVIII).

case of accidental degeneracy appears between the $a^1\Sigma^+(v=2)$ and $X^3\Pi(v=4)$ levels (the sudden decrease of lifetime of the former level).

In Fig. 4, the lifetimes due to coexisting SO predissociation and tunneling are compared with "pure" tunneling lifetimes. As expected, the tunneling lifetimes of low v levels attain huge values. For $v < 2$ levels, they exceed the predissociation lifetimes by about 40 orders of magnitude (in the least extreme case of the X state levels). Obviously, it is not the absolute values of these tunneling lifetimes but how sensitive they are to the differences existing between the JCP06 and JP04 potentials that are noteworthy. As seen in Fig. 1(a), the wells in the JP04 potentials are slightly shallower but their barriers are evidently lower and thinner. Though the former feature can cause some increase of lifetimes, it is the opposite effect of the latter which is overwhelming. The lifetimes of the X state levels from the JP04 potential are from two to six orders of magnitude smaller than the lifetimes from the JCP06 potential.

The two curves labeled with $\{X, a, b\}$ in Fig. 5 describe lifetimes of $a^1\Sigma^+(v=0-6)$ and $b^1\Pi(v=0-6)$ states due to SO mixing with levels formed within the X potential well and subsequent tunneling through the X potential barrier. Such a pathway of decay of these states is by far more probable than tunneling through the barriers of their own poten-

tials. Still, the corresponding lifetimes are 5–40 orders of magnitude larger than the actual lifetimes due to transition to the repulsive $^3\Sigma^-$ state. This provides a justification of the approximation of the closing of the channels in the subspace $Q = \{X, a, b\}$ mentioned in Sec. III B.

2. Quantitative description

Approximately half of the results shown in Fig. 1(b) are presented in numerical form in Tables I–III. Apart from energies and widths of the vibronic states obtained in the formally exact SQ calculations, results of the perturbative (CM) calculations are enclosed. Very good consistency of the SQ and CM results is demonstrated. In the majority of cases, relative deviations of the widths do not exceed 1%. Even smaller are the deviations between the SQ and CM values of the shifts of the energy levels from their zero-order positions in the chosen Q subspaces. Adequacy of these choices is thereby confirmed. The choice of the Q subspace is particularly important in the cases of the states $a^1\Sigma^+(v \leq 2)$, which predissociate via mixing with the $X^3\Pi(v)$ states. Namely, due to inclusion of both the X and the a channel into the Q subspace, the mixing is accounted for exactly. Therefore, the consistency of the perturbative and nonperturbative widths of the states demonstrated in Table II is so much better than that

TABLE VI. Positions (E) and widths (Γ), both in cm⁻¹, of selected rotation-vibration energy levels of CO²⁺($X^3\Pi$) from the JP04r-v model (a larger set of results from the model is presented in Tables AX and AXI using analytical representations of J dependencies of energies and widths). Data in lines marked with asterisk concern ¹³C¹⁶O²⁺. Underlined are the numbers to be used in comparison with the existing experimental data for lifetimes (cf. Fig. 8 and Table V).

		$E(^3\Pi_{\Omega^p}Jv)$				$\Gamma(^3\Pi_{\Omega^p}Jv)$					
		$\Omega=2$	$\Omega=1$	$\Omega=0$		$\Omega=2$		$\Omega=1$	$\Omega=0$		
v	J	$p=e$ ^a	e ^a	e	$e-f$	e	e/f	e	e/f	e	f
0	0			780.5	-0.5					2.91(-13)	7.00(-56) ^b
	1		719.0	784.0	-0.3			4.95(-14)	1.006	1.51(-13)	3.62(-16)
*	1		703.1	768.1	-0.3			1.86(-14)	1.006	5.91(-14)	1.30(-16)
	2	655.5	725.2	790.6	-0.3	5.85(-17)	1.009	5.28(-14)	1.019	1.59(-13)	1.14(-15)
	6	709.3	781.4	849.6	-0.2	9.68(-16)	1.061	9.31(-14)	1.133	2.60(-12)	1.26(-14)
*	6	691.2	762.8	830.7	-0.2	3.24(-16) ^c	1.058	3.49(-14)	1.125	1.02(-13)	4.57(-15)
*	7	711.3	783.6	852.5	-0.2	5.31(-16) ^c	1.076	4.32(-14)	1.166	1.23(-13)	7.25(-15)
1	0			2161.2	-8.5 ^d					6.15(-7)	8.64(-48) ^b
	1		2107.5	2168.4	-4.5			2.79(-7)	1.003	3.36(-7)	8.54(-10)
*	1		2062.0	2124.2	-3.1			1.50(-7)	1.003	1.93(-7)	4.27(-10)
	2	2044.0	2113.6	2174.9	-4.4	7.73(-10)	1.004	2.82(-7)	1.010	3.41(-7)	2.57(-9)
	6	2096.9	2168.7	2233.4	-3.8	8.23(-9)	1.024	3.13(-7)	1.070	3.89(-7)	1.89(-8)
*	6	2049.2	2120.5	2185.9	-2.7	4.05(-9) ^e	1.023	1.69(-7)	1.066	2.20(-7)	9.52(-9)
*	7	2068.9	2141.0	2207.5	-2.6	5.61(-9) ^e	1.030	1.76(-7)	1.087	2.30(-7)	1.30(-8)
2	0			3504.0	-0.1					1.18(-3)	1.29(-40) ^b
	1		3442.0	3507.3	0.0			4.97(-4)	1.003	5.90(-4)	1.28(-6)
	2	3378.5	3448.0	3513.6	0.0	1.53(-6)	1.003	4.99(-4)	1.008	5.94(-4)	3.83(-6)
	6	3430.4	3502.0	3570.2	0.0	1.54(-5) ^f	1.018	5.20(-4)	1.059	6.28(-4)	2.66(-5)
	7	3450.5	3523.0	3592.2	0.0	2.08(-5) ^f	1.023	5.28(-4)	1.078	6.42(-4)	3.54(-5)

^aEnergies of the corresponding f parity states are higher at most by 0.1 cm⁻¹ (for the $J=6,7$ cases).

^bThe f parity $J=\Omega=0$ states cannot predissociate by the SO coupling with the $^3\Sigma^-$ state. The widths describe tunneling through the barrier of $V_X(r) + 1/2\mu r^2$.

^cBasing on these values, the lifetime of the ground vibronic state of ¹³C¹⁶O²⁺ can be predicted to be of the size of 3–4 h instead of $\tau=5$ min, predicted by the JP04 model.

^dThese relatively large differences arise because the levels $X^3\Pi_0(Jv=1)$ of e parity are perturbed by the nearby levels $a^1\Sigma^+(Jv=0)$.

^eThe corresponding lifetimes, $\tau=1311$ and 946 μ s, should be compared with the experimental value $\tau^{\text{expt}}=800 \pm 200$ μ s.

^fThe corresponding lifetimes, 0.34 and 0.26 μ s, are to compare with $\tau^{\text{expt}}=0.32 \pm 0.22$ or 0.2 ± 0.1 μ s.

achieved in the previous calculations^{9,14} on the ion. As shown in Table II of Ref. 14, the lifetimes of the states $a^1\Sigma^+(v=0)$ and ($v=1$) (of ¹³C¹⁶O²⁺) obtained in calculations that treated as perturbations both the $a-X$ mixing and the $X-^3\Sigma^-$ coupling deviate from the nonperturbative results of Ref. 9 by 59% and 40%, respectively. The additional approximation of the present implementation of the CM approach, which is the neglect of couplings in the P subspaces, deteriorates slightly the consistency of the CM and SQ results for v levels lying above the lowest barrier, especially for the levels bound to the state $b^1\Pi$. The deviations of the widths of these levels are of the size of several percent (3% in most cases). As a whole, the contents of Tables I–III are believed to provide a convincing demonstration that good numerical accuracy has been achieved in the present calculations with the chosen quantum-mechanical methods.

B. Perturbative analysis of predissociation

Apart from confirming numerical reliability of the SQ results for very small widths, $\Gamma \ll 10^{-8}$ cm⁻¹ (see Sec. IV E), the perturbative calculations of this work have provided quite a detailed insight into dynamics of predissociation of the CO²⁺ ion. First of all, the CM formulas (30) allow for explicit resolutions of the level shifts and widths into parts

which describe three distinct paths of bound-continuum mixing, labeled “direct,” “indirect,” and “interference” [see Eqs. (A1)–(A3) in Ref. 43]. Such resolutions have been made for about 25 lowest sv states. The main fact revealed is (see Fig. A2) that the predissociation dynamics of the ion is actually very simple. The states $b^1\Pi(v=0-6)$ decay almost entirely along the direct pathway; the relations $92 < \Gamma(\text{dir})/\Gamma < 99.5\%$ and $\Gamma(\text{indir})/\Gamma < 0.2\%$ are found. The decay of the states $X^3\Pi(v=0-10)$ is not much different. For most of them, $\Gamma(\text{dir})/\Gamma \approx 103\%$ and $\Gamma(\text{interf})/\Gamma \approx -3\%$. Only the three lowest $a^1\Sigma^+$ state levels, $v=0-2$, appear to predissociate indirectly.

Because of the dominant role of the direct predissociation pathway, it is natural to expect that the widths $\Gamma_{sv \rightarrow \tilde{s}}$ of the majority of sv states of the ion can be reasonably accurately determined in two-channel calculations, including only the channels s and \tilde{s} . This expectation is essentially confirmed (in Table AVI) by a comparison of results of two- and four-channel SQ calculations for several sv states in the energy range below the barrier top of V_X . In most cases, the deviations $|\Gamma(2)/\Gamma(4)-1| \times 100\%$ are well below 10%. Exceptions are obviously the cases $a(v=0-2)$ and cases of strong perturbations (especially in the JP04 model).

Most of the results of two-channel quantum-mechanical calculations appear well reproducible in a semi-analytical

TABLE VII. Energies and widths (both in cm^{-1}) of selected rotation-vibration states of $\text{CO}^{2+}(A^3\Sigma^+)$ from the JP04r-v model.

ν	N	$E(F_i N \nu)^a$			$\Gamma(F_i N \nu)^a$			
		F_1^b	F_1^c	$[F_1]^d$	F_2	$[F_2]^d$	F_3^c	$[F_3]^d$
0	0	21 320.5	2.95(-4)	2.40(-4)				
	1	21 324.3	2.85(-4)	1.97(-4)	3.43(-4)	3.47(-4)	3.91(-4)	3.91(-4)
	2	21 331.9	2.82(-4)	1.69(-4)	3.44(-4)	3.61(-4)	2.50(-4)	3.16(-4)
	3	21 343.3	2.80(-4)	1.49(-4)	3.44(-4)	3.83(-4)	2.59(-4)	3.86(-4)
	4	21 358.5	2.79(-4)	1.38(-4)	3.46(-4)	4.11(-4)	2.63(-4)	4.56(-4)
	5	21 377.5	2.78(-4)	1.34(-4)	3.47(-4)	4.47(-4)	2.64(-4)	5.31(-4)
1	0	23 324.5	2.48(-3)	2.19(-3)				
	1	23 328.2	2.34(-3)	1.88(-3)	3.21(-3)	3.23(-3)	1.97(-3)	1.97(-3)
	2	23 335.7	2.28(-3)	1.69(-3)	3.21(-3)	3.30(-3)	1.77(-3)	2.11(-3)
	3	23 347.0	2.25(-3)	1.56(-3)	3.21(-3)	3.41(-3)	1.91(-3)	2.57(-3)
	4	23 361.9	2.22(-3)	1.49(-3)	3.21(-3)	3.55(-3)	1.97(-3)	2.97(-3)

^a $(F_1 N) \equiv (\Omega^p = 1^l J = N + 1)$, $(F_2 N) \equiv (\Omega^p = 1^c J = N)$, and $(F_3 N) \equiv (\Omega^p = 0^l J = N - 1)$.

^bThe energies are nearly degenerate in the model. A small splitting arises only due to the different SO couplings of the $^3\Sigma_{1e}$, $^3\Sigma_{1f}$, and $^3\Sigma_{0f}$ components with the lower electronic states. The separations $E(F_2) - [E(F_1) + E(F_3)]/2$ and $E(F_3) - E(F_1)$ are of the order of 0.05 cm^{-1} .

^cThese widths may change if second-order SO and spin-spin interactions are included. Assuming that the resulting splitting $E(^3\Sigma_1) - E(^3\Sigma_0)$ is of the size of $\pm 6 \text{ cm}^{-1}$, the widths are found to change at most by $\pm 35\%$.

^dResults obtained after the inclusion into the JP04r-v model of the (artificial) L-uncoupling perturbations specified in the text [Eq. (9)]. The perturbations affect slightly the near degeneracy of F_i components; the energy splitting $E(F_3) - E(F_1)$ grows with N , assuming values close to 0.2 cm^{-1} for $N=6$.

way by evaluations of the SC formulas for level shifts and widths due to curve crossing. Thus, advantages can be taken of the fact that the SC formulas explicitly show how the predissociation characteristics are linked to the particular potentials and couplings.

First of all, one can precisely describe the origin of the widths of the lowest $X\nu$ states from the JCP06 model deviating so much from their JP04 counterparts, by ten orders of

magnitude in the $\nu=0$ case. This is made in Table IV by comparing separately the particular factors of the SC expression for the width, Γ_ν^0 , P_ν^{LZ} , and $\xi(E_\nu^{\text{BS}})$ [cf. Eq. (32)]. For levels with $\xi \ll -1$, the factor $P_\nu = \Gamma_\nu / \Gamma_\nu^0$ acquires the meaning of the probability of tunneling through the effective barrier formed by the crossing potentials; it depends exponentially on the phase integral $-2\Delta\phi(E_\nu^{\text{BS}})$. The large differences in values of this integral (or ξ) obtained from the two mod-

TABLE VIII. Tunneling widths of selected vibrational states of $\text{CO}^{2+}(X^3\Pi)$ from the JCP06 model. Comparison of results obtained for the widths and energies of the states with various methods: SQ, perturbative (TP), SC, and combined quantum-semiclassical (qTP, qSC).

ν	Γ^a cm^{-1}	$\delta\Gamma(x/y)^b$				E^a	$\Delta E(x-y)^c$		
		TP/SQ	qTP ^d /SQ	qSC ^e /SQ	SC ^f /SQ		SQ-TP	SQ-qTP ^g	SQ-SC ^h
0	6.05(-62)	-0.0000	-0.18	-0.10[-7.0]	0.05	733.31	-1(-7) ⁱ	-1(-7) ⁱ	-0.11
1	2.42(-53)	0.0000	-0.15	-0.03[-2.7]	0.07	2165.46	-2(-7)	-2(-7)	-0.08
2	1.09(-45)	0.0000	-0.27	-0.09[-1.7]	-0.05	3549.42	1(-7)	1(-7)	-0.03
3	8.48(-39)	-0.0000	-0.28	-0.11[-1.3]	-0.13	4884.09	4(-8)	4(-8)	0.02
7	4.34(-17)	-0.0002	-0.83	-0.67[-1.2]	-0.98	9703.47	-2(-6) ⁱ	-2(-6) ⁱ	0.33
9	5.10(-9)	0.0012	-1.17	-1.15[-1.5]	-1.56	11775.28	-3(-6)	-5(-6)	0.49
10	1.41(-5)	-0.0063	-1.35	-1.43[-1.7]	-1.84	12714.64	-2(-6)	-3(-4)	0.51
11	1.54(-2)	-0.0397	-1.35	-1.67[-1.7]	-1.98	13577.63	-1(-5)	-3(-2)	0.40
12	5.30	0.5260	0.57	0.49[2.7]	0.59	14335.93	-4(-2)	-1.06	-0.11

^aResults of SQ calculations using one-channel Hamiltonian \mathbf{H}_{XX} of Eq. (1).

^bDefined as $[\Gamma^x/\Gamma^y - 1] \times 100\%$ with x and y denoting the method.

^c $E^x - E^y$ in cm^{-1} .

^d Γ_ν^{qTP} is evaluated in the quasiclassical limit of the TP approach which is described in Gurvitz's paper (Ref. 48).

^e $\Gamma_\nu^{\text{qSC}} \equiv \Gamma_\nu^{\text{SC}}(E_\nu^{\text{SQ}})$, where E_ν^{SQ} is the energy shown in the column "E". The number in brackets is the width obtained by evaluation of the Gamow formula at the energy E_ν^{SQ} .

^f Γ_ν^{SC} is evaluated according to Eqs. (4.5) and (4.6) of Ref. 53. Applied is also the correction of Ref. 54.

^g $E_\nu^{\text{qTP}} = E_\nu^{(0)}$, where $E_\nu^{(0)}$ is the exact energy level in the potential U [cf. Eqs. (26) and (31)].

^h E_ν^{qSC} is obtained from the generalized Bohr-Sommerfeld quantization condition [Eq. (4.2) of Ref. 53].

ⁱThe differences $E_\nu^{\text{TP}} - E_\nu^{\text{qTP}}$, evaluated according to Eq. (31), range from -5×10^{-30} for $\nu=0$ to $-10^{-10} \text{ cm}^{-1}$ for $\nu=7$ and are thus definitely smaller than the errors of the energies $\text{Re } \mathcal{E}_\nu$ and $E_\nu^{(0)}$ determined in double-precision calculations (Ref. 43). Consequently, the deviations $\Delta E(\text{SQ}-y)$ for y-TP, qTP can be informative only when $|E_\nu^{\text{sh}}| \ll 10^{-8} \text{ cm}^{-1}$, here, in the $\nu \geq 9$ cases.

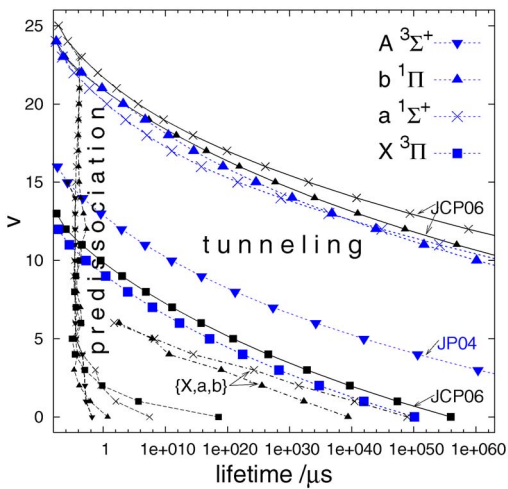


FIG. 4. (Color online) Comparison of lifetimes of vibronic states of CO²⁺ due to predissociation and tunneling. The four predissociation curves are those described in Fig. 1. The two lowest horizontally oriented (dash-dotted) curves represent results of three-channel calculations in the subspace $\{X, a, b\}$; they give lifetimes of the $a^1\Sigma^+(v=0-6)$ and $b^1\Pi(v=0-6)$ states due to transition to the well and subsequent tunneling through the barrier of the $X^3\Pi$ state potential. The other curves describe “pure” tunneling lifetimes; they are results of one-channel calculations using the particular potentials of the JCP06 and of the JP04 (larger blue symbols) models.

els, especially for the states $X(v=0-1)$, are evidently caused by the different falloffs of the respective potentials $V_{3\Sigma^-}(r)$ in the region right to the crossings with the bounding potentials; the effective barriers are much wider in the JCP06 model [see Fig. 1(a)]. The differences in the factors $\Gamma_v^{(0)}$ of the widths shown in the 12th column of Table IV are too small to contribute to the largest discrepancies $\Gamma_v^{JP04}/\Gamma_v^{JCP06}$; they become, however, significant for v levels near the crossing points. These differences stem mostly from the fact that the crossings $V_s - V_{3\Sigma^-}$ occur in the JCP06 model at higher energies relative to the minima of the potentials V_s .

The presentation of the SC results in Table IV is confined to the lowest sv states, up to the first ones above the crossings $s - ^3\Sigma^-$ for $s = X^3\Pi$, and $b^1\Pi$, and stresses sensitivity of the widths to the medium-range behavior of the repulsive potential. Figures 5 and 6 concern all the states $a^1\Sigma^+(v)$ and $b^1\Pi(v)$ that decay by predissociation and expose the presence of two open decay channels $\bar{s} = ^3\Sigma^-$ and $X^3\Pi$ for states with $v > 6$, lying above the crossings.

Figure 5 presents the level shifts yielded by the SC formula of Ref. 52 together with results of the quantum-mechanical CM calculations. Consistency of the two kinds of results is comparable to that demonstrated in Table IV. It can be thus deduced from the bottom panel of the figure that the energy shifts $E_{av} - E_{av}^{(0)}(Q_1 = \{a\})$ for $v > 6$ are, to a very good approximation, sums of two separate shifts caused by the crossings of the a state potential with the potential $V_{3\Sigma^-}$ and V_X , respectively. The shift due to the crossing $V_a - V_{3\Sigma^-}$ prevails for levels with $v > 12$. The growth with v of this shift starting at $v = 12$ resembles the variation in r of the coupling $a - ^3\Sigma^-$ (cf. Fig. 2). As a matter of fact, the shifts of the levels $av \geq 12$ displayed in Fig. 5 are the main effect of this SO coupling, the largest in the system. Dissimilarly to the a state case, the crossing $V_b - V_{3\Sigma^-}$ and the respective SO coupling

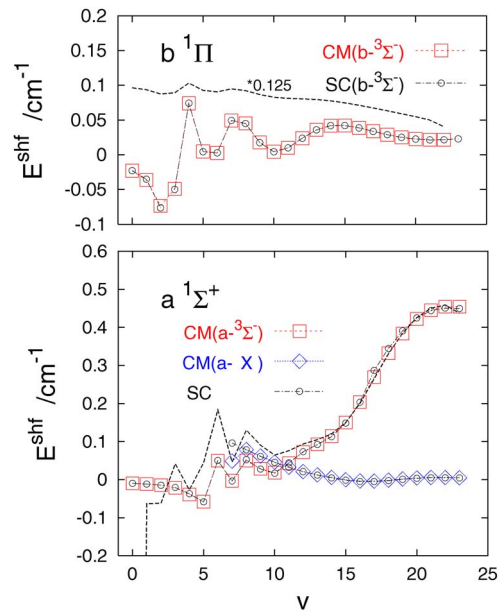


FIG. 5. (Color online) Energy shifts of $b^1\Pi(v)$ and $a^1\Sigma^+$ states of CO²⁺ due to the curve crossings $V_b - V_{3\Sigma^-}$, $V_a - V_{3\Sigma^-}$, and $V_a - V_X$ in the JCP06 model. CM($s - \bar{s}$)—results of the perturbative quantum-mechanical calculations with the subspaces $Q_1 = \{s\}$ and $P = \{\bar{s}\}$. SC($s - \bar{s}$)—results of evaluation of the SC formulas given in Ref. 52 (see also Fig. A5 in Ref. 43). The dashed lines (without symbols) denote the exact shifts $E_{sv} - E_{sv}^{(0)}$ between energies obtained in the four-channel Siegert quantization calculations and the corresponding bound state energies in the subspaces $Q_1 = \{s\}$ for $s = b$ and $s = a$, respectively. Note that these shifts are diminished eight times in the upper panel. The oscillations of the dashed line in the lower panel reflect the $a - X$ level mixing.

make only small contributions to the shifts $E_{bv} - E_{bv}^{(0)}(Q_1 = \{b\})$, as shown in the upper panel of the figure. These shifts stem mostly from the $b - X$ interaction. It is not only the strength of this interaction (the second largest in the system) that is important here. The configuration of the potentials $V_b(r)$ and $V_X(r)$ (nearly parallel in the short-range parts) is also a favorable circumstance.

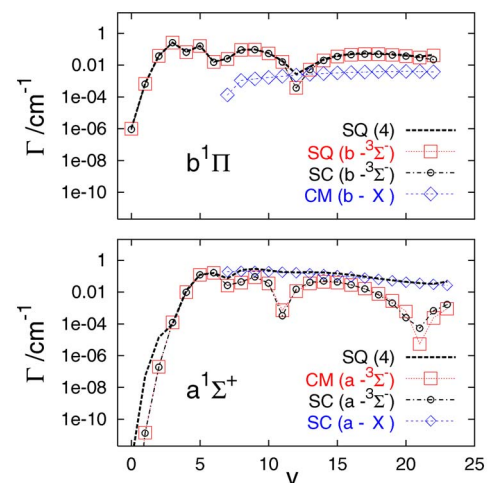


FIG. 6. (Color online) Widths of $b^1\Pi(v)$ and $a^1\Sigma^+(v)$ states of CO²⁺ from the JCP06 model. SQ—the “exact” four-channel Siegert quantization results for the total widths Γ_{sv} for $s = b, a$. SQ($s - \bar{s}$) and CM($s - \bar{s}$)—results of two-channel exact and perturbative quantum-mechanical calculations giving the partial widths $\Gamma_{sv \rightarrow \bar{s}}$. SC($s - \bar{s}$)—semiclassical results.

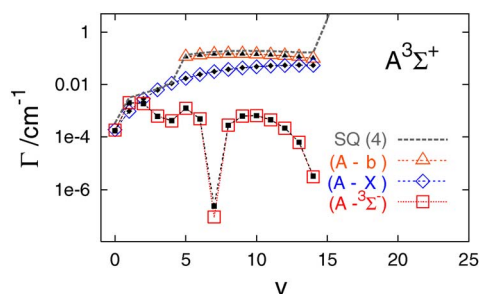


FIG. 7. (Color online) Widths of $A^3\Sigma^+(v)$ states of CO_2^+ from the JP04A model. SQ(4) denotes the “exact” total widths Γ_{Av} obtained in four-channel Siegert quantization calculations. The open (color) symbols represent partial widths $\Gamma_{Av\rightarrow\tilde{s}}$ for $\tilde{s}=\tilde{3}\Sigma^-, X^3\Pi$, and $b^1\Pi$ obtained in two-channel CM calculations using $Q_1=\{A\}$ and $P=\{\tilde{s}\}$. The small full symbols show results of application of the SC formula(32) to the $A-\tilde{s}$ curve crossings.

Figure 6 provides the corresponding information on the widths of the states $a(v=0-23)$ and $b(v=0-22)$. Like the energy shifts, the total widths of the a state levels with $v > 6$ are well approximated by sums of SC results for the curve crossings $V_a-V_{3\Sigma^-}$ and V_a-V_X . Unlike the shifts E_{av}^{shf} , however, the widths $\Gamma_{av>6}$ are dominated by contributions of the latter crossing. The probability of decay into the X channel, $\Gamma_{av\rightarrow X}/\Gamma_{av}$, ranges from about 70% for $v=6, 14-16$ to nearly 100% for $v=11, 21$. The relations between the partial widths $\Gamma_{av\rightarrow 3\Sigma^-}$ and $\Gamma_{av\rightarrow X}$ and their distinct dependencies on v number can be rationalized with the help of the analytical representation [Eq. (32)] (see Ref. 43, Fig. A3, for some comments on this matter).

The upper panel of Fig. 6 displays that the SO coupling between the crossing potentials V_b and $V_{3\Sigma^-}$ produces much larger widths than the coupling between the noncrossing potentials V_b and V_X . This is in contrast to the relative role of these couplings in producing the shifts E_{bv}^{shf} seen in Fig. 5.

Figure 7 together with Figs. A4 and A5 summarize results of all calculations (SQ, CM, and SC) which have been done for the states $A^3\Sigma^+(v=0-14)$ using the JP04A model. The results of SC calculations of the widths are shown to agree well with the quantum-mechanical results for all the states. The agreement of the energy shifts is equally good in the $v \leq 6$ cases; relative deviations do not exceed $\pm 6\%$ (see the last two columns of Table III). A difficulty arose in applying the SC formulas to energy shifts of higher states, with $v \geq 8$. Details are described in the comment to Fig. A5. Undoubtedly, all $A^3\Sigma^+(v)$ states predissociate almost entirely along direct path. Both their predissociation characteristics E_v^{shf} and Γ_v are sums of contributions of two or three $A-\tilde{s}$ curve crossings, with $\tilde{s}=\tilde{3}\Sigma^-, X^3\Pi$, and $b^1\Pi$. The most important observation to make is the relatively small role of the crossing with the repulsive curve. Even states $v=0$ and $v=1$, the closest in energy to the $A-\tilde{3}\Sigma^-$ crossing, decay only in 50% and 70%, respectively, to the $\tilde{3}\Sigma^-$ channel. The probabilities of decay of these states into the X channel are big despite the fact that the $A-X$ crossing lies so much higher, between levels E_{13} and E_{14} . The reasons are the smallness of the coupling $A-\tilde{3}\Sigma^-$ see (Fig. 2) and the inner type of the $A-X$ crossing (slow increase of $|\xi(E)|$ with E decreasing below the crossing, see Fig. A4).

C. Comparison with experiment

As stated in Sec. I, the question of primary interest in the present study is what progress in converging the theoretical simulations to the measured lifetimes of the CO_2^+ ion has become possible due to the potentials and couplings of the JCP06 and the JP04 models as compared to the previously available electronic structure data.⁹ The previous data are called hereafter the PRL93 model. Material concerning this question is collected in Table V.

There are listed the well-established experimental results for lifetimes of the $^{12}\text{C}^{16}\text{O}_2^+$ ion in three of its vibronic states: $X^3\Pi(v=2)$, $a^1\Sigma^+(v=1)$, and $b^1\Pi(v=0)$. The JCP06 model is seen to reproduce very well the result for the $X^3\Pi(v=2)$ state. The calculated value is larger only by the factor of ~ 3 . For the other two states, the lifetimes calculated from the model exceed the experimental data by about two orders of magnitude. There are also listed the two lifetimes measured in the millisecond range⁹ that pertain most likely to the $X^3\Pi(v=1)$ and $a^1\Sigma^+(v=0)$ states¹³ of the $^{13}\text{C}^{16}\text{O}_2^+$ isotopomer. For these states, the JCP06 model yields results more than three orders of magnitude too large. In the most stable ground state, $X^3\Pi(v=0)$, the ion lives longer than 1 s, according to the experimentally established⁹ lower bound for $^{13}\text{C}^{16}\text{O}_2^+$. The JCP06 model fails in predicting the actual lifetime of this state, giving practically worthless value of $\sim 10^{13}$ s. As to lifetimes of higher excited states of the ion, there is an upper bound (50 ns) available from the experimental work of Ref. 11. Somewhat higher value (100 ns) was given in Ref. 13. The lifetimes calculated from the JCP06 model are consistent with these estimations except for the case of state $a^1\Sigma^+(v=2)$ (for which $\tau=380$ ns is obtained).

The values of $\tau^{\text{Cal}}/\tau^{\text{Exp}}$ listed in the last three columns of Table V for τ 's calculated from the PRL93, JCP06, and JP04 models, respectively, should be summarized as follows. The JCP06 model improves over the PRL93 model in that it gives lifetimes too long by factors ranging from ~ 3 to about 6000 (if the bracketed numbers are not taken into account!), while the PRL93 lifetimes are all too short, on average, 1800 times. The improvement may thus seem somewhat problematic. The JP04 model, however, is evidently better than the other two; the lifetimes resulting from it are only one (at worst, one and one third) order of magnitude off the experimental values.

Consistency with the experimental upper bound of the lifetimes of the states $A^3\Sigma^+(v=0-2)$ calculated from the JP04A model is also noteworthy. Previously, an estimation of the partial width of the lowest A state level for decay into the $\tilde{3}\Sigma^-$ channel has only been available; this is the value of $6\pi \times 10^{-6} \text{ cm}^{-1}$, which was obtained in Ref. 21 assuming that the SO coupling between the $A^3\Sigma^+$ and $\tilde{3}\Sigma^-$ states is 1 cm^{-1} . Upon multiplication by the factor of 9 [since $V_{1,2}(r_c)=3 \text{ cm}^{-1}$ is the value at the crossing point of the coupling used here], this estimate becomes close to the present approximate results $\Gamma_{Av=0\rightarrow\tilde{3}\Sigma^-}^{\text{SC}}=1.72 \times 10^{-4} \text{ cm}^{-1}$ and $\Gamma_{Av=0\rightarrow\tilde{3}\Sigma^-}^{\text{CM}}(\text{dir})=1.82 \times 10^{-4} \text{ cm}^{-1}$ (see Table AVII).

As it follows from the considerations presented in Sec. IV B, the overall increases of lifetimes given by the JCP06

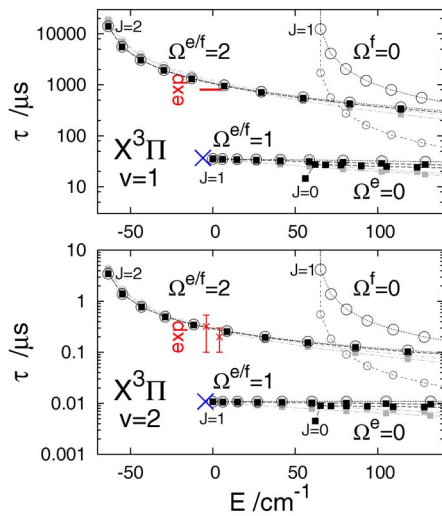


FIG. 8. (Color online) Rotation-vibration states of CO²⁺(³Π) from the JP04r-*v* model. Energies and lifetimes as functions of *J* number for the Ω = 2, 1, 0 components of *e* (squares) and *f* parity (circles). The smaller circles and gray squares indicate effects of adding of the L-uncoupling terms to the model [see Eq. (9) and Fig. A1]. The upper panel concerns ¹³C¹⁶O²⁺; the bottom panel is for ¹²C¹⁶O²⁺. Zero of energy in each panel is at the respective $E(^3\Pi_{\Omega=1} J=1 v)$ level (see Table VI). Large (blue) crosses denote the corresponding results from the JP04 model. The experimental data for lifetimes are shown at the theoretical energies of the Ω = 1 = *J* states (shifted by ±5 cm⁻¹).

and JP04 models over those from the PRL93 model should mostly be attributed to the behavior of the respective repulsive potentials $V_{3\Sigma^+}(r)$ in the region outside the crossing with the ground state potential. One has to conclude that the repulsive potential of the JCP06 model is severely inaccurate in this region; the yielded increase of lifetimes is by far too big. A comparison of the calculated and measured vibronic energies of the ion reveals (see Fig. A6) that also the JCP06 potential of the ground state is insufficiently accurate in the same region; the barrier is definitely too high. With growing *v*, the energies E_{Xv} depart from their experimental counterparts even more than the energies from the PRL93 potential. The level spacings from the JCP06 potential of state *b* ¹Π compare more favorably with the experimental data, especially with those of Ref. 10 for $v \leq 5$ levels. However, deviations start to grow for higher *v*'s, evidently because of the barrier too high in this potential, too.

There are short reports in Ref. 43 (Figs. A7 and A8) about calculations which have been done on vibronic states of the CO²⁺ ion not considered in the main text here, namely, on states *c* ¹Δ(*v*) and *d* ¹Σ⁺(*v*). Results obtained for the latter states are commented on in reference to the first hypothesis,⁹ recalled in Sec. I, about the origin of the observed ms lifetimes.

D. Rovibronic states

Though lifetimes of individual rotation-vibration states of the CO²⁺ ion have not been measured yet, a provisional theoretical simulation is possible with the existing electronic structure data. The present JP04r-*v* model serves such a purpose. The most interesting results obtained from this model, for the triplet states $X^3\Pi$ and $A^3\Sigma^+$, are presented in Fig. 8

and Tables VI and VII. Some results concerning states $a^1\Sigma^+$ and $b^1\Pi$ are presented in Figs. A9 and A10.

Figure 8 shows the lifetimes of the states $X^3\Pi_{\Omega v}(Jv)$ which lie in the energy ranges $[-70, 200]$ cm⁻¹ around the $E(^3\Pi_{\Omega=1} J=1 v)$ levels for $v=1$ and 2. (These levels are nearly coincident with the respective energies E_{Xv} from the purely vibronic JP04 model.) Correlations of the lifetimes with the quantum numbers characterizing the states are exposed. A clear distinction is seen between the multiplet components Ω = 0 of *e* parity and Ω = 1 of both parities from one side and the components Ω^{*f*} = 0 and Ω^{*ef*} = 2 from the other side. Lifetimes pertaining to the three latter components reveal a strong variation with *J* number and are at least one order of magnitude larger. The reason obviously lies in the structure of the Hamiltonian matrices \mathbf{H}^{Je} and \mathbf{H}^{Jf} (see Fig. A1). The longer lived Ω components of the ³Π state are just the ones which can predissociate only indirectly, via the rotational coupling with the ³Π_{Ω=1} component of respective symmetry.

The limited validity of the JP04r-*v* model should be noted at this point. Interactions neglected in this model may obviously induce some quantitative changes in the present picture of lifetimes of the different multiplet components. A simulation of possible impact of L-uncoupling perturbations was made by adding the terms of Eq. (9) to matrices \mathbf{H}^{Je} and \mathbf{H}^{Jf} . The impact on low *J* levels appears substantial only if they pertain to Ω^{*f*} = 0 components, as illustrated by the light gray symbols in Fig. 8.

Most intriguing is the finding marked with the vertical (red) labels: the experimental lifetimes assigned to the two $X^3\Pi(v)$ states, $v=1$ and $v=2$ (see Table V), match very well the values calculated here for the rotation-vibration states Ω = 2^{*ef*} *J* = 6 - 7*v* = 1 and Ω = 2^{*ef*} *J* = 6 - 7*v* = 2, respectively, whose energies are close to the central $E(\Omega=1^e J=1v)$ levels. A more precise comparison is made in Table VI where the positions and widths of the relevant levels are listed. Assuming that the indicated rotational components could be responsible for the measured lifetimes of states $X^3\Pi(v=1)$ and $v=2$, the values 1311–946 and 0.34–0.26 μs, respectively, are obtained as their calculated counterparts. The latter agree nearly perfectly with the experimental data (are within the experimental error bounds) and the former are only slightly (1.6–1.2 times) too high. Thus, the two largest deviations from experiment of the results calculated from the JP04 model (see Table V) become reduced ten times, roughly estimating. This should be taken as a suggestion that the diagonal SO coupling is not to be neglected in future simulations of lifetimes of the CO²⁺ ion in its $X^3\Pi(v)$ states. Accounting for “true” L-uncoupling perturbations in the system would be desirable to fully confirm the present predictions for the rotational components of these states.

The accounting for rotational structure and symmetry of the states in the JP04r-*v* model may seem to introduce only small corrections to the picture of stability of the ion in its $A^3\Sigma^+(v)$ states. Indeed, the widths $\Gamma(F_2 N v)$ listed in Table VII are practically the same as the widths Γ_{Av} from the vibrational JP04A model shown in Table III. The widths of the components F_1 and F_3 are smaller by factors not exceeding 2 in most cases. The lifetimes of all $F_i N$ components of *v* states are below the experimental upper bound (0.05 μs). An

important point is, however, that this estimation concerns also the $J=0(F_1N=1)$ component. Although predissociation of this component to the repulsive state $^3\Sigma^-$ is forbidden by symmetry, it can decay quickly due to the coupling with $\Omega^f=0$ component of state $X^3\Pi$. This fact is of direct relevance to the question about the possible fluorescence of CO^{2+} .^{2,8,16,22}

It was suggested in Ref. 22 that there is a chance to observe six emission lines due to the transitions $A^3\Sigma_0^+(J'=0, v'=0) \rightarrow X^3\Pi_{\Omega''f}(J''=1, v'')$ for $\Omega''=0, 1$ and $v''=0-2$. The respective radiative lifetime of the upper state was estimated to be about 5–7 μs . The argument about stability of this state against predissociation²¹ was crucial to the suggestion. The present calculations raise severe doubts as to the validity of this argument. The calculated predissociation lifetime of state $A^3\Sigma_0^+(J'=0, v'=0)$ is only 0.01 μs , i.e., above 500 times shorter than the estimated radiative lifetime. The estimation of the radiative lifetimes has been recently confirmed in *ab initio* calculations.²⁵ Strictly, values ranging from 8.97 to 5.49 μs have been obtained for the vibronic states $A^3\Sigma^+(v=0-3)$.

Reference 25 reports also predissociation lifetimes of the rovibronic states $A^3\Sigma_{0,1}^+(v=0-2, J=1-5)$. The results are claimed to provide evidence that a large increase of lifetimes (even by two orders of magnitude) may occur for several $J > 0$ levels due to relatively small centrifugal distortion barriers (pertaining to $J < 5$). No such a “spectacular” effect is displayed by the present results in Table VII, neither by those from the JP04r-v model nor by the results obtained after supplementing the model with the L-uncoupling terms. It seems that the finding of Ref. 25 is a spurious effect produced mostly by the complex-scaling method used (highly uncertain accuracy of this method in determining lifetimes of CO^{2+} is amply documented in Table AVIII; see also the comment to Fig. A1).

E. Comments on determining very long lifetimes

The perturbative TP approach to tunneling is applied here probably for the first time in the context of molecular dications. The approach is especially well suited to the determination of ultralong lifetimes. Very long lifetimes, corresponding to widths as small as 10^{-25} cm^{-1} , are obtainable with the modified-Milne method of Ref. 56. Quadruple precision of calculations is required, however. Widths smaller than 10^{-25} cm^{-1} have been obtainable so far only with the help of SC formulas,⁵⁷ see, e.g., Ref. 23. It is therefore noteworthy that because of its quantum-mechanical character, the TP approach is superior with respect to the accuracy to the most sophisticated SC approaches available.^{53,54} This is demonstrated exemplarily in Table VIII. A more extensive comparison of results obtained with the quantum-mechanical (TP and SQ) and SC methods for shape resonances in the potentials of the JP04 model is given in Tables AXII and AXIII.

Unlike the TP approach, the SQ method is widely exploited in calculations on molecular resonances. The present implementation of the method⁴³ is largely based on the work^{36,37} published in the early 1980s. It is all the more worth noting that (quantum-mechanical) SQ calculations

which would provide accurate results for widths as small as those obtained here [$\sim 10^{-25} \text{ cm}^{-1}$ (Table I), $\sim 10^{-62}$ (Table VIII), or even smaller (Table AXIII)] seem not to have been reported in the literature so far.

V. SUMMARY

Using the best available electronic structure data, the potentials generated in Refs. 23 and 24, the SO couplings generated in Ref. 24, and the SO constant of Ref. 22, several models have been constructed to study metastable vibronic and rovibronic states of the CO^{2+} dication. About 90 vibronic states in the energy range up to 5.3 eV above the bottom of the $X^3\Pi$ potential well have been studied. Methods of three distinct categories (quantum-mechanical “exact,” perturbative, and semiclassical) have been exploited to calculate the energies and lifetimes of the states. Lifetimes for predissociation and tunneling, varying over a wide range (tens of orders of magnitude), have been determined, demonstrating a remarkably good agreement between results yielded by the exact (SQ) and the perturbative (bound-continuum CM and TP) methods. Reasonably good consistency (deviations $\leq 10\%$) has also been observed between the quantum-mechanical and SC results. Taking advantages of this consistency, a detailed analysis has been performed of how the calculated predissociation characteristics (level widths and shifts) depend on the individual potentials and SO couplings. The main findings are as follows.

- (i) The widths of the vibronic levels bound to the potentials of the $X^3\Pi$ and $b^1\Sigma^+$ states are almost entirely determined by the crossings and couplings of these potentials with the repulsive potential of the $^3\Sigma^-$ state.
- (ii) The indirect predissociation $a^1\Sigma^+ \rightarrow X^3\Pi \rightarrow ^3\Sigma^-$ is the dominant decay mechanism of only the three lowest ($v=0-2$) levels of state $a^1\Sigma^+$. The predissociation characteristics of the levels $a^1\Sigma^+(v \geq 7)$ are well representable by sums of independent contributions of two curve crossings: $V_a - V_{^3\Sigma^-}$ and $V_a - V_X$. The latter crossing contributes mostly to the widths, and the former to the shifts.
- (iii) Two crossings of the $A^3\Sigma^+$ state potential, the outer crossing with the potential $V_{^3\Sigma^-}$ and the inner crossing with the potential V_X , contribute comparable amounts to the widths of the levels $A^3\Sigma^+(v=0-2)$. The widths of the higher A state levels are almost entirely determined by the inner crossings $V_A - V_X$ and $V_A - V_b$ (for $v \geq 6$).

The results obtained for the vibronic states of the ion from two (sets of) models, the (JCP06) model built entirely of the electronic structure data of Ref. 24 and the (JP04, JP04A) models compiled of the potentials of Ref. 23 and the SO couplings of Ref. 24, have been confronted with the existing experimental data. The main conclusions are as follows.

- (i) The JCP06 model is incapable of giving realistic lifetimes of the three lowest vibronic states of the ion, $X^3\Pi(v=0, 1)$ and $a^1\Sigma^+(v=0)$, because of insufficient accuracy of the repulsive potential of the $^3\Sigma^-$

state in the medium range of the C–O distance. Of the two cases of good consistency between the calculated and measured lifetimes in the microsecond range that are reported in Ref. 24, for states $a^1\Sigma^+(v=1)$ and $X^3\Pi(v=2)$, only the latter is confirmed by the present calculations.

- (ii) The JP04 model represents a factual improvement over the models based on the old electronic structure data,^{21,9} giving lifetimes in a reasonable agreement with all existing experimental values and estimates. The largest deviations remaining, $\tau^{\text{expt}}/\tau^{\text{calc}} \simeq 20$, concern the $X^3\Pi$ state levels, $v=1$ and $v=2$. The omission of the diagonal SO coupling terms ($\pm A_{\Pi}$) may be partly responsible for these deviations. This points to the need for refining the treatment of dynamics of the ion (since the role of the $\pm A_{\Pi}$ terms cannot be fully investigated within the nonrotating molecule models).

The first simulation of rotationally resolved lifetimes of several vibronic levels assigned to each of the four bounding electronic states $X^3\Pi$, $a^1\Sigma^+$, $b^1\Pi$, and $A^3\Sigma^+$ has been made using appropriately extended versions of the JP04 model. The main findings are as follows.

- (i) The diagonal SO coupling terms together with the rotational **S**-uncoupling perturbations create a sizable splitting of lifetimes between two groups of multiplet components ($\Omega^p=1^{ef}, 0^e$ and $\Omega^p=2^{ef}, 0^f$) of the states $X^3\Pi_{\Omega^p}(Jv=0-2)$. Lifetimes of some rotational sublevels ($\Omega^p=2^{ef}, J=6-7$) of the two vibronic levels $X^3\Pi(v=1)$ and $X^3\Pi(v=2)$ match very well ($\tau^{\text{cal}}/\tau^{\text{exp}} < 2$) the experimental values of 800 and 0.2 μs , respectively.
- (ii) The impact of rotational perturbations (of **S**- and **L**-uncoupling types) on lifetimes of the multiplet (F_{1-3}) components of the states $A^3\Sigma^+(Nv)$ is not especially large [$\tau(F_{1-3})/\tau(F_{2,3}) \leq 5$ for $N \leq 6$ and $v = 0-2, 6$]. No component is characterized by lifetime longer than 0.05 μs . Thus, with no exception, the $A^3\Sigma^+$ state levels decay (more than 100 times) faster by predissociation than by photon emission.

¹D. Mathur, *Phys. Rep.* **391**, 1 (2004).

²S. G. Cox, A. D. J. Crichley, P. S. Kreymin, I. R. McNab, R. C. Shiell, and F. Smith, *Phys. Chem. Chem. Phys.* **5**, 663 (2003).

³S. D. Price, *Int. J. Mass. Spectrom.* **260**, 1 (2007).

⁴E. Friedländer, H. Kallmann, W. Lasereff, and B. Rosen, *Z. Phys.* **76**, 60 (1932); **76**, 70 (1932).

⁵A. S. Newton and A. F. Sciamanna, *J. Chem. Phys.* **53**, 132 (1970).

⁶J. M. Curtis and R. K. Boyd, *J. Chem. Phys.* **80**, 1150 (1984).

⁷N. Correia, A. Flores-Riveros, H. Ågren, K. Helenelund, L. Asplund, and U. Gelius, *J. Chem. Phys.* **83**, 2035 (1985).

⁸G. Dujardin, L. Hellner, M. Hamdan, A. G. Brenton, B. J. Olsson, and M. J. Besnard-Ramage, *J. Phys. B* **23**, 1165 (1990).

⁹L. H. Andersen, J. H. Posthumus, O. Vahtras, H. Ågren, N. Elander, A. Nunez, A. Scrinzi, M. Natiello, and M. Larsson, *Phys. Rev. Lett.* **71**, 1812 (1993).

¹⁰G. Dawber, A. G. McConkey, L. Avaldi, M. A. MacDonald, G. C. King, and R. I. Hall, *J. Phys. B* **27**, 2191 (1994).

¹¹M. Lundqvist, P. Baltzer, D. Edvardsson, L. Karlsson, and B. Wannberg, *Phys. Rev. Lett.* **75**, 1058 (1995).

¹²M. Hochlaf, R. I. Hall, F. Penent, H. Kjeldsen, P. Lablanquie, M.

Lavollée, and J. H. D. Eland, *Chem. Phys.* **207**, 159 (1996).

¹³F. Penent, R. I. Hall, R. Panajotović, J. H. D. Eland, G. Chaplier, and P. Lablanquie, *Phys. Rev. Lett.* **81**, 3619 (1998).

¹⁴J. P. Bouhnik, I. Gertner, B. Rosner, Z. Amitay, O. Heber, D. Zajfman, E. Y. Sidky, and I. Ben-Itzhak, *Phys. Rev. A* **63**, 032509 (2001).

¹⁵J. H. D. Eland, *Chem. Phys.* **294**, 171 (2003).

¹⁶S. Taylor and J. H. D. Eland, *Chem. Phys.* **315**, 8 (2005).

¹⁷A. C. Hurley and V. W. Maslen, *J. Chem. Phys.* **34**, 1919 (1961).

¹⁸A. C. Hurley, *J. Chem. Phys.* **54**, 3656 (1971).

¹⁹R. W. Wetmore, R. J. Le Roy, and R. K. Boyd, *J. Phys. Chem.* **88**, 6318 (1984).

²⁰P. Lablanquie, J. Delwiche, M.-J. Hubin-Franskin, I. Nenner, P. Morin, K. Ito, J. H. D. Eland, J. M. Robbe, G. Gandara, J. Fournier, and P. G. Fournier, *Phys. Rev. A* **40**, 5673 (1989).

²¹M. Larsson, B. J. Olsson, and P. Sigray, *Chem. Phys.* **139**, 457 (1989).

²²D. Cossart and J. M. Robbe, *Chem. Phys. Lett.* **311**, 248 (1999).

²³J. H. D. Eland, M. Hochlaf, G. C. King, P. S. Kreymin, R. J. Le Roy, I. R. McNab, and J. M. Robbe, *J. Phys. B* **37**, 3197 (2004).

²⁴T. Šedivcová, P. R. Ždánská, V. Špirko, and J. Fišer, *J. Chem. Phys.* **124**, 214303 (2006).

²⁵T. Šedivcová-Uhlíková, P. R. Kaprálová-Ždánská, and V. Špirko, *Int. J. Quantum Chem.* **107**, 2654 (2007).

²⁶O. K. Rice, *J. Chem. Phys.* **1**, 375 (1933).

²⁷U. Fano, *Phys. Rev.* **124**, 1866 (1961).

²⁸J. N. Bardsley, *J. Phys. B* **1**, 349 (1968).

²⁹F. H. Mies, *Phys. Rev.* **175**, 164 (1968).

³⁰H. Lefebvre-Brion and R. E. Field, *Perturbations in the Spectra of Diatomic Molecules* (Academic, New York, 1986).

³¹A. Scrinzi and N. Elander, *J. Chem. Phys.* **98**, 3866 (1993).

³²A. Mandelshtam, H. S. Taylor, V. Rayaboy, and N. Moiseyev, *Phys. Rev. A* **50**, 2764 (1994).

³³N. Moiseyev, *Phys. Rep.* **302**, 212 (1998).

³⁴Some justification of this choice is given in Ref. 43 (in the comments to Fig. A1).

³⁵A. F. J. Siegert, *Phys. Rev.* **56**, 750 (1939).

³⁶O. Atabek and R. Lefebvre, *Phys. Rev. A* **22**, 1817 (1980).

³⁷J. N. L. Connor and A. D. Smith, *J. Chem. Phys.* **78**, 6161 (1983).

³⁸H. W. Jang and J. C. Light, *Phys. Rev. A* **51**, 1277 (1995).

³⁹*Handbook of Mathematical Functions*, edited by M. Abramowitz and I. A. Stegun.

⁴⁰G. V. Sitnikov and O. I. Tolstikhin, *Phys. Rev. A* **67**, 032714 (2003).

⁴¹B. R. Johnson, *J. Comput. Phys.* **13**, 445 (1973).

⁴²F. Mrugała, *Int. Rev. Phys. Chem.* **12**, 1 (1993).

⁴³See EPAPS Document No. E-JCPSA6-129-635826 for a pdf file containing: 1) some details on the implementation and the accuracy of the Siebert quantization and the two-potential methods, 2) complete set of results from the JP04 model, 3) detailed comparison of present results from the JCP06 model with results of Ref. 24, 4) extended presentation of the perturbative results, 5) some predictions for lifetimes of the states $c^1\Delta(v)$ and $d^1\Sigma^+(v)$. For more information on EPAPS, see (<http://www.aip.org/pubservs/epaps.html>).

⁴⁴W. H. Press, S. A. Teukolsky, W. T. Vetterling, and B. P. Flannery, *Numerical Recipes in FORTRAN* (Cambridge University Press, Cambridge, 1992), Sec. 9.7.

⁴⁵H. Feshbach, *Ann. Phys.* **5**, 357 (1957); H. Feshbach, *ibid.* **19**, 287 (1962); H. Feshbach, *ibid.* **43**, 410 (1967).

⁴⁶R. D. Levine, *Quantum Mechanics of Molecular Rate Processes* (Clarendon, Oxford, 1969).

⁴⁷M. Desouter-Lecomte, J. Lièvin, and V. Brems, *J. Chem. Phys.* **103**, 4524 (1995); V. Brems, M. Desouter-Lecomte, and J. Lièvin, *ibid.* **104**, 2222 (1996).

⁴⁸S. A. Gurvitz, *Phys. Rev. A* **38**, 1747 (1988).

⁴⁹F. Mrugała, *J. Chem. Phys.* **91**, 874 (1989).

⁵⁰F. Mrugała, *Mol. Phys.* **65**, 377 (1988); F. Mrugała, *J. Chem. Phys.* **93**, 1257 (1990); F. Mrugała, *ibid.* **115**, 3155 (2001).

⁵¹M. S. Child, in *Semiclassical Methods in Molecular Scattering and Spectroscopy*, edited by M. S. Child (Reidel, Dordrecht, 1980), p. 127.

⁵²M. S. Child and R. Lefebvre, *Mol. Phys.* **34**, 979 (1977).

⁵³J. N. L. Connor and A. D. Smith, *Mol. Phys.* **43**, 397 (1981).

⁵⁴J. N. L. Connor and A. D. Smith, *Mol. Phys.* **45**, 149 (1982).

⁵⁵R. S. Mulliken, *J. Chem. Phys.* **33**, 247 (1960).

⁵⁶E. Y. Sidky and I. Ben-Itzhak, *Phys. Rev.* **60**, 3586 (1999).

⁵⁷R. J. Le Roy and W.-Ki. Liu, *J. Chem. Phys.* **69**, 3622 (1978).

A. SUPPLEMENTARY MATERIAL

TABLE AI: Tests of the Siegert quantization method in four-channel calculations for vibronic states of CO^{2+} . Dependence of the eigenvalues $E - i\Gamma/2$ on the form and the position of the asymptotic boundary condition (bc) shown in terms of relative mean square deviations, $\text{dev } X^{(\text{bc})} \equiv \frac{1}{5} \left[\sum_{k=0}^4 (X_k^{(\text{bc})}/X_{\text{ref}} - 1)^2 \right]^{1/2}$ for $X=E, \Gamma$ and $\text{bc} = \text{exact}^a, \text{WKB}^b$, where $X_k^{(\text{bc})}$ denotes the value obtained with bc at $r_\infty = 9.0 - k \times 0.5 a_0$, and X_{ref} is the most accurate result generated: $X_0^{(\text{WKB})}$.

State	v	E^c cm^{-1}	$\text{dev } E^d$	Γ cm^{-1}	$\text{dev } \Gamma^{(\text{bc})}$	
					bc=WKB	exact
$X^3\Pi$	0	732.20	2(-12)	1.48(-24)	3(-6)	8(-3)
	1	2168.28	1(-12)	1.10(-11)	5(-6)	3(-3)
	2	3548.53	1(-12)	7.70(-6)	6(-6)	8(-3)
	e	3437.62	1(-12)	4.90(-4)	3(-6)	5(-3)
	3	4883.30	2(-12)	4.97(-3)	3(-6)	4(-3)
$a^1\Sigma^+$	4	6167.37	2(-11)	1.88(-1)	4(-6)	6(-3)
	0	980.23	4(-12)	1.85(-13)	7(-6)	9(-3)
	1	2923.04	3(-12)	5.06(-8)	5(-6)	5(-3)
	e	2841.46	5(-13)	2.48(-6)	2(-6)	3(-3)
$b^1\Pi$	2	4820.46	2(-12)	1.39(-5)	2(-6)	6(-3)
	0	753.64	6(-12)	1.04(-6)	3(-6)	5(-3)
	e	740.46	2(-12)	1.91(-5)	4(-6)	4(-3)
	1	2234.34	4(-12)	6.84(-4)	2(-6)	6(-3)

^aConsists here in solving the Riccati equation satisfied by $\mathbf{L}_{O^+}(r; \mathcal{E})$,

$$\frac{d}{dr} \mathbf{L}_{O^+} + \mathbf{L}_{O^+}^2 + \mathbf{W}_\infty = 0 \quad \text{with} \quad \mathbf{W}_\infty(r; \mathcal{E}) \equiv \mathbf{k}^2(\mathcal{E}) - \frac{2\mu}{r} \mathbf{I},$$

starting from the values $[\mathbf{L}_{O^+}(r_s^{\text{trn}}; \mathcal{E})]_{s,s}$ at the turning points r_s^{trn} , $\text{Re}[\mathbf{W}_\infty(r_s^{\text{trn}}; \mathcal{E})]_{s,s} = 0$, for $s=1, \dots, 4$. These values are obtained by exploiting the expansion of the Coulomb functions in terms of Airy integrals, Ref. 1.

^bThe condition described in the paper, Eqs.(21) and (23).

^cGiven relative to the minimum of the potential well of the respective electronic state. The positions of the well minima V_a^{min} and V_b^{min} relative to V_X^{min} in the potentials of Ref. 4 (the JCP06 model) and in the potentials of Ref. 5 (the JP04 model) are listed in the caption of Fig. 1 in the paper. Information on asymptotes of the states is necessary for evaluation of $[\mathbf{k}^2(\mathcal{E})]_{s,s}$, see footnote *a*. It is obtained from the extrapolation procedure described in Sec. II of the paper. The position of the asymptote of the repulsive state $V_{3\Sigma^-}^{\text{th}}$ relative to V_X^{min} is $-0.1916 E_H$ in the JCP06 model and $-0.198751 E_H$ in the JP04 model. $V_s^{\text{th}} - V_s^{\text{min}}$ for $s=X, a, b$ are $-0.191106, -0.088624, -0.073143 E_H$ in the JCP06 model, and $-0.196176, -0.088134, -0.092550 E_H$ in the JP04 model.

^dThe deviations are essentially the same for both bc-forms tried. The small values are only an indication of numerical stability of the energies E against shifts of the boundary condition. Because of the accuracy of the input potentials, the energies themselves can be physically meaningful only up to 0.1 cm^{-1} .

^eResults from the JP04 model.

TABLE AII: Exemplary results of the Siegert quantization calculations for shape resonances in the potentials of the $X^3\Pi$ and $b^1\Pi$ states of CO^{2+} . Dependence of the widths on the form and the position of the asymptotic boundary condition (bc) shown in terms of relative mean square deviations, $\text{dev } \Gamma^{(\text{bc})} \equiv \frac{1}{5} \left[\sum_{k=0}^4 (\Gamma_k^{(\text{bc})}/\Gamma_{\text{ref}} - 1)^2 \right]^{1/2}$ for bc=exact, WKB, asmt^a, where $\Gamma_k^{(\text{bc})}$ denotes the value obtained with bc at $r_\infty = 17.5 - k \times 1.0 a_0$, and $\Gamma_{\text{ref}} = \Gamma_0^{(\text{exct})}$. For each resonance shown, the entries in the second line concern the JP04 model.

State	v	E^b cm ⁻¹	Γ cm ⁻¹	dev $\Gamma^{(\text{bc})}$			r_{trn}^c a_0
				bc=exact	WKB	asmt	
$X^3\Pi$	0	733.31	6.05 (-62)	4 (-9)	8 (-8)	7 (-3)	5.14
		715.29	4.51 (-56)	4 (-9)	9 (-8)	7 (-3)	5.01
	10	12714.64	1.41 (-5)	9 (-9)	4 (-8)	4 (-3)	4.01
		12111.36	3.15 (-3)	8 (-9)	3 (-8)	3 (-3)	3.98
$b^1\Pi$	0	752.87	3.72 (-238)	1 (-8)	7 (-6)	6 (-1)	10.86
		739.68	8.95 (-224)	6 (-10)	2 (-6)	4 (-1)	10.42

^a‘exact’ and WKB denote the forms described in Table AI and ‘asmt’ denotes the following asymptotic form of \mathbf{L}_{O^+}

$$\mathbf{L}_{O^+}^{\text{as}}(r_\infty; \mathcal{E}) = \imath \left[\mathbf{k}(\mathcal{E}) - \frac{\mu}{r_\infty} \mathbf{k}^{-1}(\mathcal{E}) \right].$$

^bGiven relative to the bottom of the well in the potential of the state.

^cThe classical turning point in the respective asymptotic potential $1/r + V^{\text{th}}$. See footnote *c* in Table AI for information on V^{th} . The ‘asmt’ form of the boundary condition is clearly inapplicable when r_∞ lies too close to r_{trn} .

COMMENT

on the accuracy of the SQ method in calculation of ultra-small resonance widths

The widths Γ^{SQ} were obtained in double-precision calculations together with the corresponding energies E^{SQ} . All these widths, even the ones of the size of $\sim 10^{-220} \text{ cm}^{-1}$, are numerically correct. The consistency with the results of the perturbative quantum-mechanical and the semi-analytical semiclassical approaches, demonstrated in Tables AXII-AXIII, AIII, and in Tables I-II, VIII of the paper, should leave no doubts about that. Thus, the smallness of the imaginary parts of the Siegert eigenvalues, which are accurately determined here, is not limited by the accuracy obtainable for the real parts of these eigenvalues (absolute errors $\sim 10^{-8} - 10^{-9} \text{ cm}^{-1}$). This is an advantageous feature of the present implementation of the Siegert quantization, apparently not easily achievable in other non-perturbative implementations (see eg. the comment on the complex scaling approaches in a recent paper on long-lived molecular hydrogen anions, Ref. 15). Most likely, the advantageous performance of the present implementation should be attributed to the convergence properties of the *Numerical Recipes*’ procedure NEWT which was exploited for finding the complex eigenvalues \mathcal{E}_n [as two roots, $\text{Re } \mathcal{E}_n \equiv x_1$ and $\text{Im } \mathcal{E}_n \equiv x_2$, of the two equations: $f_1(x_1, x_2) \equiv \text{Re } \det[\mathbf{L}(r_m; \mathcal{E}) - \bar{\mathbf{L}}(r_m; \mathcal{E})] = 0$ and $f_2(x_1, x_2) \equiv \text{Im } \det[\dots] = 0$, cf. Eq. (17) in the paper].

TABLE AIII: Energies and widths (all in cm^{-1}) of vibrational states of $\text{CO}^{2+}(X^3\Pi)$ from the JP04 model (potentials of four electronic states: $X^3\Pi$, $^3\Sigma^-$, $a^1\Sigma^+$, and $b^1\Pi$ taken from Ref. 4 plus spin-orbit couplings from Ref. 5). Comparison of Siegert quantization results with results obtained within the perturbative bound-continuum configuration mixing (CM) approach using the partitioning: $\{X, a, b\} + \{^3\Sigma^-\} \equiv \text{Q} + \text{P}$.

v	E^a	Γ	$E^{\text{shf}d}$	$\delta E^{\text{shf}e}$	$\delta\Gamma^f$
0	714.19 ^b	4.66 (−14)	−0.025	0.0	−1.2
^c	698.5	1.76 (−14)			
1	2101.04	2.66 (−7)	−0.035	0.0	−0.2
^c	2056.0	1.44 (−7)			
2	3437.62	4.90 (−4)	−0.059	0.0	−0.1
3	4721.41	4.80 (−2)	−0.124	0.0	−0.0
4	5953.86	2.60 (−1)	−0.077	−2.7 ^g	1.7 ^g
5	7128.46	1.74 (−1)	0.160	0.0	0.0
6	8248.75	2.87 (−1)	0.009	0.1	0.0
7	9310.92	2.69 (−2)	0.017	−0.9	0.7
8	10312.60	3.10 (−2)	0.092	−0.0	−0.0
9	11247.84	7.84 (−2)	0.077	−0.0	0.9
10	12110.80	1.59 (−1)	0.052	17.3	−2.0
11	12879.01	1.65	^h		

^aZero of energy is at V_X^{min} , the bottom of well in $V_X(r)$.

^bLies 41.064 eV above the energy of the $X^1\Sigma^+(v=0, J=0)$ state of CO; taken from Table 8 of Ref. 5.

^cFor $^{13}\text{C}^{16}\text{O}^{2+}$.

^dEvaluated within the CM approach, Eqs. (29-30) in the paper.

^eDefined as $[E^{\text{shf}}/(E - E^{(0)}) - 1] \times 100\%$, where $E^{(0)}$ denotes energy of related bound state in the Q-subspace.

^fDefined as $(\Gamma^{\text{CM}}/\Gamma - 1) \times 100\%$.

^gSee Table AV for a refined CM treatment of this case.

^hThe state decays by tunneling. The present choice of the P and Q subspaces is inadequate. See Tables AXII-AXIII for results of perturbative treatment of tunneling.

TABLE AIV: Energies and widths (all in cm^{-1}) of the vibronic states $a^1\Sigma^+(v)$ and $b^1\Pi(v)$ of CO^{2+} from the JP04 model. Comparison of Siegert quantization results with results obtained within the perturbative bound-continuum configuration mixing (CM) approach. In the treatment of $v < 7$ states, the partitioning into subspaces of bound (Q) and continuum (P) configurations was: $\text{Q}+\text{P}=\{X, a, b\}+\{^3\Sigma^-\}$. In the cases of the states $a^1\Sigma^+(v \geq 7)$, the values of E^{shf} and Γ^{CM} were obtained as sums of respective results of two separate calculations, with $\text{Q}+\text{P}=\{a\}+\{^3\Sigma^-\}$ and $\text{Q}+\text{P}=\{a\}+\{X\}$. The same approximation was applied to the states $b^1\Pi(v \geq 7)$ except $\text{Q}=\{b\}$.

v	$a^1\Sigma^+$					$b^1\Pi$				
	E^a	Γ	$E^{\text{shf}d}$	$\delta E^{\text{shf}e}$	$\delta\Gamma^f$	E^a	Γ	$E^{\text{shf}d}$	$\delta E^{\text{shf}e}$	$\delta\Gamma^f$
0	2218.57	1.03 (-8)	-0.012	0.0	-0.1	4938.89	1.91 (-5)	-0.027	0.0	0.1
^c	2197.1	4.71 (-9)				4922.5	1.45 (-5)			
1	4102.05	2.48 (-6)	-0.013	0.0	-0.0	6392.19	4.33 (-3)	-0.047	0.0	0.1
2	5948.69	2.04 (-1)	-0.056	3.8 ^g	-2.1 ^g	7810.98	1.07 (-1)	-0.089	0.0	-0.0
3	7762.86	9.14 (-4)	-0.026	0.0	-0.6	9195.45	2.82 (-1)	0.026	0.6	-0.0
4	9537.09	3.31 (-2)	-0.052	0.0	0.0	10545.32	2.90 (-3)	0.013	-0.1	-0.0
5	11272.92	2.31 (-1)	-0.011	0.7	-0.3	11860.87	1.14 (-1)	0.060	-0.0	-0.0
6	12966.62	6.03 (-2)	0.049	3.9	-13.4	13141.97	1.17 (-1)	0.003	-0.1	-0.0
7	14617.92	2.93 (-1)	0.093	0.7	0.1	14388.92	2.36 (-2)	0.708	0.0	-2.1
8	16225.32	2.15 (-1)	0.097	-0.1	0.1	15601.75	6.08 (-3)	0.723	-0.1	-2.2
9	17786.33	2.60 (-1)	0.105	-0.2	-0.0	16780.41	4.68 (-2)	0.719	-0.1	-2.9
10	19297.80	2.76 (-1)	0.073	-0.2	-0.2	17924.91	8.00 (-2)	0.690	-0.1	-2.9
11	20755.13	2.25 (-1)	0.053	-0.1	-0.0	19035.14	8.17 (-2)	0.654	-0.0	-2.6
12	22150.91	1.71 (-1)	0.062	1.0	0.6	20110.90	6.16 (-2)	0.623	0.0	-2.5
13	23472.60	1.45 (-1)	0.087	-0.3	0.1	21151.83	3.63 (-2)	0.599	0.0	-2.2
14	24698.89	1.33 (-1)	0.123	-0.3	-0.0	22157.40	1.76 (-2)	0.582	-0.2	-6.4
15	25795.38	1.18 (-1)	0.183	0.0	0.2	23127.01	6.82 (-3)	0.565	-0.0	-0.0
16	26722.75	9.74 (-2)	0.282	-0.1	-0.2	24059.85	5.38 (-3)	0.546	-0.1	-0.1
17	27488.40	7.95 (-2)	0.373	-0.0	-0.2	24954.81	9.48 (-3)	0.525	-0.1	-1.7
18	28157.21	6.81 (-2)	0.417	0.0	-0.3	25810.34	1.64 (-2)	0.500	-0.2	-4.4
19	28764.37	5.87 (-2)	0.446	-0.0	-0.9	26624.10	2.26 (-3)	0.470	-0.1	-2.2
20	29327.40	5.12 (-2)	0.456	0.0	-0.4	27392.17	2.79 (-2)	0.437	-0.1	-2.4
21	29864.30	4.51 (-2)	0.455	0.6	-2.0	28107.99	3.09 (-3)	0.399	0.0	-2.3
22	30356.20	3.02 (-1)	^h			28764.37	5.87 (-2)			
23	30787.86	2.14 (+1)	^h			29308.85	1.52 (+1)			

See the respective footnotes in Table AIII.

TABLE AV: Results of perturbative (CM) calculations for the case of accidental degeneracy in the JP04 model.

State	v	$E^{(0)a}$ $(\rho_X, \rho_a, \rho_b)^b$	$E^c - E^{(0)}$	Γ^c	CM f		CM (2×2 \mathbf{H}^{eff}) g	
					$\delta E^{\text{shf } d}$	$\delta \Gamma^e$	$\delta E^{\text{shf } d}$	$\delta \Gamma^e$
$X^3\Pi$	4	5953.9350 (56.07, 43.92, 0.01)	-0.0773	0.2597	-2.7	+1.7	0.06	0.01
$a^1\Sigma^+$	2	5948.7436 (43.92, 56.07, 0.01)	-0.0563	0.2039	+3.8	-2.1	0.04	0.01

E and Γ are given in cm^{-1} .

a Energy of the related bound state in the subspace $Q=\{X, a, b\}$, see Eq. (29) in the text.

$^b\rho_s \equiv \langle \Phi_s | \Phi_s \rangle \times 100\%$ for $s=X, a, b$, where Φ_s denotes component of the bound state function $\Phi^T = (\Phi_X, \Phi_a, \Phi_b)$.

c Obtained in four-channel Siegert quantization calculations.

d Defined as $[E^{\text{shf}} / (E - E^{(0)}) - 1] \times 100\%$.

e Defined as $[\Gamma^{\text{CM}} / \Gamma - 1] \times 100\%$.

f The isolated resonance version of the approach, see Eq. (30) in the paper. Results given by this version are evidently less accurate than most other (low v) results shown Tables I-II and AIII-AIV.

g An extended resonance search procedure. Instead of the single diagonal element $\langle \Phi_i | \mathcal{H}_Q(E) | \Phi_i \rangle \equiv \mathbf{H}_{i,i}^{\text{eff}}(E)$ defined in Eq. (30), the 2×2 matrix $\mathbf{H}^{\text{eff}}(E)$ is determined in the basis of the functions Φ_i and Φ_{i+1} that pertain to the nearly coinciding 0-th order energies, $E_i^{(0)} \approx E_{i+1}^{(0)}$. The two eigenvalues of this matrix, $\mathcal{E}_k(E)$ with $k=0, 1$, give the resonance energies E_{i+k} , as roots of the equations $E = \text{Re } \mathcal{E}_k(E)$, and the widths as $\Gamma_{i+k} = -2 \text{Im } \mathcal{E}_k(E_{i+k})$.

As demonstrated in the Table, the application of this procedure reduces the relative errors of the widths and shifts to the size typical of the present calculations for isolated resonance cases.

TABLE AVI: Energies and widths of s ($v=0-6$) vibronic states of CO^{2+} for $s=X^3\Pi$, $a^1\Sigma^+$, and $b^1\Pi$ from the JCP06 and JP04 models. Deviations between results of two- ($s+\tilde{s}=^3\Sigma^-$) and four-channel calculations using the Siegert quantization method.

v	JCP06								
	$X^3\Pi$			$b^1\Pi$			$a^1\Sigma^+$		
	ΔE^a	$\underline{\delta}E^{\text{sh}b}$	$\underline{\delta}\Gamma^c$	ΔE^d	$\underline{\delta}E^{\text{sh}f}$	$\underline{\delta}\Gamma$	ΔE^e	$\underline{\delta}E^{\text{sh}f}$	$\underline{\delta}\Gamma$
0	1.09	4.0	3.5	-0.79	-3.1	-6.5	3.74 ^f	15.9	-100 *
1	-2.85 ^f	-1.5	1.9	-0.79	-3.1	-3.6	0.05	-0.7	-100 *
2	0.84	3.0	3.0	-0.77	-3.0	-2.9	0.05	-0.5	-98.6*
3	0.71	2.6	2.7	-0.76	-3.1	-2.8	-0.06	-1.0	32.7
4	0.73	2.5	2.7	-0.75	-3.0	-8.0	-0.01	2.0	-23.9
5	0.77	2.9	2.4	-0.74	2.8	-2.6	-0.10	3.0	-1.2
6	0.76	-0.9	3.4	-0.72	7.1	-1.9	-0.13	-1.0	2.8
JP04									
0	1.08	3.9	3.3	-0.81	-3.2	-6.2	-1.93	-16.5	-100 *
1	2.88	9.0	6.0	-0.80	-3.1	-3.5	0.12	-0.3	-99.9*
2	0.79	2.8	2.8	-0.78	-2.8	-2.7	2.31	-71.4 ^g	-100 *
3	0.67	2.6	2.7	-0.77	0.3	-3.0	-0.06	-1.2	-6.0
4	-1.55 ^g	55.1 ^g	82.8 ^{*g}	-0.75	-2.5	-1.6	-0.14	-2.6	-6.5
5	0.76	2.2	2.3	-0.74	-2.3	-3.2	-0.85	197.0 ^h	-20.8
6	0.75	-0.0	2.5	-0.72	10.5	-2.6	-0.32	-0.1	16.1

^a $\Delta E=E(2)-E(4)$ given in cm^{-1} . See Tables I–II and AIII–AIV for the values of $E(4)$. ΔE reflects almost exclusively the difference between the respective $E^{(0)}$'s in the subspaces $Q_1=\{s\}$ and $Q=\{X, a, b\}$.

^b $\underline{\delta}E^{\text{sh}f}=[E^{\text{sh}f}(2)/E^{\text{sh}f}(4)-1]\times 100\%$, where $E^{\text{sh}f}(2)=E(2)-E^{(0)}(Q_1)$ and $E^{\text{sh}f}(4)=E(4)-E^{(0)}(Q)$.

^c $\underline{\delta}\Gamma=[\Gamma(2)/\Gamma(4)-1]\times 100\%$. Gives approximately the ratio $(-)\frac{\Gamma(\text{interf})}{\Gamma}\times 100\%$ plotted in Fig. A2; exception are the cases marked with asterisk.

^dGives approximately the $(-)$ shift from $E^{(0)}$ in $Q_1=\{b\}$ caused by the coupling $b-X$, see Fig. 5 in the paper.

^eClose to $(-)$ shift from $E^{(0)}$ in $Q_1=\{a\}$ caused by the coupling $a-X$, see Fig. 5.

^fEffect of repulsion between the levels $X v=1$ and $a v=0$.

^gEffect of the strongest accidental degeneracy encountered in both models.

^hEffect of perturbation by the $X(v=9)$ state. See the right panels of Fig. A2 and note the large contributions of interference paths to Γ and $E^{\text{sh}f}$ in the $X(v=9)$ and $a(v=5)$ cases.

TABLE AVII: Partial widths $\Gamma_{A v \rightarrow \tilde{s}}$ for $v=0-2$ and $\tilde{s}=^3\Sigma^-, X^3\Pi$ from the JP04A model. Perturbative quantum-mechanical (CM) results, obtained with the subspaces $Q=\{b, A\}$ and $P=\{\tilde{s}\}$, and semiclassical (SC) results for the $A-\tilde{s}$ crossings.

v	\tilde{s}	Γ^{CM} cm^{-1}	$\Gamma(\text{dir})^a$	$\Gamma(\text{intrf})^a/\Gamma$ $\times 100\%$	Γ^{SC}	Γ^{0b}
0	$^3\Sigma^-$	1.54 (-4)	1.82 (-4)	-19.5	1.72 (-4)	8.48 (-4)
1		2.19 (-3)	2.03 (-3)	7.1	2.01 (-3)	1.40 (-3)
2		1.77 (-3)	1.86 (-3)	-5.1	1.88 (-3)	6.24 (-4)
0	$X^3\Pi$	1.80 (-4)	1.88 (-4)	-4.4	1.79 (-4)	6.21 (-2)
1		9.17 (-4)	9.50 (-4)	-3.5	9.68 (-4)	6.37 (-2)
2		2.78 (-3)	2.83 (-3)	0.9	2.86 (-3)	6.54 (-2)

^aSee the caption of Fig. A2 for the definitions of the ‘direct’, and ‘interference’ contributions to the widths. The ‘indirect path’ contributions are very small in all cases shown here.

^bThe factor defined in the paper, in Eq. (32). See also Fig. A4.

TABLE AVIII: Deviations between energies and lifetimes of thirteen lowest vibronic states of CO²⁺ obtained from the JCP06 model in this work and in the calculations of Ref. 4.

State	v	E (cm ⁻¹)	$E^{\text{Ref.4}} - E$		τ (μ s)	$(\tau^x/\tau - 1) \times 100\%$	
			CS ^a	stab ^b		x=CS ^a	x=stab ^b
$X^3\Pi$	0	732.2	0.3	0.5	3.6 (18)	l	l
	1	2168.3	1.3 ^d	6.7 ^d	4.8 (5)	l	l
	c	2168.9	0.7 ^d		4.8 (5)		
	2	3548.5	1.0	1.7	6.9 (-1)	465 ^j	-12
	3	4883.3	1.1	1.8	1.1 (-3)	355 ^j	9
	4	6167.4	1.5	1.5	2.8 (-5)	329 ^j	1043 ^g
	5	7399.9	1.7	1.6	9.7 (-6)	55 ^j	-8
$a^1\Sigma^+$	0	2101.8	-0.4 ^d	37.0 ^{df}	2.9 (7)	l	l
	c	2101.2	0.1 ^d		2.5 (7)		
	1	4044.6	0.3	17.9 ^f	1.0 (2)	-95	-99 ^h
	c	4044.7	0.2		8.8 (1)	-94	
	2	5942.0	0.4	-0.8	3.8 (-1)	-61	-93 ^h
	c	5941.1	0.3		3.0 (-1)	-50	
	3	7796.5	-37.5 ^e	-11.9 ^f	5.6 (-2)	-99.6	-98 ^h
	c	7796.5	-37.5 ^e		1.4	-99.99	
$b^1\Pi$	0	5030.8	0.0	-0.2	5.1	351	63
	1	6511.5	-0.1	1.1	7.8 (-3)	-81 ^k	-97 ⁱ
	2	7959.1	-0.1	1.8	1.3 (-4)	-96 ^k	-92 ⁱ

TABLE AVIII: continued

^aThe complex scaling calculations of Ref. 4 in which the four-state model called here ‘the original JCP06’ model was used.

^bThe stabilization calculations of Ref. 4 which accounted additionally for two higher electronic states of the ion, $A^3\Sigma^+$ and $c^1\Delta$; the impact of these states on the lifetimes shown here is negligible, however.

^cResults obtained in this work using the original JCP06 model. The $^1\Sigma^+-^3\Sigma^-$ coupling, suppressed in the original model, contributes little (about 20%) to the lifetimes of the a ($v=0-2$) states.

^dObtained after relabelling of the energies given in Table III of Ref. 4 for the $X^3\Pi$ ($v=1$) and $a^1\Sigma^+$ ($v=0$) states. Apart from evidence provided by the present perturbative calculations the relabelling is strongly suggested by the comparison of the energy spacings $E_{v=1}(X)-E_{v=0}(X)$ and $E_{v=2}(X)-E_{v=1}(X)$ shown in Table III of Ref. 4 with the spectroscopic constants listed in Table A of that paper.

^eThere seems to be a missprint in the CS value given in Table III of Ref. 4.

^fRelatively large deviation suggesting that somewhat different potential V_a was used in the ‘stab’ calculations.

^gUnexpectedly large, perhaps related to the fact that the energy $E_{X v=4}$ nearly coincides with the crossing of the potentials V_X and $V_{3\Sigma^-}$. The present result is obtained by three different methods with relative deviations not exceeding 3%, see Tables I, IV, and AVI.

^hRather big discrepancy. Tests documented in Table AIX suggest a possible cause: the use in the ‘stab’ calculations of an effectively bigger coupling $a-X$, i.e. different from that presented in Fig. 2 of Ref. 4, in addition to the use of different potential V_a , as mentioned in footnote *f*.

ⁱThe origin of this discrepancy is unclear. Within the four-state model, above 95% of the width comes from the $b^1\Pi-^3\Sigma^-$ coupling, see Table AVI. Any reasonable modification of other couplings in the model, even as large as that described in Table AIX, can increase the width merely by a few per cent. A disturbance of order of 100% from the side of the higher state $A^3\Sigma^+$ is improbable.

^jLarge values of these deviations can not be explained by differences in the input potentials and couplings. They rather reflect some technical problems with the implementation of the CS method in Ref. 4.

^kCS calculations of Ref. 6 gave completely different lifetimes for these cases, deviating from the present accurate results for $b v=1$ and $v=2$ by 426 and 1054 %, respectively. The errors of the lifetimes obtained in those calculations for the levels b ($v=3-10$) are similarly large. It is evident that the CS method did not work properly in determining the lifetimes of the system.

^lNo method used in Ref. 4 was capable of determining the long lifetimes of these states.

TABLE AIX: Test of sensitivity of energies and widths of the lowest vibronic states of CO^{2+} to the strength of spin-orbit couplings. \tilde{E} and $\tilde{\Gamma}$ — results from the JCP06 model with the couplings $X^3\Pi-a^1\Sigma^+$ and $X^3\Pi-^3\Sigma^-$ multiplied by factors of 4 and 2^a , respectively, are compared to the values E and Γ listed in Tables I and II. $\tilde{\tau}(\tau)$ — lifetimes from the modified (unmodified) couplings are compared to the available experimental data, cf. Table AVIII and Table V in the paper. Lines marked with an asterisk concern $^{13}\text{C}^{16}\text{O}^{2+}$.

State	v	$\tilde{E}-E^b$	$\tilde{\Gamma}/\Gamma$	$\log_{10} \tilde{\tau}(\tau)/\tau^{\text{Exp}}$
$X^3\Pi$	0	-4.5	3.7 ^c	
	1	33.4	5.5	
	*	39.3	6.2	2.6 (3.4)
	2	-1.2	3.9	-0.1 (0.5) ^f
	3	0.5	4.0	
	4	-0.3	4.0	
$a^1\Sigma^+$	0	-35.2	10.3 ^d	
	*	-41.2	5.0 ^d	3.1 (3.8)
	1	-0.8	65.4	0.4 (2.2) ^g
	2	-0.7	76.4	
	3	1.0	0.0 ^e	
	4	0.2	3.6 ^e	
$b^1\Pi$	5	1.5	1.1 ^e	
	0	0.0	1.1	2.2 (2.3)
	1	0.0	1.0 ^h	

^aThe factors are chosen to make the strength of the multiplied JPC06 couplings comparable, in the curve-crossing region, to the strength of their older counterparts, generated in Ref. 10.

^bGiven in cm^{-1} .

^cThis ratio being close to 2^2 testifies on dominance of the direct $X \rightarrow ^3\Sigma^-$ pathway of decay.

^dWidths due to the indirect $a \rightarrow X \rightarrow ^3\Sigma^-$ decay depend sensitively on the position of the a state level relative to levels in the X state potential. The simple perturbative estimate $\tilde{\Gamma}/\Gamma \approx (4 \times 2)^2$ may not be good.

^eThe direct $a \rightarrow ^3\Sigma^-$ pathway of decay becomes dominant, see Fig. A2.

^fThe modification does not change essentially the consistency of τ with τ^{Exp} in this case.

^gThe significant improvement of $\tilde{\tau}/\tau^{\text{Exp}}$ over τ/τ^{Exp} is to note in this case.

^hAlmost insensitive to the modification, cf. footnote i in Table AVIII.

TABLE AX: Rotation-vibration states of $\text{CO}^{2+}(X^3\Pi)$ from the JP04r-v model. Analytical representation of rotational energies, $E^J(^3\Pi_\Omega)=E^0+B[J(J+1)+1-2\Omega(\Omega-1)]+C[J(J+1)+1-2\Omega(\Omega-1)]^2$. Parameters $E^0(\Omega^p, v)$, $B(\Omega^p, v)$, and $C(\Omega^p, v)$ (all in cm^{-1}) of fitting to the calculated values $E(X^3\Pi_{\Omega^p} J v)$ in the range $J=1-10$.

v	p	E^0			B			$C \times 10^6$		
		$\Omega=0^a$	$\Omega=1$	$\Omega=2^a$	$\Omega=0$	$\Omega=1$	$\Omega=2$	$\Omega=0$	$\Omega=1$	$\Omega=2$
$^{12}\text{C}^{16}\text{O}^{2+}$										
0	f	65.12	714.27	-63.27	1.640	1.560	1.495	-46	0	23
	e	64.86	b					-47		
1		65.13	2102.94	-63.30	1.607	1.531	1.468	-44	-1	21
		60.58			1.628	1.529		-95	5	
2		65.13	3437.45	-63.29	1.575	1.501	1.440	-42	-2	19
		65.09								
$^{13}\text{C}^{16}\text{O}^{2+}$										
0	f	65.11	698.60	-63.27	1.565	1.492	1.432	-40	-1	19
	e	64.85								
1		65.13	2057.59	-63.30	1.535	1.465	1.406	-38	-2	18
		61.97			1.546	1.463		-60	3	17

^aGiven relative to the value for $\Omega=1$.

^bEmpty space means that the number is identical to that listed above for f parity.

TABLE AXI: Rotation-vibration states of $\text{CO}^{2+}(X^3\Pi)$ from the JP04r-v model. Analytical representation^a of J dependence of the widths, $\Gamma^J(^3\Pi_\Omega)=\bar{\Gamma}[J(J+1)-\Omega]^{(\alpha+\beta J^\varepsilon)}$. Parameters $\bar{\Gamma}(\Omega^p, v)$ (in cm^{-1}), $\alpha(\Omega^p, v)$, $\beta(\Omega^p, v)$, and $\varepsilon(\Omega^p, v)$ of fitting to the calculated values $\Gamma(X^3\Pi_{\Omega^p} J v)$ in the range $J=1-10$. a) strong J dependence, b) weak J dependence.

a)	v	$\Omega^f = 0$				$\Omega^{f/e} = 2^b$				
		$\bar{\Gamma}$	α	β	ε	$\bar{\Gamma}$	α	β	ε	
$^{12}\text{C}^{16}\text{O}^{2+}$	0	1.791 (-16)	1.005	1.13 (-2)	1.38	1.387 (-17)	1.007	8.46 (-3)	1.51	
						1.392 (-17)	1.008	9.79 (-3)	1.49	
	1	4.259 (-10)	1.002	4.91 (-4)	1.78	1.916 (-10)	1.002	3.86 (-4)	1.82	
						1.920 (-10)	1.002	8.09 (-4)	1.67	
	2	6.348 (-7)	0.998	1.10 (-2)	-1.03	3.789 (-7)	0.995	1.55 (-2)	-0.71	
						3.819 (-7)	1.001	1.72 (-5)	2.47	
$^{13}\text{C}^{16}\text{O}^{2+}$	0	6.435 (-17)	1.006	1.10 (-2)	1.40	4.649 (-18)	1.008	8.29 (-3)	1.52	
						4.679 (-18)	1.006	9.82 (-3)	1.49	
	1	2.131 (-10)	1.003	6.29 (-4)	1.72	9.385 (-11)	1.002	5.14 (-4)	1.75	
						9.401 (-11)	1.002	9.20 (-4)	1.64	
	b)		$\Omega^e = 0$				$\Omega^{f/e} = 1$			
$^{12}\text{C}^{16}\text{O}^{2+}$	0					4.917 (-14)	0.005	1.00 (-2)	1.44	
			1.488 (-13)	0.006	1.18 (-2)	1.39	4.951 (-14)	0.003	1.37 (-2)	1.39
	1					2.783 (-7)	0.002	4.81 (-4)	1.77	
			3.349 (-7)	0.003	2.77 (-3)	1.44	2.792 (-7)	0.002	1.68 (-3)	1.57
	2					4.951 (-4)	-0.005	6.25 (-3)	-0.55	
			5.884 (-4)	0.002	8.67 (-4)	1.59	4.965 (-4)	0.001	5.85 (-4)	1.64
$^{13}\text{C}^{16}\text{O}^{2+}$	0					1.852 (-14)	0.007	9.53 (-3)	1.47	
			5.836 (-14)	0.008	1.12 (-2)	1.42	1.864 (-14)	0.005	1.29 (-2)	1.42
	1					1.499 (-7)	0.002	6.04 (-4)	1.72	
			1.923 (-7)	0.003	2.13 (-3)	1.52	1.504 (-7)	0.002	1.83 (-3)	1.54

^aNote, the representation is well justified for $\Omega=2$ and $\Omega^f=0$ states only (by the form of the matrix elements $C_{2,1}$ and $C_{0,1}$ of the S -uncoupling operator, see Eq. (8) in the paper. In the $\Omega=1$ and $\Omega^e=0$ cases, the widths are determined by the direct SO coupling with the respective Ω^p components of the $^3\Sigma^-$ state. The weak J dependence of these widths is demonstrated in part b) by smallness of the parameter α .

^bData for e parity states are in the lower lines.

TABLE AXII: Energies and widths of shape resonances from the JP04 potential of the $X^3\Pi$ state of CO^{2+} . Comparison of quantum-mechanical perturbative (TP) and non-perturbative (SQ) results with the semiclassical results obtained in this work and in Ref. 5. All entries are given in cm^{-1} except for the relative deviations $\delta\Gamma(x/y)\equiv(\Gamma^x/\Gamma^y-1)\times 100\%$.

v	TP			TP vs SQ		$\delta\Gamma(\text{Ref. 5}/y)$	
	E^a	Γ	E^{shf}	ΔE^b	$\delta\Gamma^c$	$y=\text{SQ}$	$y=\text{qSC}^d$
0	715.29	4.51 (-56)	-2.67 (-28)	1 (-7)	0.0000	-7.5	-0.8
1	2103.96	5.81 (-48)	-7.34 (-25)	1 (-7)	0.0000	-3.4	-0.7
2	3438.47	8.99 (-41)	-8.83 (-22)	5 (-7)	-0.0000	-2.2	-0.6
3	4722.21	2.71 (-34)	-6.36 (-19)	5 (-7)	-0.0000	-1.8	-0.5
4	5952.43	1.97 (-28)	-3.03 (-16)	4 (-7)	-0.0000	-1.6	-0.4
5	7129.05	4.12 (-23)	-1.02 (-13)	9 (-6)	-0.0000	-1.5	-0.5
6	8249.49	2.75 (-18)	-2.50 (-11)	2 (-6)	-0.0001	-1.7	-0.5
7	9311.67	6.48 (-14)	-4.62 (-9)	7 (-7)	-0.0003	-2.0	-0.5
8	10313.21	5.88 (-10)	-6.65 (-7)	1 (-6)	-0.0009	-1.8	-0.5
9	11249.14	2.16 (-6)	-7.97 (-5)	3 (-6)	-0.0042	-1.9	-0.5
10	12111.36	3.15 (-3)	-9.03 (-3)	3 (-6)	-0.0296	-2.2	-0.7
11	12879.76	1.55	-6.18 (-1)	2 (-3)	0.3042	-2.9	-3.1

^aObtained as $E_v^{(0)} + E_v^{\text{shf}}$, where $E_v^{(0)}$ denotes the energy of related bound state in the respective inner potential U , cf. Eq. (26) in the paper, and E_v^{shf} , shown in the fourth column, is evaluated from Eq. (31).

^b $E^{\text{TP}} - E^{\text{SQ}}$. Note, $\Delta E \gg |E^{\text{shf}}|$ in low v cases, reflecting merely the accuracy of the energies E^{SQ} and $E^{(0)}$ that was achieved in double-precision calculations.

^c $\delta\Gamma(x/y)$ for $x=\text{TP}$ and $y=\text{SQ}$ method.

^dObtained by applying the Gamow formula at energy $E^{(0)}$.

TABLE AXIII: Same as Table AXII for the potential of $\text{CO}^{2+}(b^1\Pi)$.

v	Γ^a	$\delta\Gamma(\text{x/SQ})$		$\delta\Gamma(\text{Ref. 5/y})$		E	$\Delta E(\text{x-y})$	
	cm^{-1}	x=TP^b	SC^c	y=SQ	SC^c	cm^{-1}	SQ-TP	SQ-SC^d
0	8.94(-224)	0.000	-0.2			4938.11	-4(-7)	0.10
1	1.59(-199)	0.000	-0.3			6391.44	9(-7)	0.12
2	4.10(-178)	0.000	-0.3			7810.29	-1(-6)	0.14
3	5.70(-159)	0.000	-0.4			9194.65	2(-7)	0.17
4	1.11(-141)	0.000	-0.0			10544.56	2(-7)	0.07
5	7.16(-126)	0.000	-0.4			11860.08	-1(-6)	0.07
6	5.51(-111)	0.000	9.4			13141.25	-2(-6)	0.21
7	2.93(-97)	0.000	-2.4			14388.22	-1(-6)	0.39
8	1.31(-85)	0.000	-2.1			15601.02	-3(-6)	0.51
9	2.22(-75)	0.000	-1.5			16779.70	-3(-6)	0.52
10	4.10(-66)	0.000	-0.8	0.2	1.0	17924.22	-5(-6)	0.45
11	1.24(-57)	0.000	-0.3	0.5	0.8	19034.49	-4(-6)	0.35
12	7.05(-50)	0.000	-0.0	-0.6	-0.6	20110.28	-5(-6)	0.25
13	8.14(-43)	0.000	-0.1	-1.1	-1.1	21151.23	-6(-6)	0.20
14	2.07(-36)	0.000	-0.5	-1.7	-1.2	22156.81	1(-6)	0.13
15	1.35(-30)	0.000	-0.7	-2.2	-1.5	23126.45	-2(-5)	0.09
16	2.78(-25)	0.000	5.0	3.1	-1.8	24059.30	-1(-5)	0.08
17	1.44(-20)	0.000	-4.0	-5.8	-1.8	24954.28	-7(-7)	0.05
18	1.71(-16)	0.000	-6.3	-8.1	-2.0	25809.84	-2(-5)	-0.04
19	9.39(-13)	0.000	-3.5	-5.5	-2.2	26623.63	-2(-5)	-0.10
20	3.30(-09)	-0.007	-2.2	-4.6	-2.4	27391.74	-9(-6)	-0.31
21	8.31(-06)	-0.008	-0.2	-2.8	-2.6	28107.59	-2(-5)	-0.44
22	1.69(-02)	-0.038	15.4	11.9	-3.0	28758.42	-3(-5)	-0.65
23	1.52(+01)	-0.610	-23.5	-24.4	-1.1	29308.57	-6(-1)	-1.14

^aThe widths of $v=0-6$ levels are affected by the extrapolation of the potential; the outer turning points are larger than the last *ab initio* point available from Ref. 5.

^b0.000 in this column denotes TP and SQ values of Γ identical at all five significant figures determined.

^c Γ_v^{SC} evaluated according to Eqs. (4.5)–(4.6) of Ref. 2. Applied is also the correction of Ref. 3.

^d E_v^{SC} is obtained from the generalized Bohr-Sommerfeld quantization condition, Eq. (4.2) of Ref. 2.

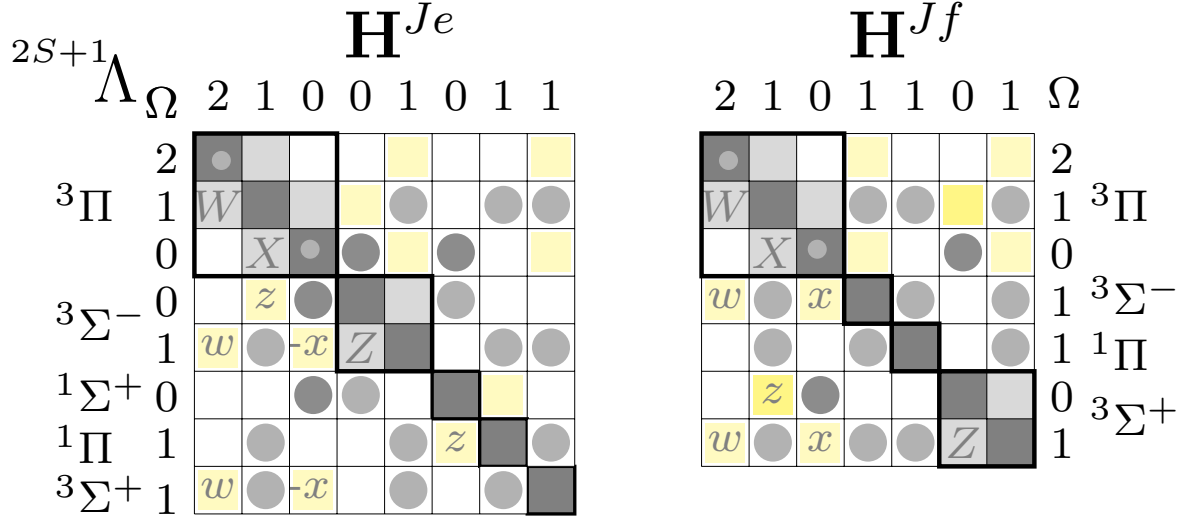


Fig. A1

The structure of the Hamiltonian matrices used in the calculations on rotation-vibration states of CO^{2+} (the JP04r-v model, Eqs. (2)–(8) in the paper). Dark squares represent all the diagonal terms of the matrices except for the SO terms ($\pm A_{\Pi}$) which are shown explicitly by the small gray circles. Large circles denote the SO couplings; with darker gray color are marked the ones multiplied by $\sqrt{2}$. Light gray squares represent the rotational couplings included into the model (the \mathbf{S} uncoupling perturbations only);

$$X \equiv -\frac{\sqrt{2J(J+1)}}{2\mu R^2}, \quad Z = \sqrt{2}X, \quad \text{and} \quad W \equiv -\frac{\sqrt{2J(J+1)-4}}{2\mu R^2}.$$

The yellow squares in the scheme denote the \mathbf{L} uncoupling terms which were used in the part of calculations aimed at testing the reliability of the lifetime predictions by the JP04r-v model (cf. Table VII and Fig. 8). The terms denoted here by x , z , and w can be found⁷ to satisfy

$$\frac{x}{X} = \frac{z}{Z} = \frac{w}{W} = \frac{\langle \Pi | L^+ | \Sigma \rangle}{\sqrt{2}} \equiv \mathcal{S}.$$

No information on the electronic matrix element(s) $\langle \Pi | L^+ | \Sigma \rangle$, determining the relative strength of the two kinds of perturbations, is available for CO^{2+} . Thus, setting $\mathcal{S}=1$ was the first natural choice to make. Moreover, it was believed that this choice would impose a rather stringent test on the adequacy of the JP04r-v model. Indeed, some information available on the magnitude of rotational perturbation parameters in other systems⁷, like N_2^{2+} ⁸, indicates that the ‘true’ factor(s) \mathcal{S} may be much smaller than 1.

COMMENT

supplementing the discussion of Sec. IVD

A comparison of the present matrices \mathbf{H}^{Je} and \mathbf{H}^{Jf} with those specified in Tables I and II of Ref. 6 reveals:

- The terms z and Z do not appear in the rotational couplings of Ref. 6. The smaller terms x and X , respectively, are used instead. A consequence of that is the rather large energy splitting (of the size of several cm^{-1}) between the F_i components of the states $A^3\Sigma^+ v N$ which is seen in Table VIII of that paper.
- The formulas of Ref. 6 do not respect the $\Delta\Omega=0$ selection rule for SO interactions. This fact might possibly contribute to the anomalous behavior of lifetimes calculated in that work for the $A^3\Sigma^+$ state levels. However, some tests (performed in this work using the JP04 potentials) indicate that it could not be the main cause.

CO²⁺

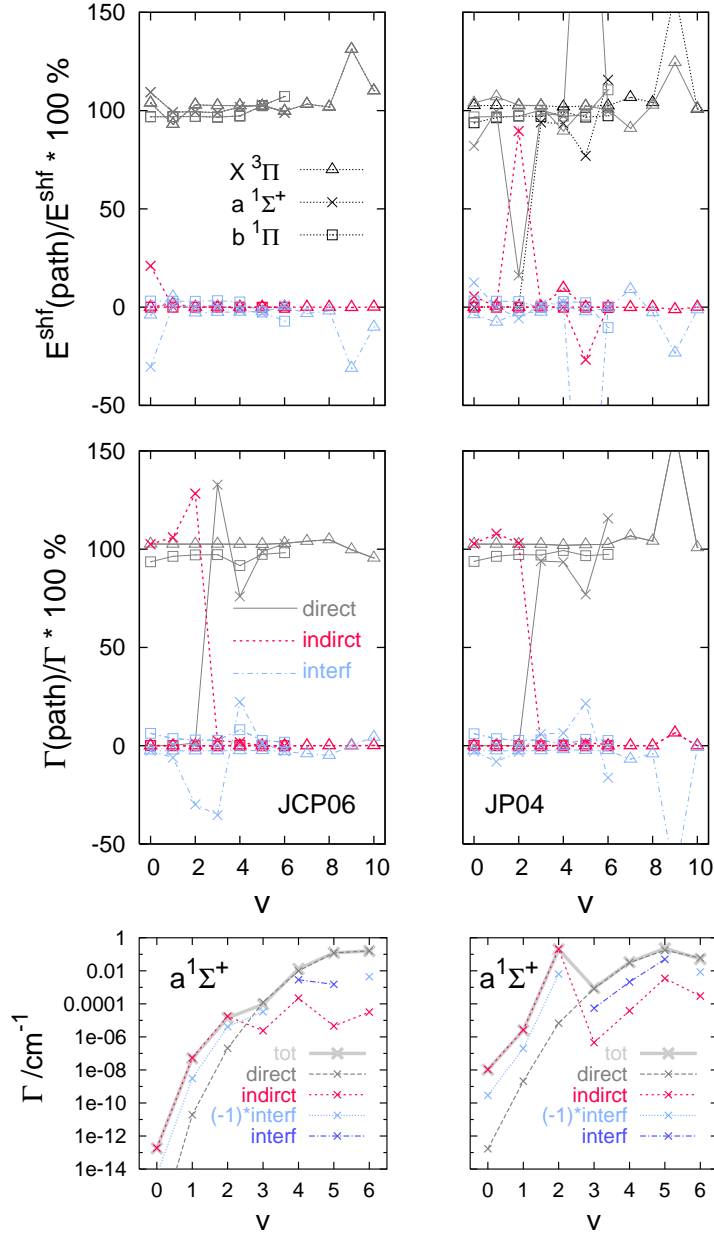


Fig. A2

Energy shifts and widths of 25 lowest vibronic states of CO²⁺ (all states have energies below the barrier top of V_X). Perturbative results from the JCP06 and JP04 models — contributions of different paths of mixing between the $Q=\{X, a, b\}$ and $P=\{^3\Sigma^-\}$ subspaces. The values of E^{shf} and Γ from the JCP06 model can be found in Tables I and II. The corresponding values from the JP04 model are given in Tables AIII and AIV. In the bottom panels: absolute values of $\Gamma(\text{direct})$, $\Gamma(\text{indirect})$, and $\Gamma(\text{interference})$ for the states $a^1\Sigma^+ v=0-6$.

cf. Fig. A2

DEFINITIONS
of 'direct', 'indirect', and 'interference' parts
of level widths and shifts

Let us rewrite the CM formulas, Eqs. (30) in the paper, in the following, more explicit, way

$$E_i^{\text{shf}} - i\frac{1}{2}\Gamma_i \approx \sum_{\tilde{s} \in \text{P}} \sum_{s' \in \text{Q}} \sum_{s'' \in \text{Q}} \langle \Phi_{s'}^i | V_{s', \tilde{s}} G_{\tilde{s}, \tilde{s}}^{(+)} V_{\tilde{s}, s''} \Phi_{s''}^i \rangle, \quad (\text{A1})$$

where Φ_s^i denotes a component of the bound state function in the Q subspace, $[E_i^{(0)} \mathbf{I}_Q - \tilde{\mathbf{H}}_{\text{QQ}}] \Phi_i = 0$, and $G_{\tilde{s}, \tilde{s}}^{(+)}$ is an element of the matrix Green function $\mathbf{G}_{\text{P}}^{(+)}(E) \equiv [E^+ \mathbf{I}_{\text{P}} - \mathbf{H}_{\text{PP}}]^{-1}$ at $E = E_i^{(0)}$; off-diagonal elements of this matrix do not appear here in consequence of neglecting the couplings in the P subspace. Obviously, the index i is a label of vibronic state under consideration, $i \equiv (sv)$ with $s \in \text{Q}$.

The terms of the first sum for the width have the meaning of partial widths, i.e.

$$\Gamma_i = \sum_{\tilde{s} \in \text{P}} \Gamma_{i \rightarrow \tilde{s}} \quad \text{with} \quad \Gamma_{i \rightarrow \tilde{s}} \approx 2\pi \sum_{s'} \sum_{s''} \langle \Phi_{s'}^i | V_{s', \tilde{s}} \Psi_{\tilde{s}}^{(+)\tilde{s}} \rangle \langle \Psi_{\tilde{s}}^{(+)\tilde{s}} | V_{\tilde{s}, s''} \Phi_{s''}^i \rangle.$$

The terms of the two sums over states in the Q subspace (s' and s'') can be divided into the following three groups, each describing a different path of bound-continuum configuration mixing or resonance decay,

$$\begin{aligned} \{ \text{terms with } s' = s'' = s \} &\equiv \text{'direct' path} \\ \{ \text{terms with } s' = s'' \neq s \} &\equiv \text{'indirect' path} \\ \{ \text{terms with } s' \neq s'' \} &\equiv \text{'interference' path}. \end{aligned} \quad (\text{A2})$$

This leads to the resolutions

$$E_{sv}^{\text{shf}} = \sum_{\text{path}} E_{sv}^{\text{shf}}(\text{path}) \quad \text{and} \quad \Gamma_{sv \rightarrow \tilde{s}} = \sum_{\text{path}} \Gamma_{sv \rightarrow \tilde{s}}(\text{path}). \quad (\text{A3})$$

COMMENTS

- The states $b^1\Pi v=0-6$ decay almost entirely along the direct pathway, $92 < \frac{\Gamma(\text{dir})}{\Gamma} < 99.5\%$ and $\frac{\Gamma(\text{indir})}{\Gamma} < 0.2\%$.
- For most of the states $X^3\Pi v=0-10$, $\frac{\Gamma(\text{dir})}{\Gamma} \approx 103\%$ and $\frac{\Gamma(\text{interf})}{\Gamma} \approx -3\%$.
- The large involvement of interference path for $v=9$, displayed in the middle right panel of the figure, stems from the presence of the nearby state $a^1\Sigma^+ v=5$ (the second closest approach of two energy levels in the JP04 model).
- Only the three lowest $a^1\Sigma^+$ state levels, $v=0-2$, appear to predissociate indirectly. The relation $\Gamma(\text{indir}) \gg \Gamma(\text{dir})$ which characterizes these cases becomes reversed already for the next a state level, $v=3$.

- In the JCP06 model, the transition from indirect to direct predissociation is accompanied by a significant participation of the interference terms $\Gamma_{av}(\text{interf})$ for $v=2-4$. No counterpart effect is observed in the JP04 model. This is certainly related to the fact that the mixing within the Q subspace, of bound states supported by the individual potentials U_X , U_a , and U_b , is quite different in the two models (despite identical SO couplings). The crucial factors are the different relative positions of the X and a state energy levels. The distance between the closest levels from the JCP06 potentials, $E_{X v=1}^{(0)}$ and $E_{a v=0}^{(0)}$, is about 42 times larger than the smallest distance between levels from the JP04 potentials $E_{X v=4}^{(0)} - E_{a v=4}^{(0)} = 1.4 \text{ cm}^{-1}$.
- The different intra Q subspace mixing in the two models manifests itself even more clearly in the resolutions of the shifts E_{av}^{shf} plotted in the upper panels.

CO²⁺

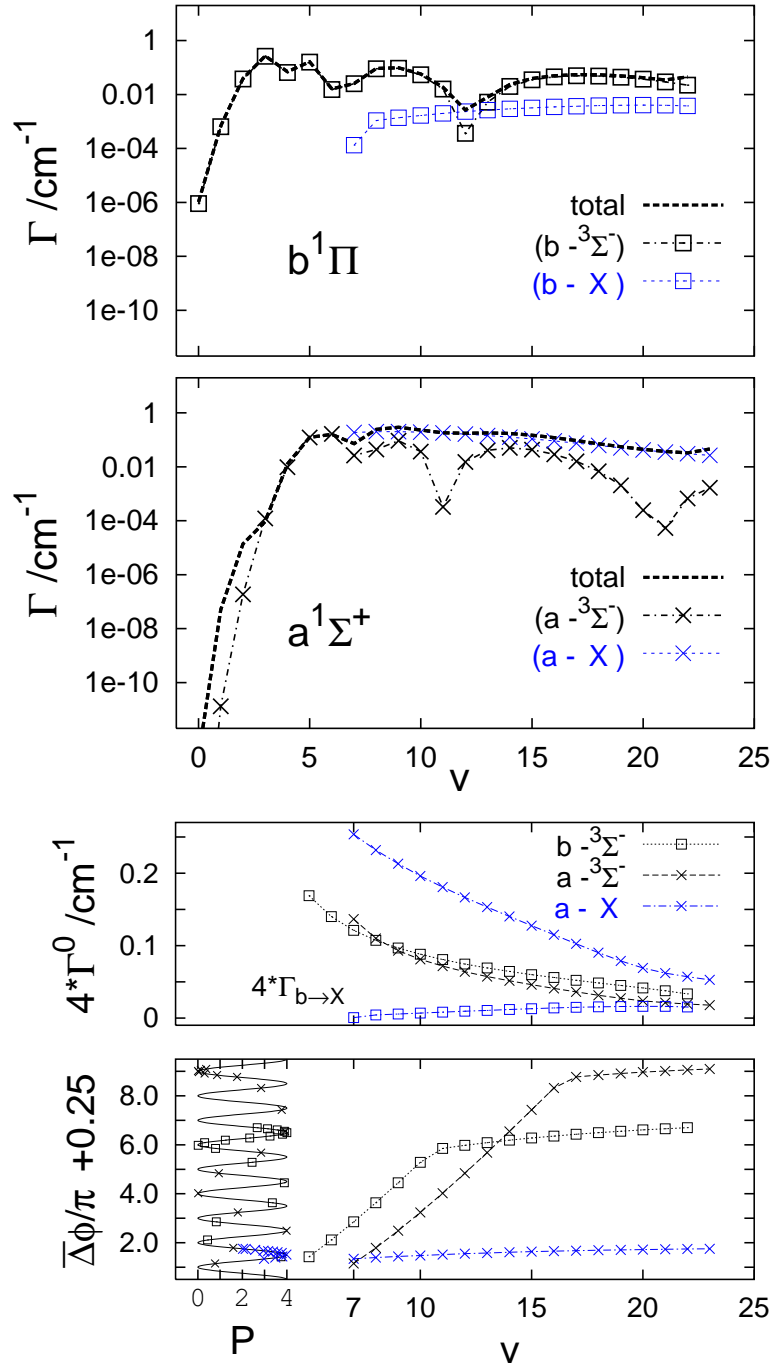


Fig. A3

Level widths from the JCP06 model, total and partial $\Gamma_{s\nu \rightarrow \tilde{s}}$ for $s=b^1\Pi$, $a^1\Sigma$ and $\tilde{s}=^3\Sigma^-$, $X^3\Pi$

Fig. A3 *continued*

In the upper panels: 'Exact' results for the total widths Γ_{bv} and Γ_{av} , perturbative quantum-mechanical results for the widths $\Gamma_{bv \rightarrow X}$, and semiclassical results for the widths $\Gamma_{bv \rightarrow 3\Sigma^-}$, $\Gamma_{av \rightarrow 3\Sigma^-}$, and $\Gamma_{av \rightarrow X}$, due to the curve-crossings.

In the lower panels: the factors Γ_v^0 and P_v of the semiclassical widths for v levels above the energies of the crossings. The factors are defined in Eq. (32) of the paper. The definition of the quantity $\xi(E)$ for energies above the crossing point is quoted in the comment to Fig. A5, Eq. (A7). For levels lying sufficiently above the crossing point, the factor P_v takes an approximate form

$$P_v \approx 4 \sin^2 ph_v \quad \text{with} \quad ph_v = \bar{\Delta}\phi(E_v^{\text{BS}}) + 0.25\pi.$$

(see Eq. A6 for definition of $\bar{\Delta}\phi$).

ANALYSIS of PARTIAL WIDTHS

in terms of the factors Γ_v^0 and P_v

- As to the relations between the widths due to the $a-3\Sigma^-$ and $a-X$ crossings,

$$\Gamma_{av \rightarrow X} > \Gamma_{av \rightarrow 3\Sigma^-};$$

Both $\Gamma_v^0(a-3\Sigma^-)$ and $\Gamma_v^0(a-X)$ are monotonically decreasing functions of v in the range shown. Any difference between them can stem only from the curve-crossing parameter p_v^{LZ} . The v -independent ingredient of this parameter, $V_{1,2}^2(r_c)/\Delta F$, is about 1.5/0.43 times larger in the $a-X$ case. The actual ratios $p_v^{\text{LZ}}(a-X)/p_v^{\text{LZ}}(a-3\Sigma^-)$ are slightly smaller ($\sim 1.9-3.0$) because of larger velocities $u_v(r_c)$ in the same $(a-X)$ case. The phases ph_v pertaining to the crossings $a-X$ and $a-3\Sigma^-$ both grow monotonically with v but with distinctly different speeds. Whereas the phase $ph_v(a-X)$ increases between $v=7$ and $v=23$ by less than 0.5π , the increase of the phase $ph_v(a-3\Sigma^-)$ in the same range is close to 8π . This obviously causes distinct (smooth vs oscillatory) variation with v of the respective factors $P_v(a-X)$ and $P_v(a-3\Sigma^-)$.

- As to the widths due to the $b-3\Sigma^-$ and $a-3\Sigma^-$ crossings;
The two crossings are of the same type. The similarity is best exposed in the shapes of the respective functions ph_v in the bottom panel. The widths are of similar size; this stems from nearly identical values of the respective factors Γ_v^0 for $v \geq 7$, as seen in the third panel.
- The widths $\Gamma_{bv \rightarrow X}$ for $v \geq 7$ due to the SO coupling between the non-crossing potentials V_b and V_X do not oscillate with v . Therefore, in order to compare with the oscillating widths $\Gamma_{bv \rightarrow 3\Sigma^-}$, it is convenient to use the Γ_v^0 parts of the latter. Such comparison is made in the third panel of the figure.

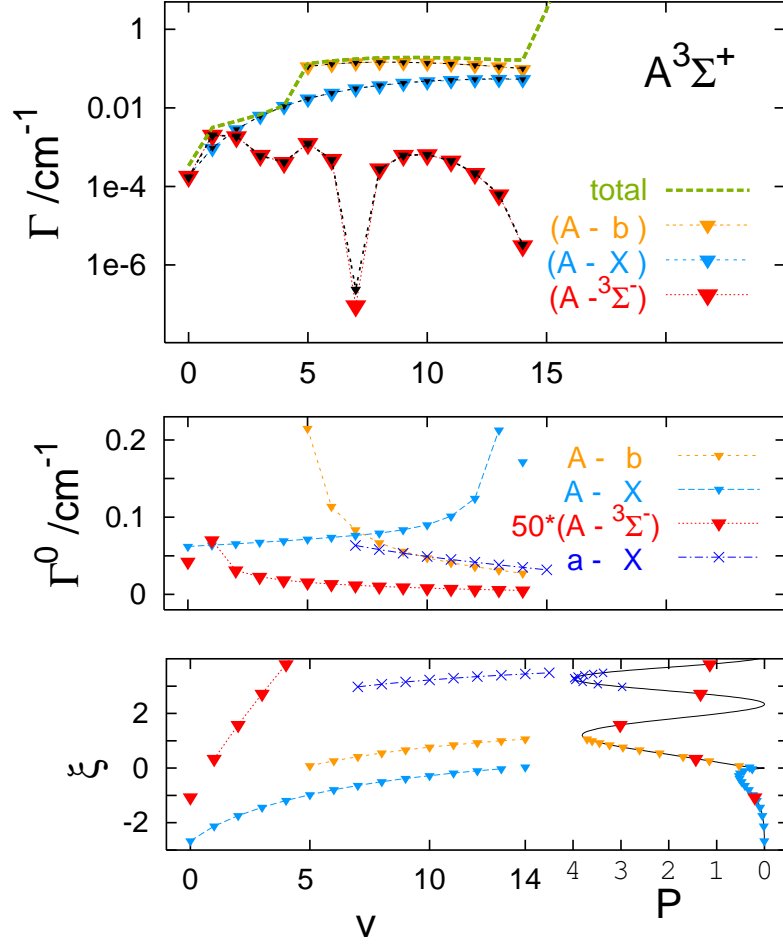


Fig. A4

Level widths from the JP04A model: Γ_{Av} and $\Gamma_{Av \rightarrow \tilde{s}}$ for $\tilde{s} = {}^3\Sigma^-$, $X {}^3\Pi$, and $b {}^1\Pi$

Upper panel: Perturbative quantum-mechanical results using $Q = \{A\}$ and $P = \{\tilde{s}\}$ (color triangles) and semiclassical results for the $A-\tilde{s}$ crossings (small black triangles), see Table AV.

Lower panel: Resolutions of the semiclassical results into Γ_v^0 and P_v factors defined in the paper, Eq. (32). Note, the factors Γ_v^0 pertaining to $A-{}^3\Sigma^-$ are magnified 50 times. For comparison shown are also the factors that pertain to the c^i type crossing $a-X$ analyzed in Fig. A3.

CO²⁺

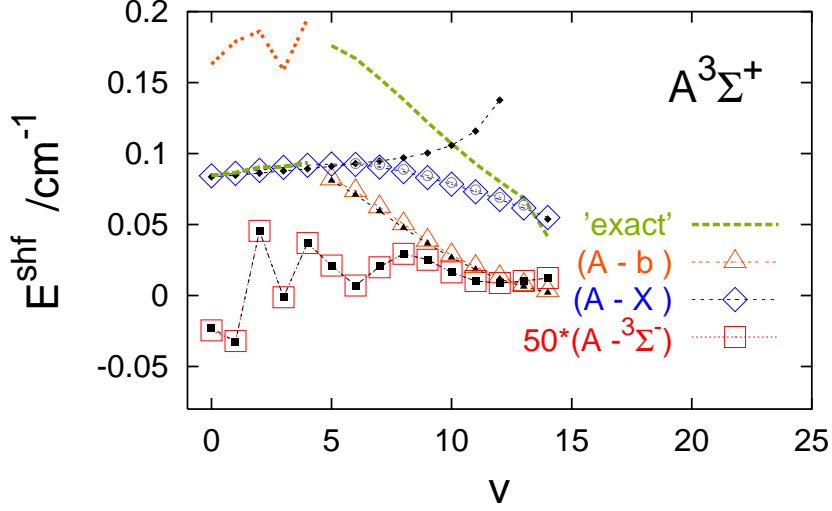


Fig. A5

Level shifts from the JP04A model

‘exact’ means the shift between E_v — the energy of the state $A^3\Sigma^+ v$ obtained in four-channel Siebert quantization calculations and $E_v^{(0)}$ — the energy of related bound state in the subspace $Q=\{b, A\}$ for $v=0-4$ and $Q_1=\{A\}$ for $v\geq 5$. The open (color) symbols represent shifts obtained in two-channel calculations within the CM approach using $Q_1=\{A\}$ and $P=\{\tilde{s}\}$ for $\tilde{s}={}^3\Sigma^-$, $X^3\Pi$, and $b^1\Pi$. Note, the values of E_v^{shf} from $Q_1+P=\{A\}+{{}^3\Sigma^-}$ calculations are magnified 50 times. The energy shifts due to the $A-b$ coupling, accounted for exactly in the subspace $Q=\{b, A\}$, are equal to the distances between the dotted orange and dashed green lines at $v=0-4$. The small full symbols show results of application of the semiclassical (SC) formulas of Ref. 9 to the three $A-\tilde{s}$ curve-crossings, with $\tilde{s}={}^3\Sigma^-$, $X^3\Pi$, and $b^1\Pi$. The crossings occur at points $r_c\approx 2.3, 1.8,$ and $1.9 a_0$, and at energies $E_{v=0}<V_A(r_c)<E_1$, $E_{13}<V_A(r_c)<E_{14}$, and $E_4<V_A(r_c)<E_5$, respectively.

COMMENT on Fig. A5

The divergence which is seen in the figure between the SC and CM energy shifts due to the $A-X$ crossing reflects a difficulty associated with the term $E_v^{\text{shf}(1)}$ of the semiclassical formulas, Eq. A4 below. The term loses its original meaning when r_1 becomes too close to the crossing point $r_c \approx 1.8 a_0$; a part of the integration range near r_1 becomes then severely outweighed by the large factor $[V_2(r) - V_1(r)]^{-1} \equiv [\Delta V(r)]^{-1}$ of the integrand. The circles, inside the blue squares, represent results obtained after a simple modification of this factor: $\Delta V_{\text{mod}} = \Delta V(r_{1;v=6})$ for $r \leq r_{1;v=6}$, where $r_{1;v=6} = 1.88 a_0$ denotes the left turning point in the potential V_A at $E = E_{v=6}^{\text{BS}}$. The problem with $E_v^{\text{shf}(1)}$ occurs also in the case of the inner crossing $A-b$ at the energy $V_A(r_c \approx 1.9 a_0)$ just above the barrier top of the potential V_b . In this case, the inaccuracies are less visible since the shifts are dominated by the term $-E_v^{\text{shf}(2)}$ (Eq. A5, the minus sign is necessary for an inner crossing⁹).

SEMICLASSICAL FORMULAS for LEVEL SHIFTS of Ref. 9

In the notation introduced in Sec. IIIC of the paper ($V_A \equiv V_1$ and $V_b \equiv V_2$), the formula for the shifts of levels lying below $V_1(r_c)$ reads

$$E_v^{\text{shf}} = -\frac{2}{T_v} \int_{r_1}^{r_2} \frac{V_{12}^2(r)}{[V_2(r) - V_1(r)]^{\frac{\hbar}{\mu}} k_1(r, E_v^{\text{BS}})} dr \equiv E_v^{\text{shf}(1)}. \quad (\text{A4})$$

For levels above the crossing-points,

$$E_v^{\text{shf}} = E_v^{\text{shf}(1)} + E_v^{\text{shf}(2)}. \quad (\text{A5})$$

Taking the principal value of the integral in the term $E_v^{\text{shf}(1)}$ becomes necessary because of singularity of the integrand at $r=r_c$. The term

$$E_v^{\text{shf}(2)} = -2\pi\Gamma_v^0 \sqrt{\xi_v} \text{Ai}(-\xi_v) \text{Bi}(-\xi_v) \quad (\text{A6})$$

causes the oscillations of the shifts with changing v since it involves the Airy functions Ai and Bi for negative arguments. The positive quantity ξ_v is defined as $\xi_v = \xi(E_v^{\text{BS}})$, where

$$\xi(E) = \left[\frac{3}{2} \bar{\Delta}\phi(E) \right]^{2/3} \quad (\text{A7})$$

with $\bar{\Delta}\phi$ denoting the smaller of the phase differences

$$\int_{r_1}^{r_c} k_1 dr - \int_{r_3}^{r_c} k_2 dr \quad \text{and} \quad \int_{r_3}^{r_c} k_2 dr + \int_{r_c}^{r_2} k_1 dr.$$

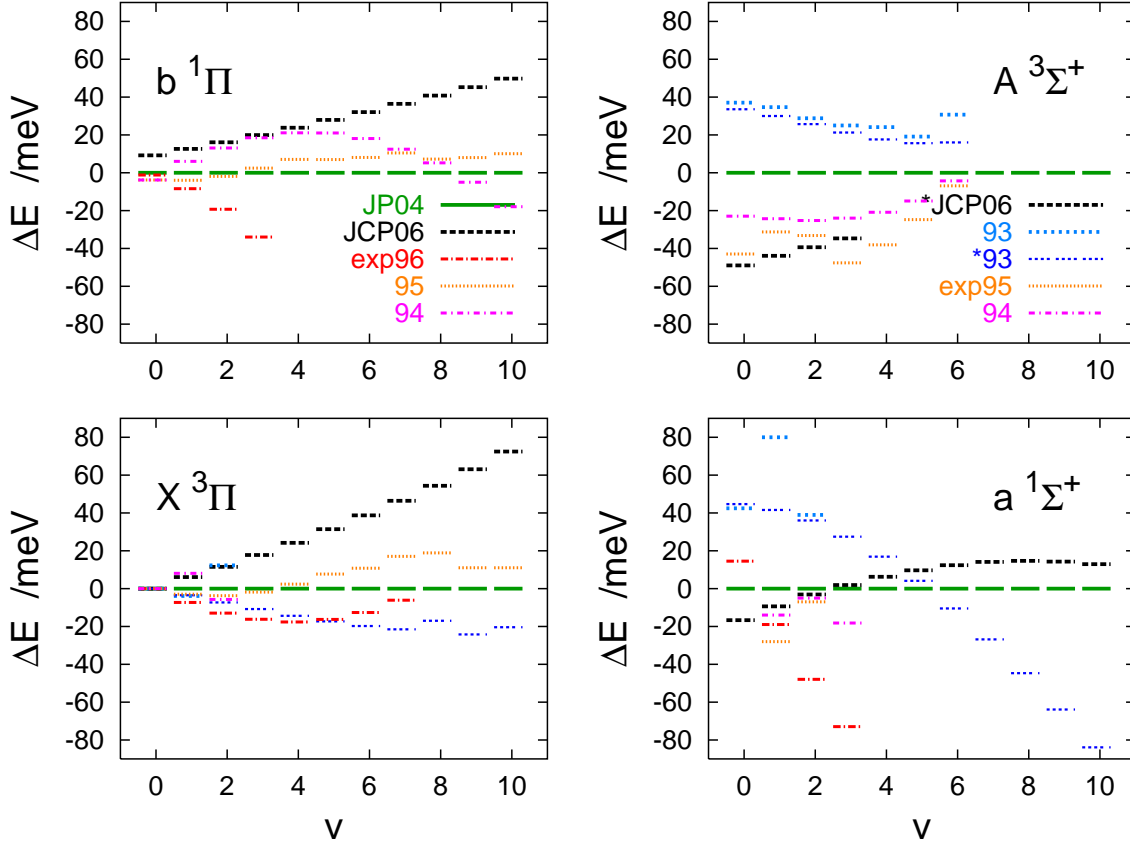


Fig. A6

Comparison of calculated and measured vibronic energies of CO^{2+}

Considered are the energies relative to the position of the lowest level, $E_{sv} - E_{Xv=0} \equiv \bar{E}_{sv}$ for $s=X, b, a, A$, and plotted are the deviations: $\Delta E_{sv} \equiv \bar{E}_v - \bar{E}_v(\text{JP04})$. ‘JP04’ stands for energies calculated from the potentials of Ref. 5. The values of $\bar{E}_{sv}(\text{JP04})$ (represented here by the green $\Delta E_{sv}=0$ lines) can be obtained from Tables AIII and AIV. ‘JCP06’ denotes energies calculated (in this work) from the potentials of Ref. 4. ‘*JPC06’ in the upper right panel denotes the energies obtained in Ref. 6. ‘93’ and ‘*93’ denote the energies calculated in Ref. 11 from the potentials of Ref. 10 and from the potentials referred to ‘Larsson (1993)’, respectively. The values of \bar{E}_{bv} from these potentials are about 170 meV smaller than the ‘JP04’ values; hence, the absence of the ‘93’ lines in the upper left panel. ‘exp96’, ‘94’, and ‘95’ denote the experimental results from Refs. 13, 11, 12, respectively. Since the state $X^3\Pi v=0$ was not observed in the latter work, the extrapolated value of 41.298 eV was used for its vertical energy to obtain the energies \bar{E}_{sv} of the higher observed states.

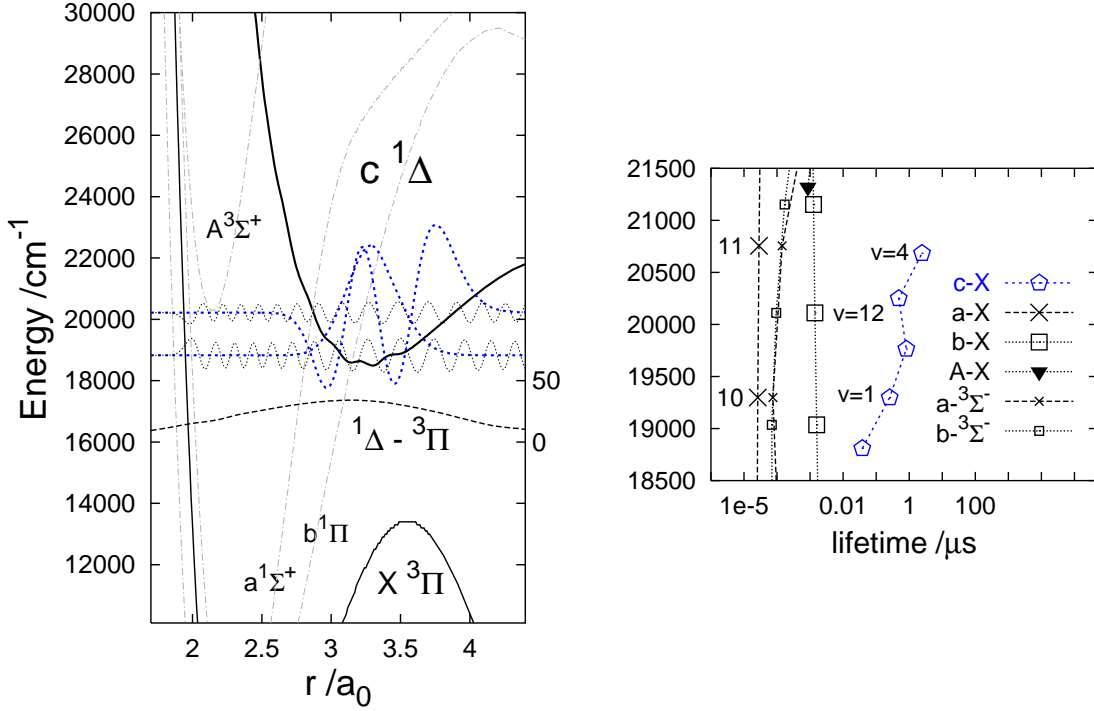
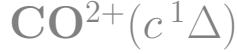


Fig. A7

Predissociation lifetimes of vibrational levels of CO^{2+} in the $c^1\Delta$ state.
A crude estimation

COMMENT

The model used in the calculations accounts for the SO coupling with the state $X^3\Pi$; the coupling is reproduced from Fig. 2 of Ref. 4. The potentials are from Ref. 5. Cubic spline interpolation between the *ab initio* points listed in Table 4 of Ref. 5 gives a rather low quality curve for the state c (un-smooth around the minimum, undetermined outer part of the barrier). Thus, lifetimes of $v \geq 6$ levels could not be calculated (tunneling prevails) and the predissociation lifetimes obtained for the lower levels can be reliable only as to their overall magnitude. They are generally in the μs range, evidently larger than lifetimes of other levels in the same energy range, $a^1\Sigma^+$ $v=10, 11$, $b^1\Pi$ $v=11-13$, and $A^3\Sigma^+$ $v=0$. Note, the partial lifetimes for decay into the X and $^3\Sigma^-$ channels are shown separately for the a and b state levels. Obviously, the relations between the lifetimes of levels in the different potentials can be rationalized with the help of the Golden Rule formula. Because of similar size of the couplings $s-X$ for $s=a, b, c, A$ (see also Fig. 2), the discrimination stems from overlapping between the bound and continuum functions which oscillate with similar or disparate frequencies.

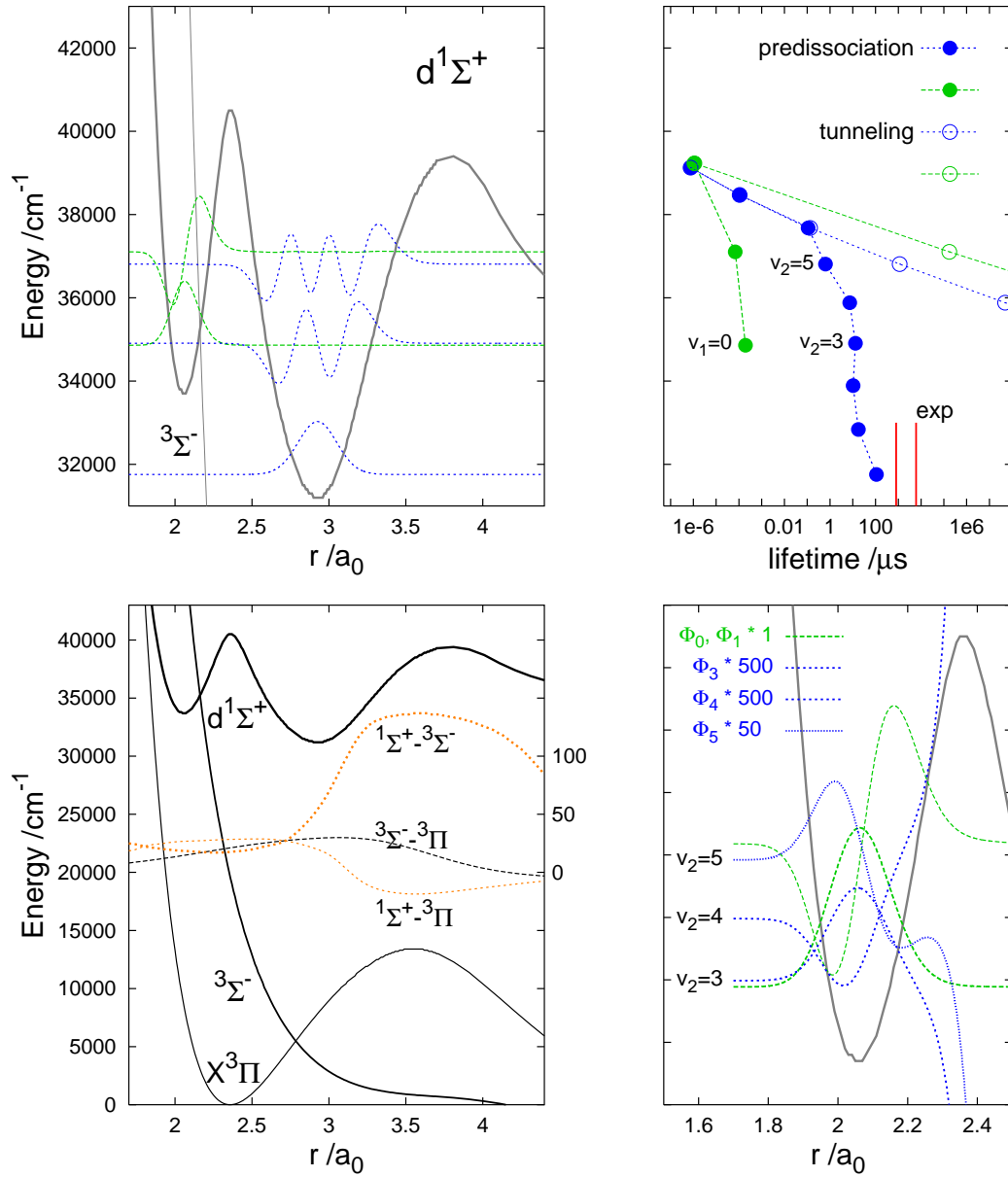
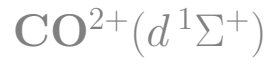


Fig. A8

Results of test calculations for predissociation and tunneling lifetimes of vibrational levels of $^{13}\text{C}^{16}\text{O}^{2+}(d^1\Sigma^+)$.

COMMENT

The tests are presented in connection with the original hypothesis of Ref. 10 that tunneling through the two barriers of the potential $d^1\Sigma^+$ might be the mechanism responsible for the observed lifetimes in the millisecond range. The potentials and couplings used in the calculations are shown in the bottom panel. The potentials are taken from Ref. 5 and the couplings are from Ref. 4. Since no SO coupling curve involving the state $d^1\Sigma^+$ is available, the respective curves for the state $a^1\Sigma^+$ are used instead (indicated by orange color). In the range of $r > 4.5a_0$, the potential $d^3\Sigma^+$ is extrapolated, somewhat artificially, with the curve $C+1/r$. This affects the tunneling lifetimes of the lowest levels and therefore these lifetimes are not shown here. It should nevertheless be evident from the two upper panels of the figure that tunneling is a rather unfavorable decay route for the two inner-well levels $v_1=0$ and $v_1=1$ which had probably the largest chances to be populated in the experiment of Ref. 10. These levels decay fast by spin-orbit predissociation which is obviously facilitated by the crossing with the state $^3\Sigma^-$. Lifetimes below 1 ns characterize this decay. However, some tiny fraction of ions excited to the $d^1\Sigma^+$ $v_1=1$ level may choose the tunneling pathway. Their lifetime would be about 170 ms, i.e. somewhat too big to account for the measured value of 6 ms. It should be added, however, that this lifetime is enormously sensitive to the barrier shapes, thus its reduction by a factor of 10 due to some refinements of the potential is quite likely.

Yet another hypothesis may be considered. An inspection of amplitudes of the vibrational functions within the inner well (the bottom right panel) indicates that the probability of populating the outer-well levels by vertical transition from ground state CO to the inner well and subsequent tunneling through the inner barrier could be non-negligible (like 1/50–1/500). Predissociation of these levels is relatively slow. Lifetimes of the size of 13, 7, and 0.6 μs are obtained for $v_2=3, 4,$ and 5, respectively. These lifetimes are also determined by interaction with the state $^3\Sigma^-$. It is likely that accounting for true coupling $d^1\Sigma^+ - ^3\Sigma^-$ will enlarge all the predissociation lifetimes shown in the upper right panel and those concerning v_2 levels will thus become closer to the red sticks denoting the experimental values. For now, however, the evidence is insufficient to decide whether tunneling through the double barrier and/or predissociation from the outer well of the potential $d^3\Sigma^+$ could contribute to the observed 6 and 0.8 ms lifetimes. Thus, one may believe that no alternative exists to the assignment of these lifetimes proposed in Ref. 14 and corroborated in the main text of the present paper.

$\text{CO}^{2+}(a^1\Sigma^+)$

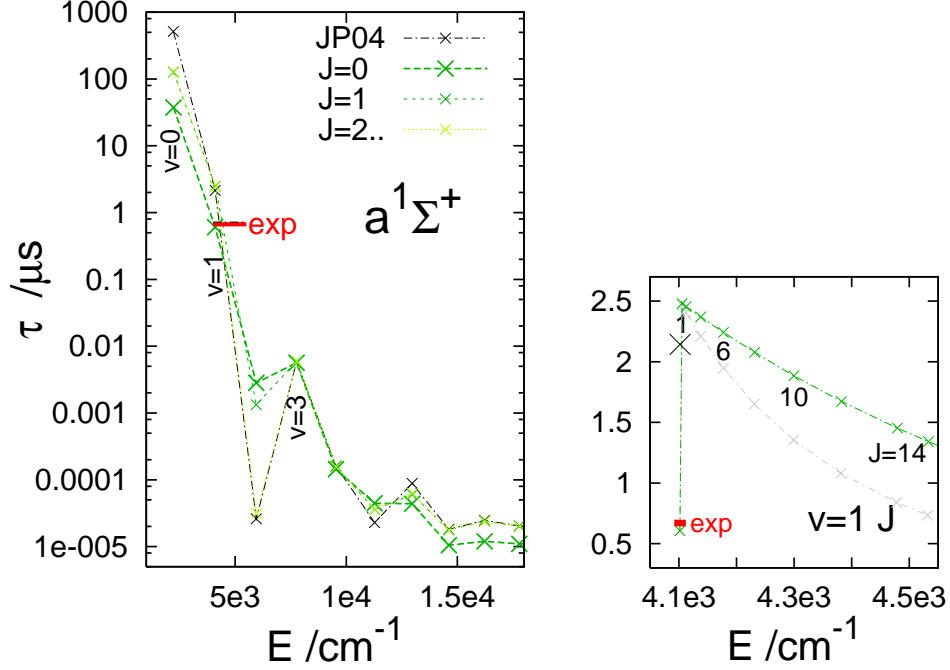


Fig. A9

Lifetimes of rotation-vibration states (Jv) of $\text{CO}^{2+}(a^1\Sigma^+)$ from the JP04r-v model

COMMENT

The lifetimes are seen to change very little (by about 30%) with J growing from 1 to 10 (the right panel). For the states $vJ=1$, they are close to the corresponding results from the purely vibrational JP04 model (denoted by black crosses). Exception is the $v=0 J=1$ level; its lifetime is about three times smaller than the $v=0$ lifetime from the JP04 model. In the case of the $^{13}\text{C}^{16}\text{O}^{2+}$ isotopomer (not shown here), the lifetimes of the states $av=0 J=1-10$ are within the range of 390-410 μs . So, they compare less favorably with the experimental value of $6000 \pm 2000 \mu\text{s}$ than the JP04 result, see Table V in the paper. The gray symbols in the right panel show the effect of the \mathbf{L} -uncoupling terms when added to the Hamiltonian \mathbf{H}^{Je} of the JP04r-v model, see Fig. A1. The faster decrease of lifetimes with growing J is almost entirely due to the couplings $^3\Sigma_0^- - ^3\Pi_1$ and $^3\Sigma_1^- - ^3\Pi_0$.

$\text{CO}^{2+}(b^1\Pi)$

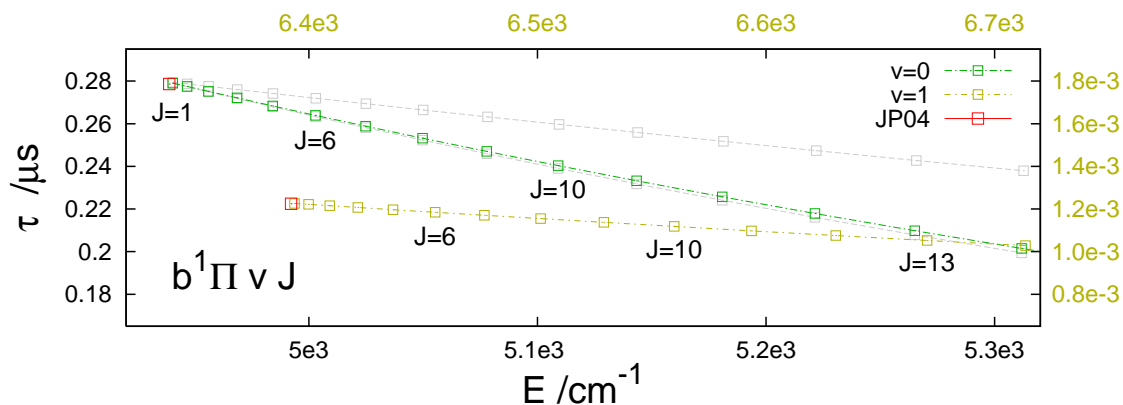


Fig. A10

Rovibronic states $b^1\Pi v=0, 1 J$ of CO^{2+} from the JP04r-v model

COMMENT

The energies and lifetimes obtained from the model for e and f parity states are practically indistinguishable. The gray symbols for $v=0 J$ levels represent results from the model supplemented with the **L**-uncoupling terms, see Fig. A1; the upper gray line pertains to e parity levels; the f parity levels remain almost unaffected by the terms. The relation to the results from the vibrational JP04 model should be noted: the lifetimes τ_{bv}^{JP04} are close to the lifetimes of the $J=1$ rotational levels. Deviations smaller than 1 % are found for nearly all v 's in the range 0-10. Obviously, this is just what one would expect. It is thereby demonstrated that the JP04r-v model passes the minimal correctness test.

-
- ¹ C-E. Froberg, *Rev. Mod. Phys.* **27**, 399 (1955).
- ² J. N. L. Connor and A. D. Smith, *Mol. Phys.* **43**, 397 (1981).
- ³ J. N. L. Connor and A. D. Smith, *Mol. Phys.* **45**, 149 (1982).
- ⁴ T. Šedivcová, P. R. Ždánská, V. Špirko, and J. Fišer, *J. Chem. Phys.* **124**, 214303 (2006).
- ⁵ J. H. D. Eland, M. Hochlaf, G. C. King, P. S. Kreynin, R. J. Le Roy, I. R. McNab, and J. M. Robbe, *J. Phys.* **B 37**, 3197 (2004).
- ⁶ T. Šedivcová, P. R. Ždánská, and V. Špirko, *Int. J. Quant. Chem.* **107**, 2654 (2007).
- ⁷ H. Lefebvre-Brion and R. E. Field, *Perturbations in the Spectra of Diatomic Molecules*, (Academic, New York, 1986).
- ⁸ M. Larsson, G. Sundström, L. Broström, and S. Mannervik, *J. Chem. Phys.* **97**, 1750 (1992).
- ⁹ M. S. Child and R. Lefebvre, *Mol. Phys.* **34**, 979 (1977).
- ¹⁰ L. H. Andersen, J. H. Posthumus, O. Vahtras, H. Ågren, N. Elander, A. Nunez, A. Scrinzi, M. Natiello, and M. Larsson, *Phys. Rev. Lett.* **71**, 1812 (1993).
- ¹¹ G. Dawber, A. G. McConkey, L. Avaldi, M. A. MacDonald, G. C. King, and R. I. Hall, *J. Phys.* **B27**, 2191 (1994).
- ¹² M. Lundquist, P. Baltzer, D. Edvardsson, L. Karlsson, and B. Wannberg, *Phys. Rev. Lett.* **75**, 1058 (1995).
- ¹³ M. Hochlaf, R. I. Hall, F. Penent, H. Kjeldsen, P. Lablanquie, M. Lavollée, and J. H. D. Eland, *Chem, Phys.* **207**, 159 (1996).
- ¹⁴ F. Penent, R. I. Hall, R. Panajotovič, J. H. D. Eland, G. Chaplier, and P. Lablanquie, *Phys. Rev. Lett.* **81** 3619 (1998).
- ¹⁵ M. Cizek, J. Horacek, and W. Domcke, *Phys. Rev.* **A75**, 012507 (2007).